

**Modelling Dutch Lower  
Shoreface Sand Transport**





# **Modelling Dutch Lower Shoreface Sand Transport**

Bart Grasmeijer  
Reinier Schrijvershof  
Jebbe van der Werf





## Title

Modelling Dutch Lower Shoreface Sand Transport

Client	Project	Attribute	Pages
Rijkswaterstaat Water, Verkeer en Leefomgeving, RIJSWIJK	1220339-005	1220339-005-ZKS-0008	74

## Keywords

Kustgenese 2.0, 3D DCSM-FM model, CGII TA model, Dutch Lower Shoreface, Sand Transport

## Summary

Dutch coastal policy aims for a safe, economically strong and attractive coast. This is achieved by maintaining the part of the coast that support these functions; the coastal foundation. The coastal foundation is maintained by means of sand nourishments.

Up to now, it has been assumed that net transports across the coastal foundation's offshore boundary at the 20 m depth contour are negligibly small. In the framework of the Coastal Genesis 2.0 program we investigate sand transports across this boundary and across other depth contours at the lower shoreface. The purpose of this report is to provide knowledge for a well-founded choice of the seaward boundary of the coastal foundation. Possibilities for an alternative offshore boundary of the coastal foundation will be discussed in a following synthesis report. The lower shoreface is the zone where the mixed action of shoreface currents (tide-, wind- and density gradient driven) and shoaling and refracting waves is predominant. Transport rates are relatively small and hence the bed levels in the lower shoreface undergo relatively slow changes.

We developed an efficient approach to compute the annual sand transport rates at the Dutch lower shoreface. It is based on the 3D Dutch Continental Shelf Model with Flexible Mesh (3D DCSM-FM), a wave transformation tool and a 1DV sand transport module. Waves and currents were decoupled to save computational time, ignoring wave-current-interaction.

The wave transformation tool was found to be an appropriate tool to derive wave parameters at the lower shoreface, indicated by a good and equal performance of the tool over the depth range studied. Comparisons against measurements at Ameland, Terschelling and Noordwijk showed that the approach is suitable to correctly model hydrodynamics during normal wind and wave conditions, yielding transport values that are comparable to calculations based on measurements. Wind- or wave-driven residual flows under high energetic conditions were, however, underestimated.

Although cross-shore transports are sensitive to the definition of the coast angle, computations showed predominantly onshore directed transports for the coastal stretch from Westkapelle to about 10 km south of Callantsoog and along the Wadden islands. The transports tend to be offshore directed at the inlets between Callantsoog and Texel (Marsdiep) and between Vlieland and Terschelling (Vliestroom). The onshore directed transport component was generally larger for smaller water depths closer to the shore, except near the inlets.

Computations show decreasing annual mean alongshore transports from Westkapelle to Scheveningen, increasing from Scheveningen to the inlet between Callantsoog and Texel (Marsdiep) and decreasing again towards Schiermonnikoog at the NAP-20 contour. Alongshore transports at the NAP-15 m contour were on average 10% smaller than at the NAP-20 m contour.




**Title**  
Modelling Dutch Lower Shoreface Sand Transport

**Client**  
Rijkswaterstaat Water,  
Verkeer en Leefomgeving,  
RIJSWIJK

**Project**  
1220339-005

**Attribute**  
1220339-005-ZKS-0008

**Pages**  
74

Version	Date	Author	Initials	Review	Initials	Approval	Initials
0.2	September 2019	Bart Grasmeijer Jebbe van der Werf Reinier Schrijvershof		Arjen Lujendijk		Frank Hoozemans	

**Status**  
final

## Samenvatting

Het Nederlandse kustbeleid streeft naar een veilige, economisch sterke en aantrekkelijke kust. Dit wordt bereikt door het deel van de kust te handhaven dat deze functies ondersteunt; het kustfundament. Het kustfundament wordt onderhouden door middel van zandsuppleties.

Tot nu toe is aangenomen dat netto transporten over de zeewaartse grens van het kustfundament op de 20 m diepte contour verwaarloosbaar klein zijn. In het kader van het Kustgenese 2.0-programma onderzoeken we zandtransporten over deze grens en over andere dieptecontouren op de diepe vooroever. Doel van dit rapport is om de kennis te leveren voor een onderbouwde keuze van de zeewaartse grens van het kustfundament. Een mogelijke alternatieve grens voor het kustfundament wordt besproken in een volgend syntheserapport. De diepe vooroever is de zone waar de gecombineerde werking van stroming (getijden-, wind- en dichtheidsgradiënt aangedreven) en shoalende en refracterende golven overheersen. Transporten zijn relatief klein waardoor de veranderingen in bodemhoogte langzaam verlopen.

We hebben een efficiënte aanpak ontwikkeld om de jaarlijkse zandtransporten op de diepe vooroever van de Nederlandse kust te berekenen. Het is gebaseerd op het 3D Dutch Continental Shelf Model met Flexible Mesh (3D DCSM-FM), een golftransformatie-tool en een 1DV-zandtransportmodel. Golven en stromingen werden onafhankelijk van elkaar berekend om rekentijd te besparen. Golf-stroom-interactie werd hiermee genegeerd.

De golftransformatie-tool blijkt een geschikt instrument om golfparameters op de diepe vooroever te bepalen. Uit een vergelijking met metingen bij Ameland, Terschelling en Noordwijk blijkt de aanpak geschikt om de hydrodynamica te modelleren tijdens normale wind- en golfomstandigheden. Transporten zijn vergelijkbaar met berekeningen op basis van metingen. De door wind of golven aangedreven reststromen en bijbehorende zandtransporten blijken onder hoog energetische condities in werkelijkheid groter te zijn dan met deze methode geschat.

Hoewel het kustdwarse transport gevoelig is voor de precieze definitie van de kusthoek laten de berekeningen voornamelijk landwaarts gerichte transporten zien voor het kusttraject van Westkapelle tot ongeveer 10 km ten zuiden van Callantsoog en langs de Waddeneilanden. De transporten zijn meestal zeewaarts gericht ter hoogte van de zeegaten tussen Callantsoog en Texel (Marsdiep) en tussen Vlieland en Terschelling (Vliestroom). De landwaarts gerichte

**Title**  
Modelling Dutch Lower Shoreface Sand Transport

<b>Client</b>	<b>Project</b>	<b>Attribute</b>	<b>Pages</b>
Rijkswaterstaat Water, Verkeer en Leefomgeving, RIJSWIJK	1220339-005	1220339-005-ZKS-0008	74

transportcomponent is over het algemeen groter voor kleinere waterdiepten dicht bij de kust, behalve bij de zeegaten.

In kustlangse richting laten de berekeningen langs de NAP-20 contour een afnemend jaargemiddeld langstransport zien Westkapelle naar Scheveningen, toenemend van Scheveningen naar het zeegat tussen Callantsoog en Texel (Marsdiep) en weer afnemend richting Schiermonnikoog. Op de NAP-15 m-contour zijn de berekende kustlangse transporten gemiddeld 10% kleiner dan bij de NAP-20 m-contour.



## Contents

<b>1</b>	<b>Introduction</b>	<b>1</b>
1.1	Background	1
1.1.1	Coastal foundation	1
1.1.2	Kustgenese 2.0	2
1.1.3	Previous work	2
1.2	Objective and research questions	2
1.3	Study approach	2
1.4	Outline report	3
<b>2</b>	<b>Methodology</b>	<b>5</b>
2.1	Introduction	5
2.2	Two-sided modelling approach	5
2.3	Measurements at Ameland, Terschelling and Noordwijk	7
2.4	Terschelling-Ameland model (CGII-TA)	8
2.5	Offline modelling approach	9
2.5.1	Overview	9
2.5.2	Wave transformation matrix	10
2.5.3	3D Dutch Continental Shelf Model-Flexible Mesh (3D DCSM-FM)	10
2.5.4	Sand transport model TSAND	12
2.5.5	Wave-driven currents	12
<b>3</b>	<b>Hydrodynamic validation</b>	<b>13</b>
3.1	Waves at Ameland Inlet	13
3.2	Velocities at Noordwijk and Ameland Inlet	15
3.2.1	Error statistics	15
3.2.2	Residual currents	16
3.2.3	Importance of wave and wind-driven flow at the lower shoreface	23
3.3	Conclusions	26
<b>4</b>	<b>Sensitivity transport modelling approaches</b>	<b>27</b>
4.1	Introduction	27
4.2	Wave input	27
4.3	Velocity input	29
4.4	Transport approach	32
4.5	Conclusions	33
<b>5</b>	<b>Quantifying transports at the lower shoreface</b>	<b>35</b>
5.1	Introduction	35
5.2	Flow velocities	36
5.2.1	Annual mean residual flow	36
5.2.2	Peak tidal velocities	38
5.3	Waves	40
5.4	Transport rates	43
5.4.1	Net annual transport rates	43
5.4.2	Effect of density and wind	57
5.4.3	Contribution of storm events to the annual transports	65
<b>6</b>	<b>Discussion, conclusions and recommendations</b>	<b>67</b>

6.1	Discussion	67
6.2	Conclusions	67
6.2.1	Hydrodynamic validation	68
6.2.2	Sensitivity analysis	68
6.2.3	Main research questions	68
6.3	Recommendations	72
<b>7</b>	<b>References</b>	<b>73</b>
<b>Appendices</b>		
<b>A</b>	<b>Wave driven currents</b>	<b>A-1</b>
A.1	Wave breaking	A-1
A.2	Wave-driven currents from a force perspective	A-4
A.3	Wave-driven currents from a continuity perspective	A-5
A.3.1	Mass flux	A-5
A.3.2	Cross-shore currents	A-6
A.3.3	Alongshore currents	A-9
A.4	Discussion	A-12
<b>B</b>	<b>Offshore wave statistics</b>	<b>B-1</b>
<b>C</b>	<b>Annual mean residual flow velocities</b>	<b>C-1</b>
<b>D</b>	<b>Annual mean peak tidal velocities</b>	<b>D-1</b>



# 1 Introduction

## 1.1 Background

### 1.1.1 Coastal foundation

Dutch coastal policy aims for a safe, economically strong and attractive coast. This is achieved by maintaining the part of the coast that support these functions; the coastal foundation.

The offshore boundary of the coastal foundation is presently taken at the NAP -20 m depth contour, the onshore limit is formed by the landward edge of the dune area (closed coast) and by the tidal inlets (open coast). The borders with Belgium and Germany are the lateral boundaries (Figure 1.1). The coastal foundation is maintained by means of sand nourishments; the total nourishment volume is approximately 12 million m<sup>3</sup>/year since 2000.

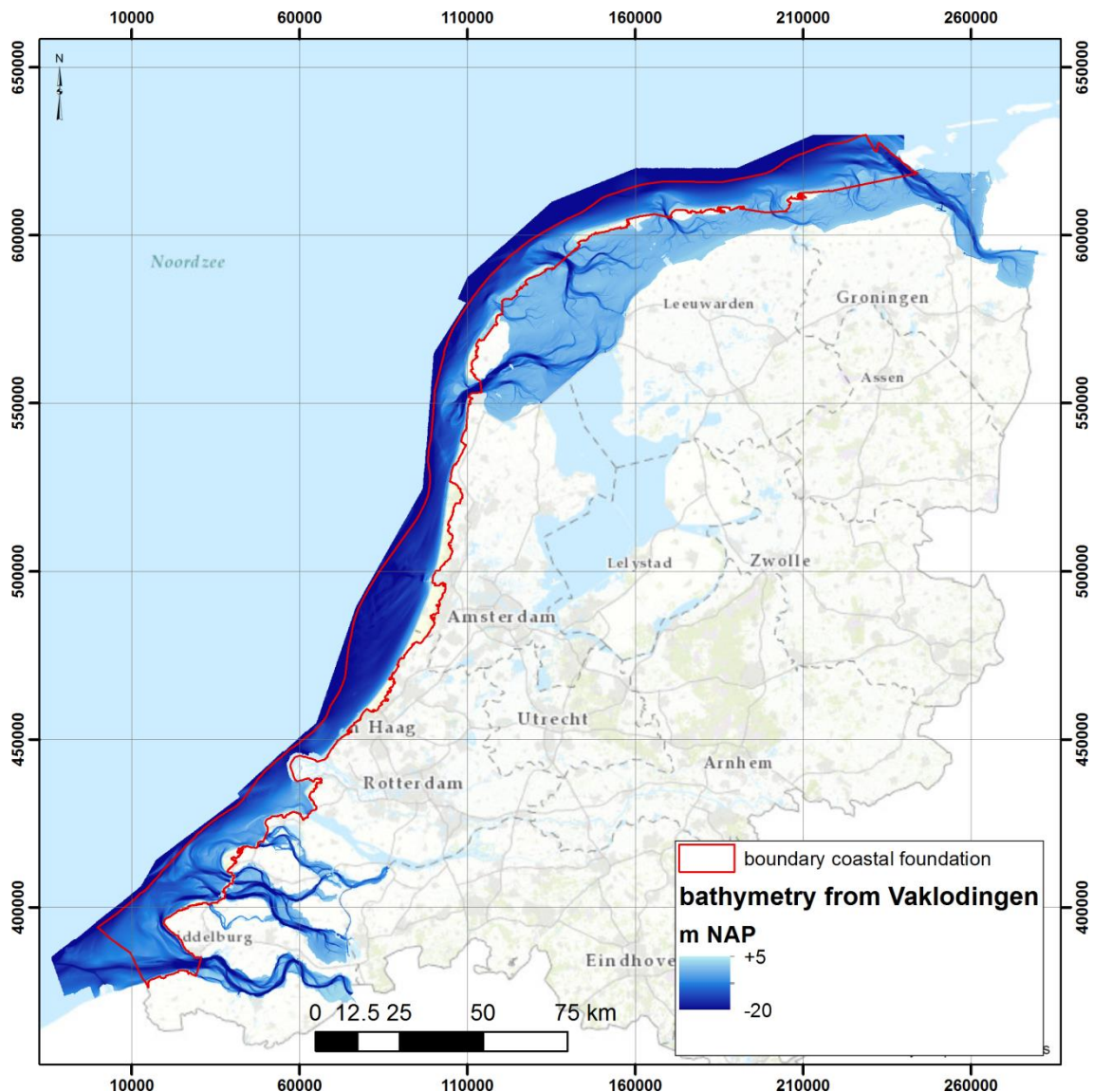


Figure 1.1 Coastal foundation on top of bathymetry from Vakklingen measurements between 2009 and 2014.

### 1.1.2 Kustgenese 2.0

In 2020 the Dutch Ministry of Infrastructure and Environment will make a decision on the nourishment volume. The Kustgenese-2.0 (KG2) programme is aimed to deliver knowledge to enable this decision making. The scope of the KG2 project commissioned by Rijkswaterstaat to Deltares is determined by two main questions:

- 1 What are possibilities for an alternative offshore boundary of the coastal foundation?
- 2 How much sediment is required for the coastal foundation to grow with sea level rise?

The Deltares KG2 subproject “Diepe Vooroever” (DV, lower shoreface), of which this report is a small part, answers both questions. The KG2-DV project studies the cross-shore and alongshore sediment transports at the Dutch lower shoreface as function of depth on the basis of field measurements, numerical modelling and system knowledge. Answers to the above main questions will be given in a synthesis report. The present report delivers knowledge required to do so.

### 1.1.3 Previous work

This report is a continuation of three previous reports, i.e. 1) a literature study by Van der Werf et al. (2017), 2) a description of a method for calculating the sediment transports on the Dutch lower shoreface by Grasmeijer (2018) and 3) a report on the set-up and validation of the 3D Dutch Continental Shelf Model – Flexible Mesh by Zijl et al. (2018).

## 1.2 Objective and research questions

The objective of this study is to estimate the net sand transport rates on the Dutch lower shoreface, with water depths between ~15 and 25 m, and to unravel the underlying mechanisms.

The main research questions are described as follows:

1. How do the hydrodynamics conditions vary along and across the Dutch Lower Shoreface?
  - a) Peak tidal velocities
  - b) Residual flow
  - c) Waves
2. What are typical net sand transport rates on the Dutch lower shoreface?
  - a) Which physical processes determine lower shoreface net sand transport?
  - b) How does net transport vary across and along the Dutch lower shoreface?
  - c) What is the effect of storms?

The first research question helps in understanding the variation of the transports along and across the lower shoreface in the second question. This knowledge will be used to answer the main questions of the KG2 project in the synthesis report (see par. 1.1.2).

## 1.3 Study approach

In the framework of the Kustgenese-2.0 (KG2) programme, the sand transport at the Dutch lower shoreface is assessed by combining field measurements, 1D, 2D and 3D models and expert judgement. This report focusses on the validation of the models with field measurements and model computations for five years. We use two different modelling approaches. The first includes the interaction of waves, flow, and the resulting sand transport (online approach). In the second approach, the waves, flow and the transport of sand are calculated separately and independently and there is no feedback between the processes (offline approach). More details on the methodology can be found in chapter 2 of this report.

#### **1.4 Outline report**

Chapter 2 describes the applied methodology, including the measurements used and models applied. Chapter 3 presents a hydrodynamic validation of the models by comparing modelled and measured waves and velocities. Chapter 4 quantifies the sensitivity of various transport modelling approaches. Chapter 5 analyses the computed transports at the Dutch lower shoreface for a period of 5 years. Chapter 6 summarizes the results and presents conclusions and recommendations.



## 2 Methodology

### 2.1 Introduction

Van der Werf et al. (2017) present an inventory of existing knowledge, field data and models of the Dutch lower shoreface. Important modelling research has been done in 1990's in the framework of the first Coastal Genesis research program of Rijkswaterstaat. Roelvink & Stive (1990) and Van Rijn (1997) published research on the sediment transport of Holland coast. In both studies, the yearly averaged transport was computed along a number of coast-normal transects. Important finding in these earlier studies is that the net sand transport on the Holland shoreface is determined by various subtle effects such as a density-gradient driven current but also that storm events play an important role and that a changing wave climate has a relatively big effect on the net transports.

Improved computer techniques facilitated the development of large scale 2D models of the Dutch coast. Van der Werf & Giardino (2009), Van der Hout et al. (2009) and Van der Spek et al. (2015) computed the hydrodynamics, sediment transport and morphodynamics (only Van der Hout et al.) along the Dutch coast with a Delft3D model. The predicted hydrodynamics and sediment transport along the Holland Coast and the Texel Inlet compared quite well with reference studies. A recent study of the large-scale sediment transport along the Dutch coast is from Knook (2013). He analyzed cross-shore sediment transport rates at various depths on the lower shoreface of the Central Holland coast. This analysis was based on computations with the Unibest-TC model, which makes the approach similar to the one by Roelvink and Stive in 1990 and Van Rijn in 1997, although density-gradient effects were not accounted for. Probably, related to this he found offshore cross-shore transport on the lower shoreface (due to tidal currents) and onshore transport at the upper shoreface (due to waves). This induced a lower shoreface flattening and an upper shoreface steepening.

The earlier work has mainly focused on the central Dutch coast between Hoek van Holland and Den Helder without the effects of tidal inlets or estuaries. The computations were based on cross-shore profile models (2DV) or horizontal depth-averaged models (2DH). This required schematizing wave and current conditions based on results from large scale models or excluding effects such as salinity and 3D circulation in order to keep the computation time limited. However, 3D circulation patterns by e.g. fluid density gradients play an important role for the total cross-shore transport rate at water depths deeper than about 8 m (e.g. Van Rijn, 1997). Process-based 3D modelling to study the transport processes along the entire Dutch coast has not been done before.

Important processes to consider are the following:

- Effects of tide, wind and waves.
- Density gradient effects, especially for the Holland Coast, which is affected by the Rhine ROFI.
- The vertical flow structure, especially density gradient driven currents, wave breaking induced undertow, Longuet-Higgins and other boundary layer streaming, up- and downwelling during storms.
- Alongshore effects, especially at outer deltas of the Delta and Wadden Coast.
- Wave effects: velocity skewness, return flow and Stokes drift.

### 2.2 Two-sided modelling approach

We follow the two-sided modelling approach as suggested by Van der Werf et al. (2017). The first is by setting up a detailed model of the Ameland-Terschelling coastal study area and calibrate and validate the model using the Coastal Genesis 2.0 measurements made in 2017

and 2018. We make sensitivity computations to investigate lower shoreface sand transport processes for different scenario's (varying input parameters and boundary conditions). This is a so-called online sand transport model approach, including wave-current interaction.

The second approach is by applying the existing 3D Dutch Continental Shelf Model – Flexible Mesh (3D DCSM-FM) of the entire Dutch coast (Zijl et al., 2018; Grasmeyer, 2018; Grasmeyer et al., 2019). This model includes effects of tide, wind and river discharge (density-driven currents). The necessary wave parameters to compute the sand transports are taken from wave observation data in combination with a wave transformation matrix to assess the wave conditions anywhere along the Dutch coast. The wave transformation matrix is described by De Fockert and Luijendijk (2011). The current and wave parameters will feed into a local 1DV sand transport model. This is the offline approach, in which wave-driven current effects are excluded or accounted for in a simplified way.

This second approach enables computing net transport rates along the entire Dutch shoreface and allows for investigating effects of wind and wave climate, tidal motion and effects of policy decisions such as changing the offshore boundary of the coastal foundation and maintenance requirements thereof.

The main difference between the online and offline approach is that the wave driven currents are included in the online approach and excluded or accounted for in a simplified way in the offline approach.

The transport of sand at the Dutch lower shoreface is calculated in this study using hydrodynamic input derived from measurements and numerical models. The advantage of using measurements is that all hydrodynamic processes are reflected in the data which gives the best possible input for a sediment transport calculation. A clear disadvantage of using measurements is the limitation of the data in time and space. Although numerical models can essentially be extended to any temporal and spatial extent and resolution the computational times usually limit the application of such models.

In the offline approach it is assumed that the sand transport flux is determined locally and that the interaction of flow and waves does not substantially alter the transport at the lower shoreface. To verify this, we compare the offline approach with measurements and the online modelling approach. Eventually, the combination of measurements, online and offline modelling lead to a substantiated result for the transport of sand at the lower shoreface. The approaches to calculate sand transport at the lower shoreface and the interaction between these approaches is visualized in a flow diagram in Figure 2.1.



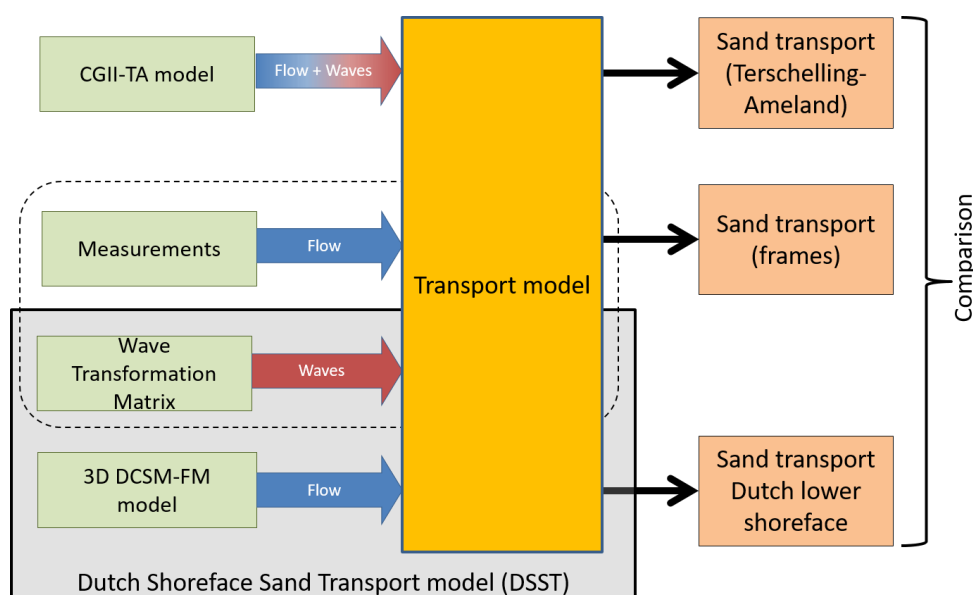


Figure 2.1 Flow diagram of the approach to estimate sand transport at the lower shoreface.

### 2.3 Measurements at Ameland, Terschelling and Noordwijk

In the Coastal Genesis II measurement campaigns stationary frames were deployed along the coasts of Ameland, Terschelling and Noordwijk with Acoustic Doppler Current Profiler (ADCP) instruments to measure flow velocity profiles. The data gathered during the campaigns is processed from raw data, checked and subsequently processed in to depth-averaged values (Van der Werf et al., in prep.). In this report the data will be used to validate the models and to use as input for sediment transport calculations. The Coastal Genesis lower shoreface campaigns and measurement frames are shown in Table 2.1 with relevant metadata and a map showing the locations of the frames is shown in Figure 2.2. The frames that are indicated with a green shade in Table 2.1 are the frames used in the analyses; the frames that are not shaded green were omitted from the analyses due to complications with the data (i.e. the data from the upward looking ADCP was missing).

Table 2.1 Overview of ADCP measurement locations used for model validation.

Campaign	Code	Frame	RDx [m]	RDy [m]	Depth [m NAP]	Start	End
Lower shoreface Ameland	DVA	F1	168339	615736	-20	8 Nov 2017	11 Dec 2017
		F3	168449	613779	-16		
		F4	168472	613485	-10		
Lower shoreface Terschelling 1	DVT1	F1	151671	611326	-20	11 Jan 2018	6 Feb 2018
		F3	152260	607627	-14		
		F4	152685	606596	-10		
Lower shoreface Terschelling 2	DVT2	F1	151993	611306	-20	12 Mar 2018	26 Mar 2018
		F3	152249	607599	-14		
		F4	152662	606583	-10		
Lower shoreface Noordwijk	DVN	F1	76940	477601	-20	4 Apr 2018	15 May 2018
		F3	86695	472149	-12		
		F4	85613	472749	-16		

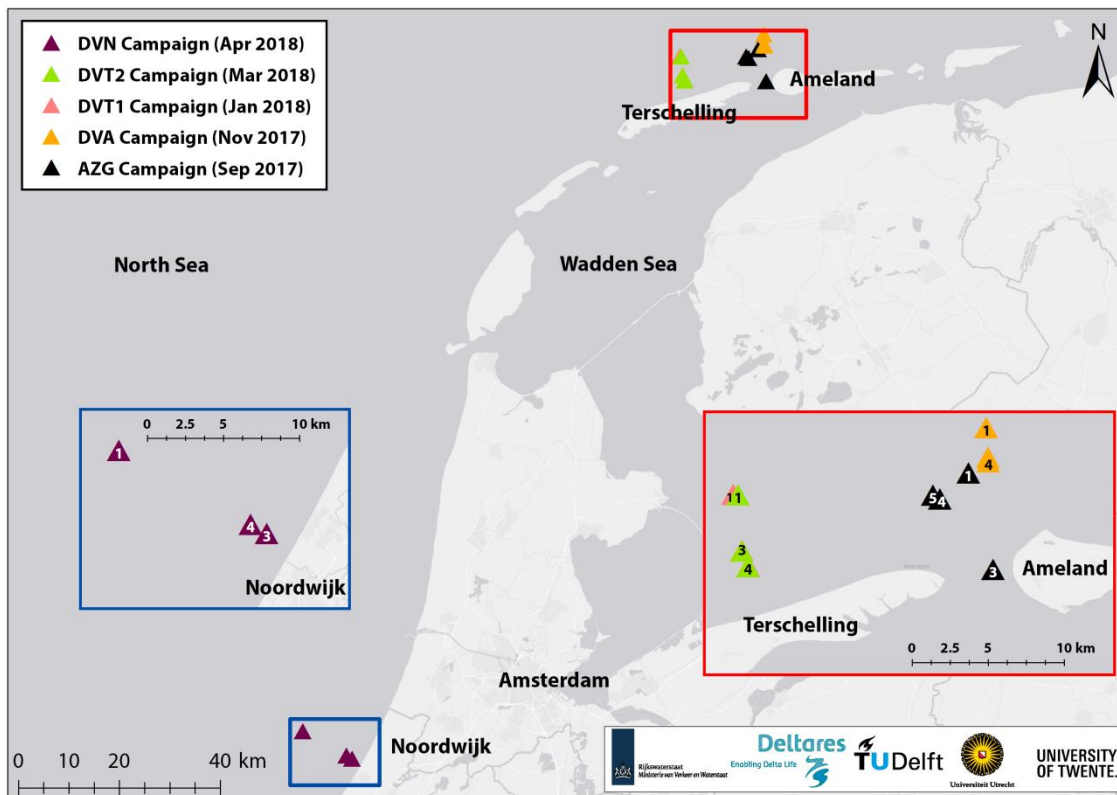


Figure 2.2 Overview of the locations of measurement frames during the Coastal Genesis II campaigns in 2017 and 2018.

## 2.4 Terschelling-Ameland model (CGII-TA)

Within the framework of the Coastal Genesis II Program a model is developed focused on the area of the Ameland tidal inlet and the Terschelling lower shoreface; the Coastal Genesis II Terschelling-Ameland model (CGII-TA model; Nederhoff et al., 2019). The model is set up to be used as a basis for modelling sediment exchange through the inlet and modelling sand transport at the lower shoreface near the Ameland inlet and Terschelling (subproject 'Lower Shoreface'). Aim is to compare this online approach with the offline modelling approach.

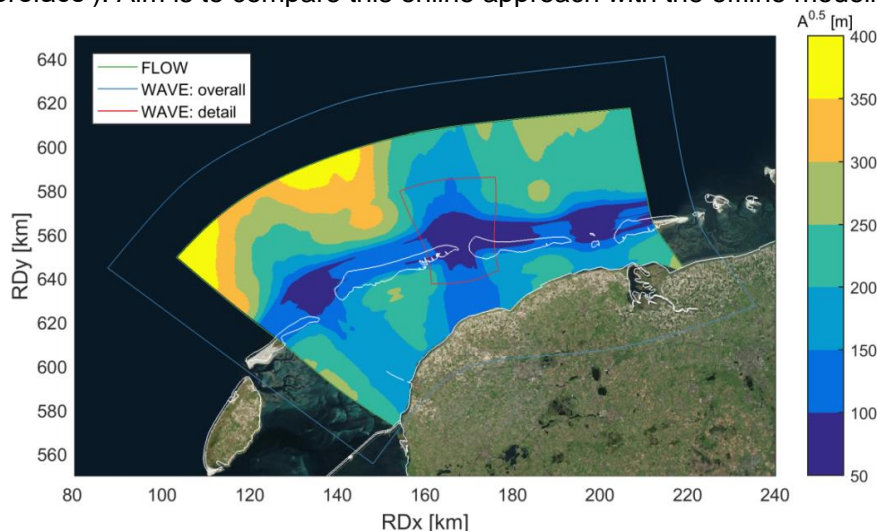


Figure 2.3 Extent of the model grids with the resolution of the FLOW grid indicated as the length [in m] of the grid cells. In red the extent of the SWAN grid is presented.

The model is set up as a coupled hydrodynamic-wave depth averaged (2DH) model using the Delft3D4 modelling package (Lesser et al., 2004). The numerical domain of the hydrodynamic module (FLOW) is centralized around the Ameland tidal inlet but includes the neighboring inlets (Vlie inlet and the Frysian inlet) as well (Figure 2.3). The resolution of the FLOW domain varies from ~50 m at the inlet to ~350 m near the seaward boundaries. The extent of the numerical domain of the wave modelling module (WAVE) is slightly larger to avoid boundary issues within the FLOW domain but the resolution is coarser by a factor 2. At the Ameland tidal inlet a nested WAVE domain is included with a resolution identical to the FLOW domain. At the boundaries the model is forced by modelled water levels obtained from the DCSMv4-ZUNOV6 model (Zijl et al., 2013), measured wave spectra obtained from offshore located wave buoys in the North Sea, and modelled meteorological (wind and pressure) data obtained from the KNMI HIRLAM model. The model bathymetry is schematized using Rijkswaterstaat vaklodingen data from the years 2012 up to and including 2018.

The model is extensively calibrated and validated using measurements of water levels, waves, discharges, and depth averaged flow velocities obtained during four Coastal Genesis II campaigns (September and November 2017 and January and March 2018). The model is well capable of reproducing the measurements and hence, is considered the most advanced model instrument to estimate sand transport rates near the Ameland inlet and the Terschelling lower shoreface. The setup, calibration, and validation of the CGII-TA model is described in detail by Nederhoff et al. (2019).

The CGII-TA model is extended for the present purpose with a sediment transport module, using the Van Rijn (2007) sediment transport formulae. A single non-cohesive sediment fraction is added to the model consisting of a median sediment diameter ( $D_{50}$ ) of 250  $\mu\text{m}$  and a 90<sup>th</sup> percentile ( $D_{90}$ ) of 400  $\mu\text{m}$ . All parameters of the sediment transport module are kept at default values except the factor to calculate the initial suspended sediment diameter, which is set at a value of 0.8 for coherence with the setting in the offline modelling approach.

## 2.5 Offline modelling approach

### 2.5.1 Overview

To answer the main research question, the sediments transports across the offshore boundaries of the Dutch coast need to be assessed. To assess the relative importance of different conditions and transport mechanisms the method to calculate these transports should include effects of tide-, wind-, density gradient driven currents and the skewed wave-induced orbital motion. We propose a method in which the tide-, wind-, density gradient driven currents are calculated with a 3D model, the waves are obtained from observations using a wave transformation matrix and transports are computed with a 1DV transport model.

This is referred to as an offline approach, which is relatively fast and easily facilitates assessing the relative importance of the different transport mechanisms, e.g. by artificially modifying density effects (for example by turning it off in the 3D model) or wave skewness effects (for example by manually changing it in the 1DV transport model) and makes sensitivity calculations by changing parameter settings relatively easy. It also facilitates application of different transport formulations.

Impact of the waves on the stratification and flow is not taken into account in this offline approach. Comparison with an online approach is made in chapter 3 of this report.

Tide-, wind-, density gradient driven currents are obtained from the 3D Dutch Continental Shelf Model-Flexible Mesh model (3D DCSM-FM). We will briefly describe the main characteristics

of the 3D DCSM-FM model here. Details are presented by Zijl and Veenstra (2018). Wave conditions are obtained from a wave transformation matrix (De Fockert and Luijendijk, 2011). The wave transformation matrix will also be described briefly.

To assess the annual transports, sediment transport computations are performed using the 1DV model by Van Rijn et al. (2018). It is an engineering approach of the Van Rijn (2007) model and described in more detail by Grasmeyer (2018). The sediment transport model requires flow and wave conditions as an input.

### 2.5.2 Wave transformation matrix

Wave conditions are obtained from a wave transformation matrix, or wave look-up table, that enables a swift transformation of measured offshore wave time series from the IJmuiden, Europlatform, Eierlandse Gat and Schiermonnikoog North waverider stations to an arbitrary location nearshore (De Fockert and Luijendijk, 2011).

The wave transformation matrix was made by analysing the offshore wave observation data and classifying these into discrete wave height, wave period and wave direction bins. These offshore wave conditions were applied to drive SWAN wave models of different parts of the Dutch coast. A set of 269 stationary SWAN computations were made to obtain good insight in the wave transformation under different hydrodynamic conditions.

A wave transformation matrix was made using the offshore wave conditions and the generated nearshore wave conditions. For the significant wave height and peak period, the transformation matrix was filled with multiplication factors and for the wave direction and surge an additional factor was applied.

In the wave transformation matrix, nearshore wave conditions depend more strongly on wave observation data that are closest by. For example, along the central Dutch coast, waves that have a direction smaller than  $280^\circ$  use the offshore wave information of Europlatform and waves with a direction larger than  $280^\circ$  use the wave information of IJmuiden. For the region above IJmuiden, waves with a direction smaller than  $300^\circ$  use the offshore wave information of IJmuiden and waves with a direction larger than  $300^\circ$  use the wave information of Eierlandse Gat as offshore wave platform

The wave transformation matrix uses the following parameters:

- a) wave height ( $H_{m0}$ ),
- b) mean period ( $T_{m02}$ ),
- c) wave direction,
- d) wind speed,
- e) wind direction
- f) surge

Transformed time series of wave data together with flow from the 3D DCSM-FM model described in par. 2.5.3 will in Chapter 5 be used as an input for sediment transport computations at more than 1300 locations along the Dutch coast for a period of 5 years.

### 2.5.3 3D Dutch Continental Shelf Model-Flexible Mesh (3D DCSM-FM)

Stratification caused by the freshwater outflow of the Rhine alters the tidal currents in front of the Dutch coast. The top and bottom layers of the flow become decoupled due to stratification. A cross-shore sediment transport may be caused by stratification. Explorative modelling research has shown that the models can indeed predict this transport (see e.g. Hop, 2017). Therefore, to answer the two main questions of the KG2 project it is important to model the effect of stratification on the velocity field. This can be done with the 3D DCSM-FM model. The

model includes the tide, wind and discharge. The 3D DCSM-FM model has originally been setup as part of Deltares' strategic research funding, with a focus on long-term water quality. Since then this model has been used for numerous studies.

Figure 2.4 shows the 3D DCSM-FM model grid. The DCSM-FM network was designed to have a resolution that increases with decreasing water depth. Figure 2.5 shows DCSM-FM model bathymetry in the southern North Sea. Zijl and Veenstra (2018) provide details on the setup and validation of the 3D DCSM-FM model.

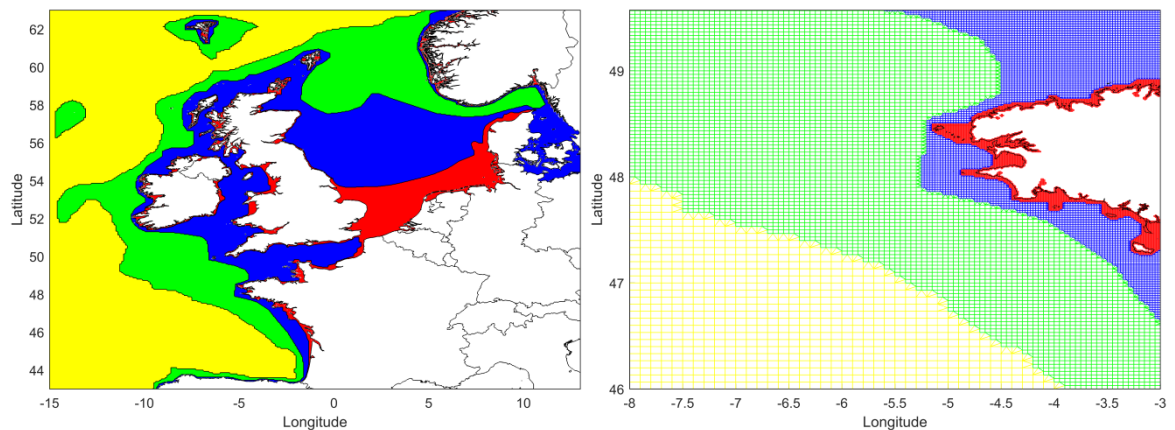


Figure 2.4. Overview (left) and detail (right) of the 3D DCSM-FM model network with the colours indicating the grid size (yellow: ~4 nm; green: ~2 nm; blue: ~1nm; red: ~0.5 nm).

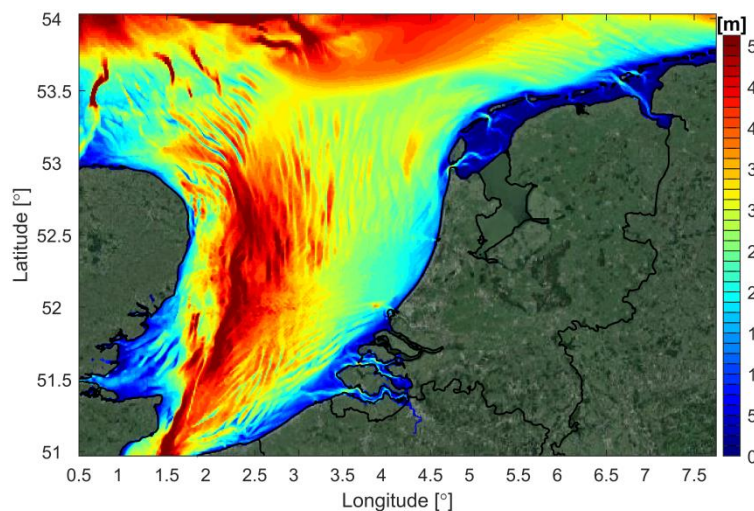


Figure 2.5. DCSM-FM model bathymetry in the southern North Sea (depths relative to MSL).

## 2.5.4 Sand transport model TSAND

The sediment transport rates are computed with the TSAND model. Grasmeijer (2018) describes the transport model in detail.

TSAND is a simplified sand transport model for tidal flow with waves. The simplified approach is based on the detailed sediment transport formulations by Van Rijn (1984, 1993, 2007, 2015), which have been verified extensively.

The TSAND-model can be used standalone or as a post-processing model to compute the instantaneous variation of the depth-integrated suspended sand transport and total transport (incl. bed-load transport). Here we use it as a post-processing model to compute annual transports.

The suspended sand transport is computed by integration of the product of velocity and concentration over the water depth:

$$q_s = \int_a^h (uc_{sand}) dz$$

The velocities ( $u$ ) and sand concentrations ( $c_{sand}$ ) are computed as a function of height above bed and time. The grid points over the depth (50 points) are distributed exponentially. Used standalone, the basic hydrodynamic parameters should be specified by the user. Used as a post-processing model, the hydrodynamic input may come from a 1D, 2DH or 3D-model.

The bedload sand transport includes the effect of wave skewness and computes the bedload transport based on the quasi-steady approach by Van Rijn (2007) as follows:

$$q_b = \int_0^T q_{b,t} dt$$

with  $q_{b,t}$  the intra-wave time-dependent bedload transport and  $T$  the wave period.

For the quasi-steady bedload transport approach, the intra-wave near-bed velocity is computed based on the parameterization by Isobe and Horikawa (1982).

The total load transport of sand is computed as the sum of the suspended load and bed load.

## 2.5.5 Wave-driven currents

In the offline approach we compute the sand transport rates on the Dutch lower shoreface using the Van Rijn et al. (2018) sand transport model with wave input from the wave transformation matrix and velocity input from the 3D DCSM-FM model (Grasmeijer, 2018; Zijl et al., 2018). These simulations include wave-driven Longuet Higgins streaming near the bed and Stokes drift due to water particles moving along elliptic orbits that are not completely closed. Appendix A discusses the wave-driven currents and in more detail.



### 3 Hydrodynamic validation

Predictions of sand transport rates at the Dutch lower shoreface using process-based numerical simulation models contain inherent uncertainties owing to model structural deficiencies, measurement errors, and parameter uncertainty. Sand transport is driven by waves and currents, which means that the predictive uncertainty of sand transport depends on the accuracy of the model's representation of waves and currents. In this chapter we therefore validate the models against measurements of waves and currents.

#### 3.1 Waves at Ameland Inlet

Wave characteristics derived via the wave transformation tool are validated using measurements in Grasmeyer (2018) at locations Meetpost Noordwijk (MPN) and Ameland Inlet 1-2 (AZB12). Here, the validity of the approach is tested for the study site (lower shoreface) specifically by comparison of the wave characteristics from the matrix and the CG-II TA (process-based) modelled wave characteristics. This comparison is shown at the locations of the measurement frames from the lower shoreface campaigns at Ameland and Terschelling. Timeseries of the wave characteristics at frame 3 (Figure 3.1) show that the matrix can reproduce the significant wave height and peak period well and the wave direction reasonable. Fluctuations in the wave characteristics on time scales shorter than days are reproduced, giving confidence that the tide-induced changing water depths are represented well in the wave parameters. Scatterplots for all frames for the Ameland lower shore face campaign (Figure 3.2) illustrate that the performance of the wave transformation tool is equal over the range of water depths studied in this report (NAP -20 m up to NAP -10 m, see Table 2.1). The ability of the tool to reproduce the mean wave direction is less than for the other two aggregated wave parameters considered which is mostly attributed to a mismatch for waves coming from a southwest to south direction (offshore directed winds). However, waves coming from this direction are less energetic due to the limited fetch length and the implications for sand transport are presumably small. The goodness-of-fit parameters for the three campaigns and all frames (Table 3.1) indicate that the wave transformation tool gives similar performances for different conditions (other time periods) and locations (other campaigns). Furthermore, the performance of the model to reproduce the significant wave height at the lower shoreface is similar to the direct comparison with measurements at other (deeper water) locations (shown by Grasmeyer, 2018). Hence, the wave transformation tool is considered appropriate for the studied environment.

Table 3.1 Goodness of fit ( $r^2$ ) parameters for the significant wave height ( $H_{m0}$ ), peak period ( $T_p$ ) and mean wave direction derived from the wave transformation tool and the CGII-TA model at the locations of the measurement frames during the coastal genesis campaigns at Ameland and Terschelling.

Campaign	Frame	$r^2 H_{m0}$ (-)	$r^2 T_p$ (-)	$r^2$ Direction (-)
DVA	F1	0.92	0.83	0.78
	F3	0.93	0.85	0.78
	F4	0.94	0.88	0.77
DVT1	F1	0.90	0.71	0.92
	F3	0.89	0.75	0.89
	F4	0.88	0.74	0.87
DVT2	F1	0.92	0.61	0.83
	F3	0.91	0.59	0.82
	F4	0.91	0.57	0.80

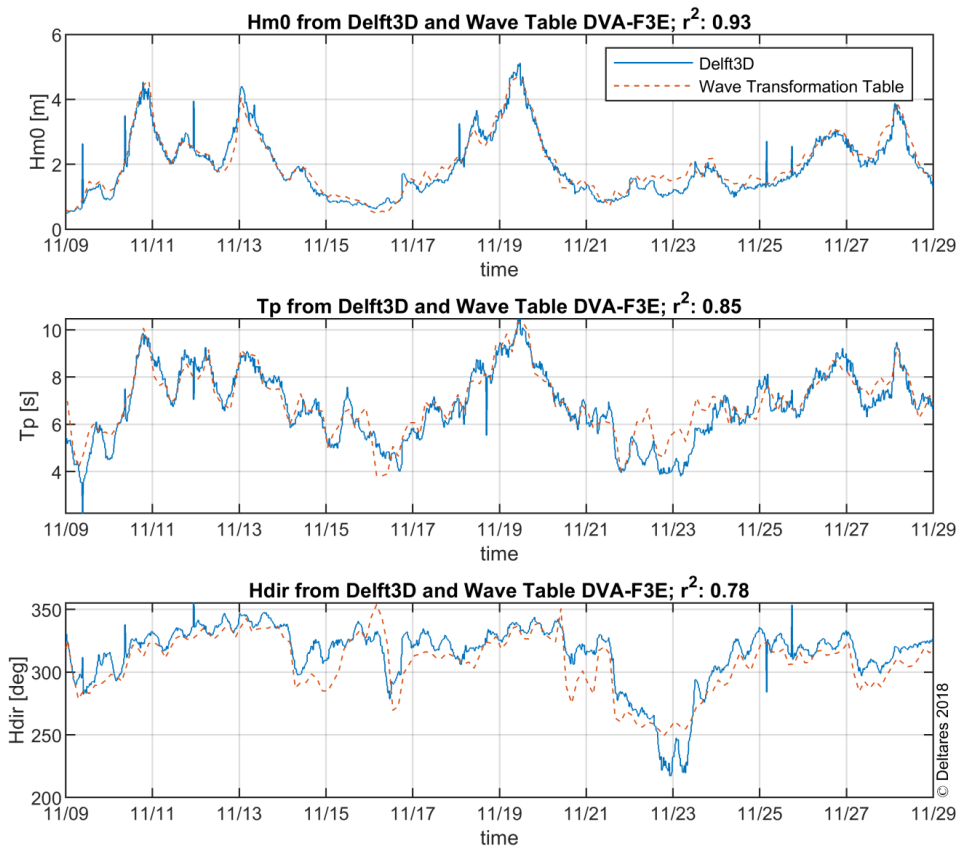


Figure 3.1 Timeseries of significant wave height ( $H_s$ , top), peak period ( $T_p$ , centre), and wave direction ( $H_{dir}$ , bottom) at the location of frame 3 during the CGII November 2017 measurement campaign (DVA-F3).

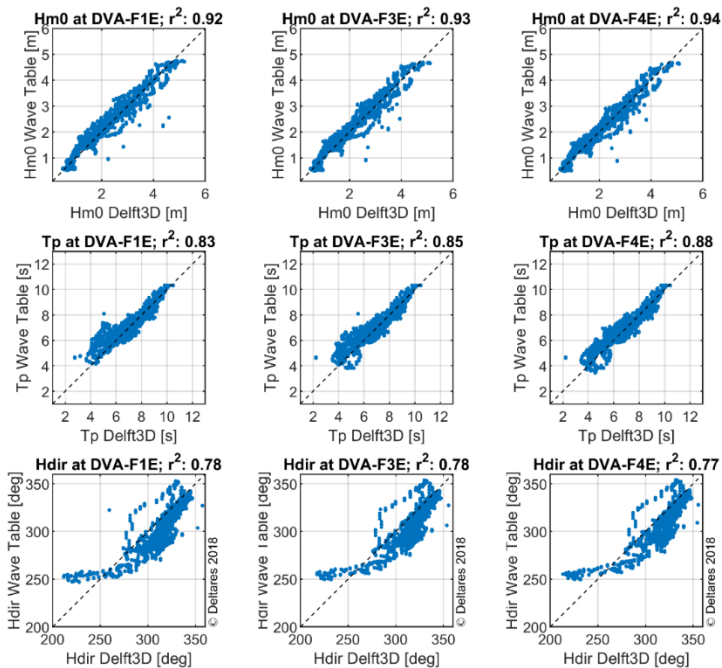


Figure 3.2 Scatterplots of significant wave height ( $H_{m0}$ , top), peak period ( $T_p$ , centre), and wave direction ( $H_{dir}$ , bottom) as modelled by the wave transformation matrix versus the Delft3D CGII-TA model. Scatterplots are shown for the locations frame 1 (left), 3 (middle), and 4 (right) of the November 2017 campaign (DVA).

## 3.2 Velocities at Noordwijk and Ameland Inlet

### 3.2.1 Error statistics

The model set-up and validation report of the 3D DCSM-FM model (Zijl et al., 2018) compares the modelled and measured depth averaged velocities during the Ameland lower shoreface campaign (DVA), showing a good reproduction with a bias less than 0.06 m/s and a root-mean-squared-error (RMSE) less than 0.15 m/s for the velocity magnitude. For this report the comparison is extended to cover all frames and Coastal Genesis Lower Shoreface campaigns (Table 3.2). The model-data comparison is presented in a compact yet complete manner by providing bias and RMSE values for the east- and northward components and the velocity magnitude of the depth averaged velocities (Table 3.3)<sup>1</sup>. Values presented are not necessarily equal to the values presented by Zijl et al. (2018) due to a change in time period analysed. The table shows a good reproduction of the magnitude with generally bias values of less than 0.09 m/s and a RMSE less than 0.20 m/s, which is in line with the analysis of Zijl et al. (2018). In general, the performance of the model decreases with decreasing water depths, most likely indicating an increasing importance of wave-induced flow which is not modelled by the 3D DCSM-FM model (the data from the wave transformation tool is only used in the sand transport calculations). Contrary to this general trend are the error statistics of the Noordwijk campaign, which show a trend of increasing performance with decreasing water depth. These trends are analysed in more detail in the next chapter by considering the residual (non-tide driven) flow.

Table 3.2 Overview of the input for the hydrodynamic validation.

Campaign	Campaign code	Period analysed	Data sources	Data code
Lower shoreface Ameland	DVA	9 Nov 2017 – 29 Nov 2017	Measured DCSM-FM CGII TA	OBS DFM D3D
Lower shoreface Terschelling 1	DVT1	12 Jan 2018 – 6 Feb 2018	Measured DCSM-FM CGII TA	OBS DFM D3D
Lower shoreface Terschelling 2	DVT2	13 Mar 2018 – 26 Mar 2018	Measured DCSM-FM CGII TA	OBS DFM D3D
Lower shoreface Noordwijk	DVN	5 Apr 2018 12h – 21 Apr 2018 12h	Measured DCSM-FM	OBS DFM

The model set-up van validation report of the CGII TA model (Nederhoff et al., 2019) gives a full analysis of reproduction of flow at the measurement frames deployed during the November 2017 (DVA), and January (DVT1) and March 2018 (DVT2) Coastal Genesis Lower Shoreface campaigns. With an absolute bias smaller than 0.05 m/s and a RMSE smaller than 0.16 m/s for the flow velocity magnitude this model performs slightly better than the DCSM-FM model in reproducing depth averaged velocities at the lower shoreface. This is not a surprising result considering the CGII TA model is specifically set-up and calibrated based on these measurements. The error statistics in Nederhoff et al. (2019) show a general trend of decreasing performance of the model with decreasing water depths as well, similar to the DCSM-FM model. This trend indicates that even a model with an online coupled wave model

<sup>1</sup> Analysing these results must be accompanied by the remark that the direction of the measurements is subjected to errors (directional shift) due to a wrong correction of the compass heading (see Van der Werf, 2019 for details). The values of the eastward and northward components of the frames that are presumably subjected to this error are given in *italic*. The error does not have effect on the magnitude of the depth averaged velocity.

and a fine grid resolution (~50 m) is not able to grasp the full complexity of non-tide driven processes at the lower shoreface.

Table 3.3 Goodness of fit ( $r^2$ ) parameters for the significant wave height ( $H_{m0}$ ), peak period ( $T_p$ ) and mean wave direction derived from the wave transformation tool and the CGII-TA model at the locations of the measurement frames during the coastal genesis campaigns at Ameland and Terschelling. At campaign DVN F3 and F4 are switched to show the values with continuous decreasing water depths.

Campaign	Frame	East comp. (m/s)		North comp. (m/s)		Magnitude (m/s)	
		Bias	RMSE	Bias	RMSE	Bias	RMSE
DVA	F1	0.01	0.10	-0.03	0.15	0.02	0.10
	F3	0.09	0.20	-0.03	0.13	0.04	0.15
	F4	0.15	0.23	-0.08	0.17	0.07	0.18
DVT1	F1	0.09	0.15	-0.04	0.10	0.02	0.14
	F3	0.05	0.12	-0.01	0.04	0.04	0.12
DVT2	F1	0.00	0.13	0.00	0.11	0.02	0.12
	F3	-0.05	0.19	-0.02	0.06	0.06	0.18
DVN	F1	0.00	0.11	-0.02	0.15	-0.05	0.13
	F4	0.02	0.08	0.02	0.11	-0.04	0.11
	F3	0.02	0.06	0.04	0.10	-0.02	0.11

### 3.2.2 Residual currents

Leummens (2018) analysed the measurements of the coastal genesis Ameland lower shoreface campaign and found that storms (characterised by north western winds and  $H_s > 4$  m) drive a strong eastward and landward residual current on the lower shoreface, increasing in strength towards shallower depths. He showed that both the DCSM-FM and CGII-TA models are not capable of reproducing these residual flows, resulting in a similar mismatch of calculated cross- and longshore sand transport rates. Here, the analysis is extended to cover all campaigns (focussed on the residual flow during storms) to determine if the conclusions of Leummens (2018) are only valid for conditions with an open coastal system (tidal inlet) or that the models are better capable of simulating the storm-induced residual flows at a closed coastal system.

Leummens (2018) analysed residual flows by applying a Fourier transform low pass filtering on the signals to filter out the non-tide induced flow (wind, wave and density driven currents). Here, this filtering approach is adopted and performed for all measurement frames from the Coastal Genesis Lower Shoreface campaigns (see Table 3.2). Timeseries for the Ameland (DVA), Terschelling March (DVT2), and Noordwijk (DVN) campaigns are shown (Figure 3.3 - Figure 3.5) for the frames positioned around NAP -15 m, showing the complete (unfiltered) velocity signals (a, c) and filtered residual flow (b, d) for the eastward (a, b) and northward (c, d) velocity components separately. Time series of wave (e) and wind (f) data from nearby measurement stations are shown in the figures as well (see figure captions for stations). Time series from the Terschelling January (DVT1) campaign are omitted from this chapter due to the absence of storm events during the campaign, which makes the dataset less suitable for the analysis.

The figure of the Ameland campaign (Figure 3.3) shows that, in accordance to the conclusions of Leummens (2018), both the models are not capable of reproducing the east- and northward residual flow during high energetic wind and wave conditions (e.g. around 19 November). For the DCSM-FM model this results in a maximum (absolute) underestimation of ~0.3 m/s in eastward direction and ~0.2 m/s in northward direction. The CGII TA model underestimates the storm induced currents as well but gives a better performance than the DCSM-FM model; the underestimation is reduced with ~50% with respect to the DCSM-FM model. The southward

(considered as landward) directed residual flow corresponds very well to the peaks in wave height ( $H_s = 4\text{--}5\text{ m}$ ) and following theory (Appendix A.1) wave breaking induced currents can become important from these water depths. During calm conditions there is a small northward directed residual current which is reproduced and even sometimes overestimates by the models.

The conditions during the March 2018 Terschelling campaign (DVT2, Figure 3.4) were predominantly mild with a single event of increased wave height and wind speed (17 till 19 March,  $H_s = \sim 4\text{ m}$ ,  $U_{\text{wind}} = \sim 20\text{ m/s}$ ). The performance of the models during the mild conditions is nearly perfect and during the storm event there is an underestimation of the eastward (longshore) and northward (cross-shore) directed currents, like the underestimation during the storm events observed at the Ameland site (Figure 3.3). A remarkable difference is a change in the behaviour of the models. The 3D DCSM-FM model is better capable of reproducing the longshore and specifically the landward directed residual flow than the CGII TA model. Because wave-breaking induced flow is not modelled by the 3D DCSM-FM model the (relative) good performance of the model suggests that this residual flux during this event is not (predominantly) wave driven. The event corresponds to a high wind event with wind speeds up to 20 m/s from eastern direction, suggesting this a predominantly wind driven signal.

The Noordwijk campaign (DVN, Figure 3.5) shows calm conditions during the first half of the campaign (8 April till 16 April) and conditions with increasing winds (maximum 15 m/s) from western direction accompanied by increasing wave heights from 16 April onwards. During the calm conditions there is, like the calm conditions during the March Terschelling (DVT2) campaign, a near perfect performance of the DCSM-FM model. During the more energetic conditions there is an eastward (here more or less considered shoreward) and northwards directed residual current of  $\sim 0.1\text{ m/s}$ . The DCSM-FM model reproduces a residual flux in the same directions but underestimates the magnitude by approximately 0.05 m/s. The underestimation of the residual flow by the model at the Noordwijk site is considerably smaller than observed at the other two sites. However, because the wind and wave conditions are not known at the exact location of the measurement frames these conditions cannot be compared directly. It is therefore not known if the better performance of the model is due to the change in site or a change in external (less stormy) conditions.

In Figure 3.6 the residual flow is shown for two campaigns (DVA and DVN) for all measurement frames and zoomed in on a specific event, showing the performance of the models with decreasing water depths. The figures show that the magnitude of the residual current during high wind and/or wave conditions is relatively small at deep water (20 m). The magnitude of the longshore velocities is  $O(0.05 - 0.1\text{ m/s})$ , which corresponds well to values found by an analytical solution (Appendix A.3.3). The magnitude of these residual fluxes increases towards shallower depths to several decimetres per second. The performance of the models becomes less as the non-tide induced currents become stronger at shallower depths.

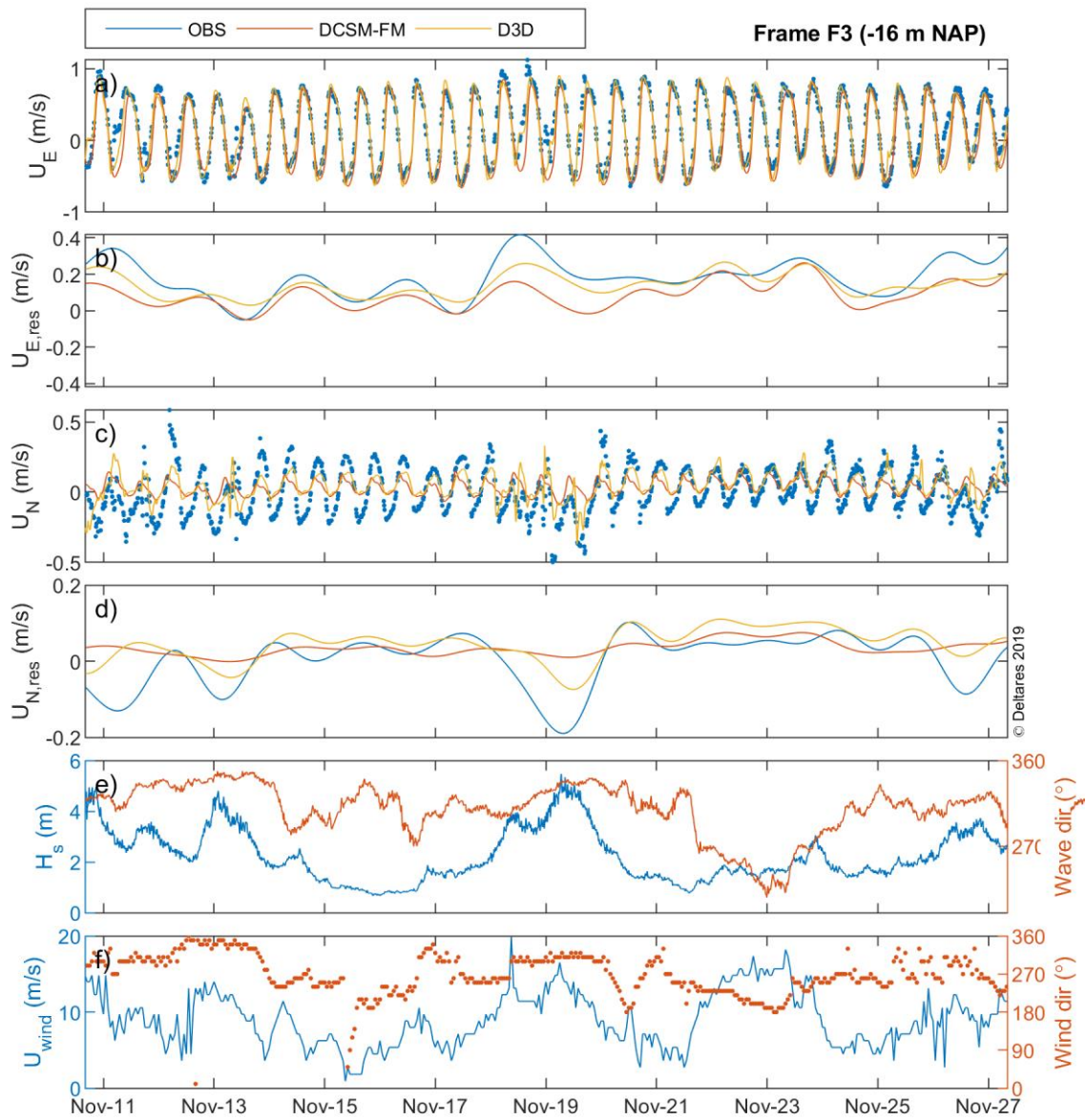


Figure 3.3 Timeseries of the velocity signal (a) and residual flow (b) in Eastern direction, and the velocity signal (c) and residual flow (d) in Northern direction derived from observations (blue), the DCSM-FM model (red) and the CGII Ta model (yellow). Timeseries of wave height and wave direction from wave buoy AZG-1-1 are shown in (e), timeseries of wind speed and direction from Terschelling Noord are shown in (f).



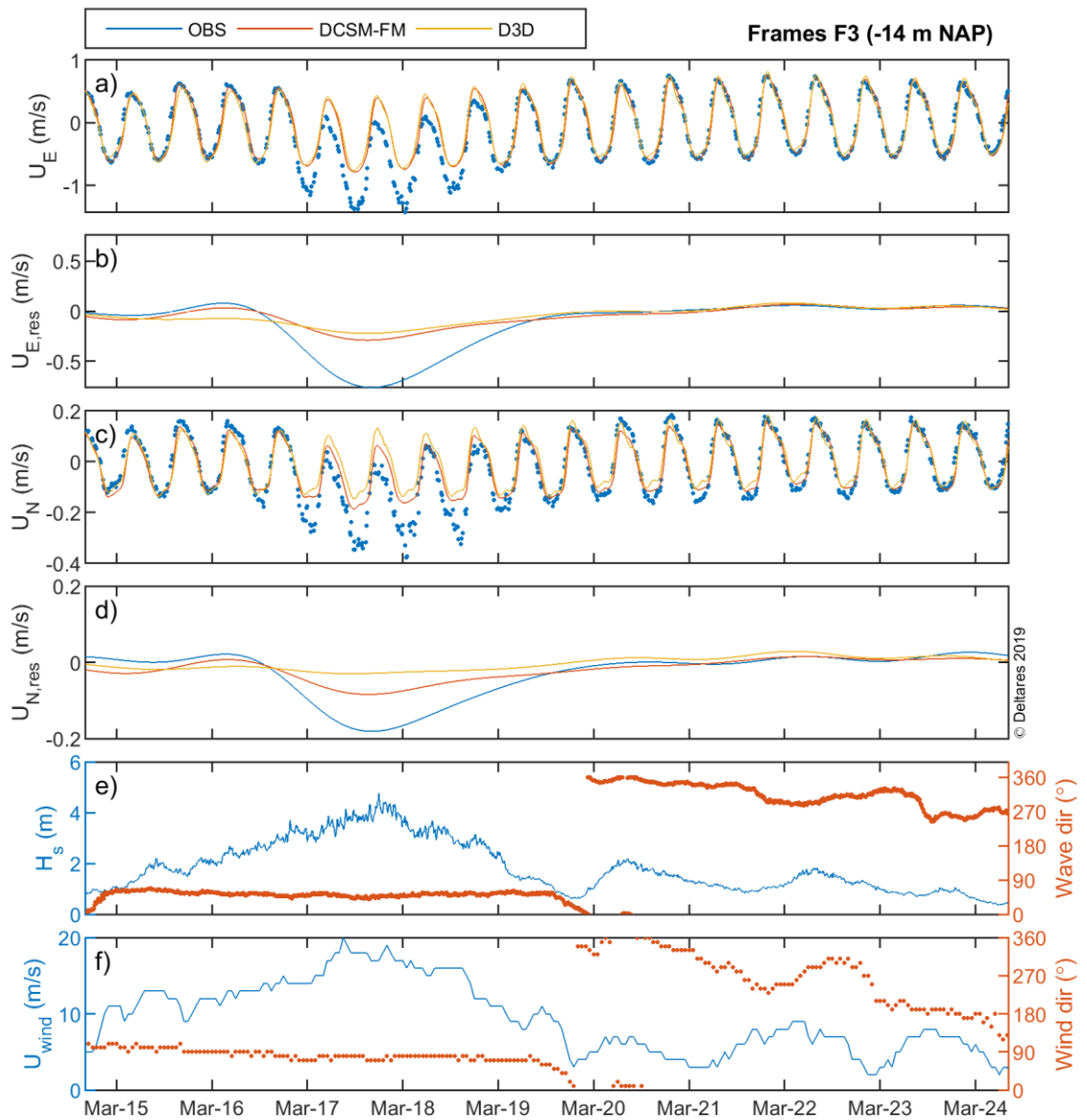


Figure 3.4 Timeseries of the velocity signal (a) and residual flow (b) in Eastern direction, and the velocity signal (c) and residual flow (d) in Northern direction derived from observations (blue), the DCSM-FM model (red) and the CGII Ta model (yellow). Timeseries of wave height and wave direction from wave buoy AZG-1-1 are shown in (e), timeseries of wind speed and direction from Terschelling Noord are shown in (f).

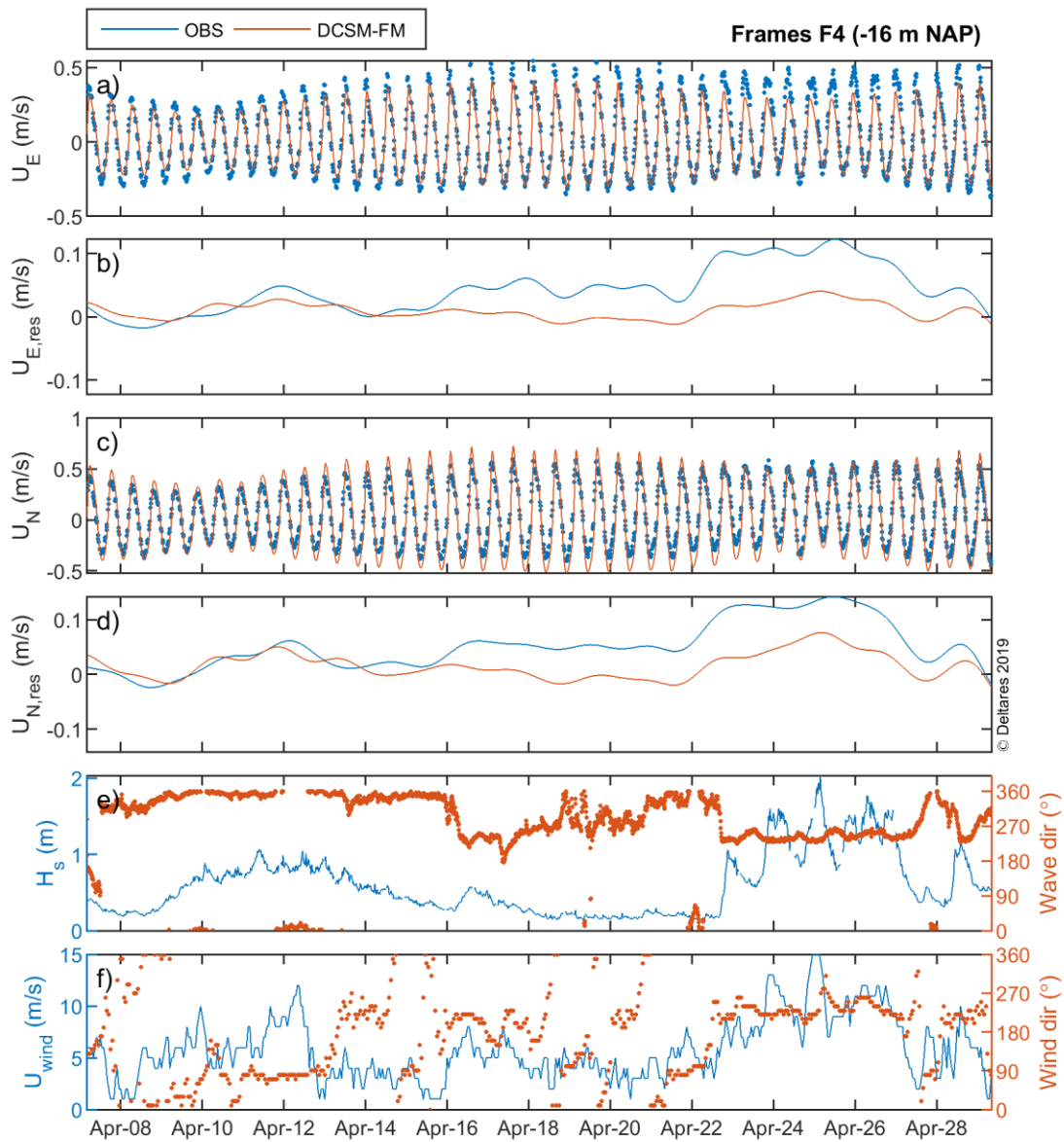


Figure 3.5 Timeseries of the velocity signal (a) and residual flow (b) in Eastern direction, and the velocity signal (c) and residual flow (d) in Northern direction derived from observations (blue) and the DCSM-FM model (red). Timeseries of wave height and direction from wave buoy Schouwenbank are shown in (e), timeseries of wind speed and direction from IJmuiden are shown in (f).

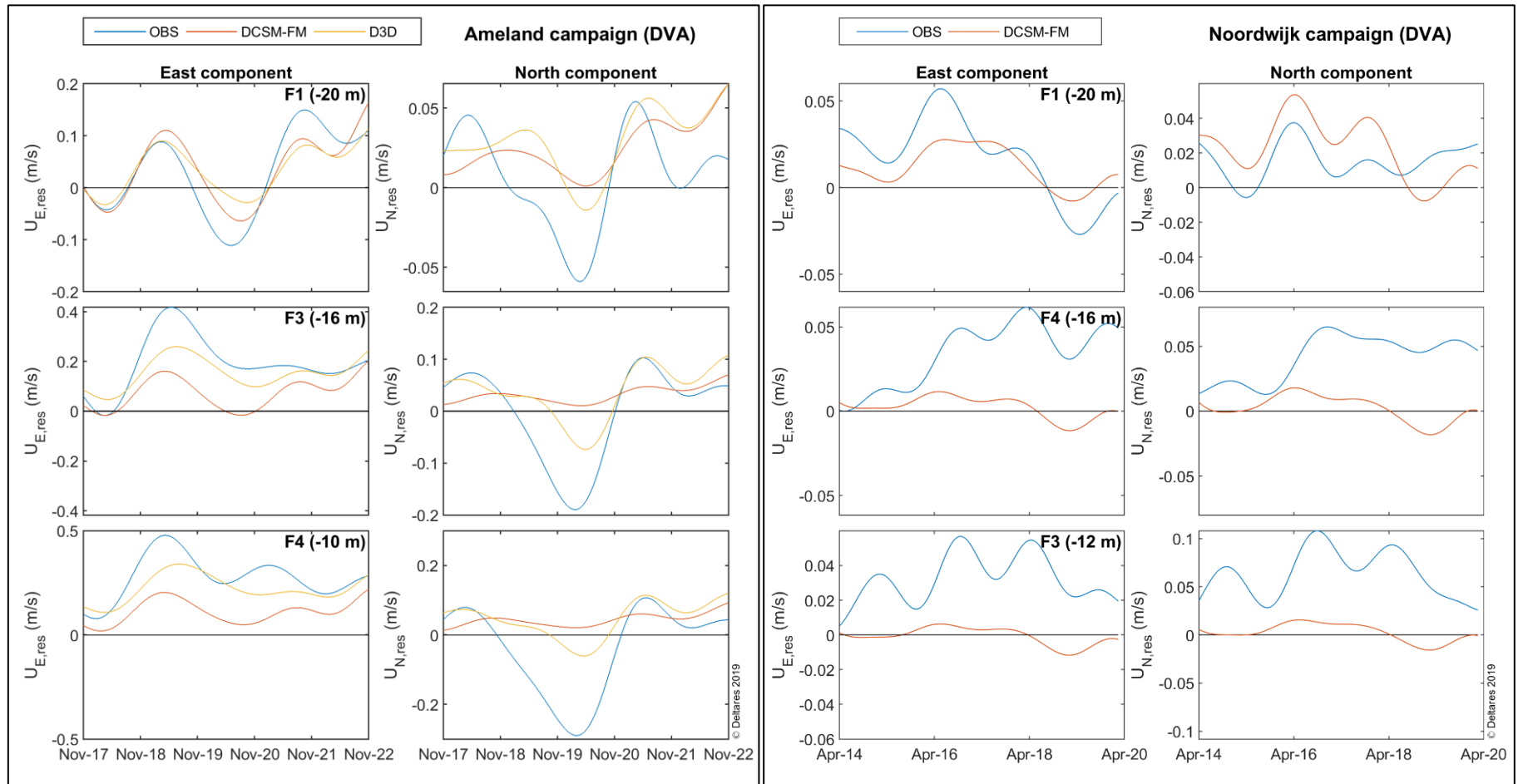


Figure 3.6 Time series of the eastward and northward components of the residual flow are shown for the Ameland (DVA) and Noordwijk (DVN) Lower Shoreface campaigns for all measurement frames, decreasing in water depth going down.



### 3.2.3 Importance of wave and wind-driven flow at the lower shoreface

The DCSM-FM and CGII TA models perform well in reproducing tide induced (depth averaged) currents at the lower shoreface. Besides flow driven by the tide there is a flow at the lower shoreface driven by waves, wind and gradients in density (e.g. due to salinity) that increase towards shallower depths. The previous analyses have shown that the models perform less in reproducing the (residual) currents driven by these mechanisms. Here, the CGII TA model is used for an analysis on the importance of including wind and waves for reproducing the residuals flows at the lower shoreface. Table 3.4 shows an overview of the configurations used for this analysis. The input for the analysis is derived from the measurements and for three variants of the CGII TA model; the default FLOW-WAVE model, a model without the online wave coupling with WAVE (only FLOW), and a model without meteorological forcing at the surface boundary (no wind and pressure, purple). In the last variant of the model (D3D no wind) there is an online coupling with the WAVE module and there are waves forced on the lateral boundaries of the model, allowing waves to propagate from offshore to nearshore. The absence of wind, however, prohibits wind induced wave growth within the model domain, yielding inevitable differences of modelled waves at the lower shoreface compared to the default model configuration.

Table 3.4 Overview of the input for the analysis of the hydrodynamic processes at the lower shoreface.

Campaign name	Campaign code	Period analysed	Data sources	Data code
Lower shoreface Ameland	DVA	9 Nov 2017 – 29 Nov 2017	Measured CGII TA CGII TA (ex. waves) CGII TA (ex. wind)	OBS D3D D3D (no waves) D3D (no wind)
Lower shoreface Terschelling 2	DVT2	13 Mar 2018 – 26 Mar 2018	Measured CGII TA CGII TA (ex. waves) CGII TA (ex. wind)	OBS D3D D3D (no waves) D3D (no wind)

Figure 3.7 shows the timeseries of the complete signals (a, c), residual flows (b, c) and wind (e) and wave (f) characteristics for the Ameland Lower Shoreface campaign. The figure shows that, as expected, the default model shows the best performance in reproducing the measurements. The model without the online wave coupling is not able to reproduce the southward directed residual flows that coincide with the peaks in the significant wave height (13 and 19 November). This indicates that these southward (onshore) directed residual fluxes are clearly wave driven events. The model without meteorological forcing is not able to reproduce the peaks in eastward (longshore) directed residual flow that coincide with wind speeds roughly exceed 10 m/s (e.g. around 11, 18, and 26 November), indicating that this is a mainly wind driven residual flux. From the figure a general pattern can be derived that shows that the model without waves performs the least in reproducing the residual flow pattern in northern (cross shore) direction and the model without wind performs the least in reproducing the residual flow in eastern (longshore) direction.

At the Terschelling site, the analysis of residual currents (§3.2.2) has shown that the DCSM-FM model is better capable of reproducing the southward (landward) directed residual flux (Figure 3.4), an unexpected result considering the behaviour of the models at the Ameland lower shoreface (Figure 3.3). In Figure 3.8 the measurements and the three CGII TA model variants are shown for the Terschelling site (DVT2) to give a more detailed analysis of the importance of wave and wind driven currents. The figure clearly visualizes that the model

without meteorological forcing is not able to reproduce the westward and southward directed residual fluxes, conforming that these are dominantly wind driven events. Furthermore, the figures show a small northward directed residual flow during this event simulated by the model without wind and a stronger southward directed residual flow by the model without waves. This indicates that the (residual) cross-shore flow at the lower shoreface is the result of a balance between offshore directed wave driven (undertow) and wind driven flow, for which the effect depends on wind direction and magnitude.

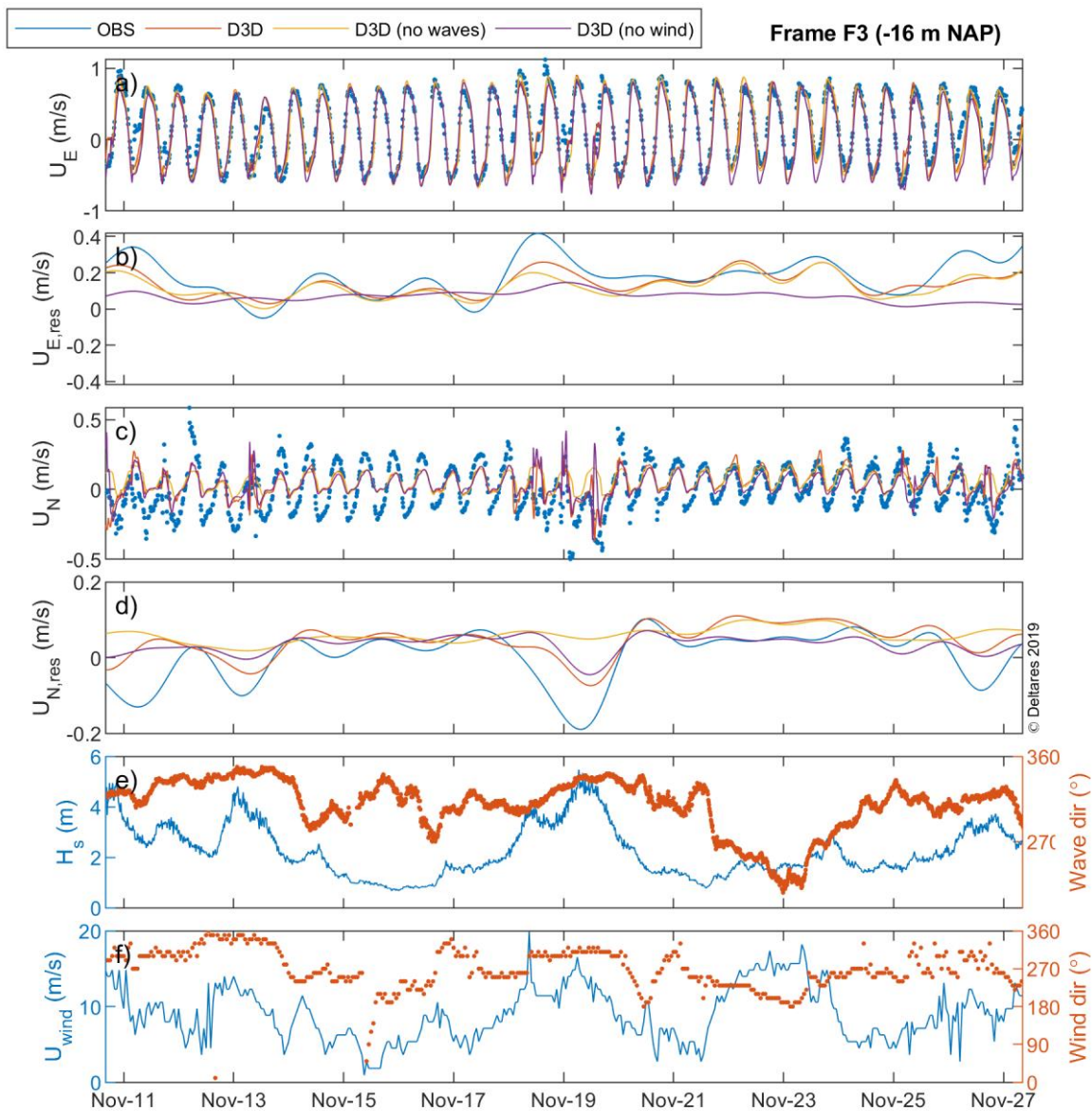


Figure 3.7 Timeseries of the depth averaged velocity signal (a) and residual flow (b) in Eastern direction, and the velocity signal (c) and residual flow (d) in Northern direction derived from observations (blue), the CGII TA model in default mode (red) without waves (yellow) and without meteorological forcing (purple). Timeseries of wave height and wave direction from wave buoy AZG-1-1 are shown in (e), timeseries of wind speed and direction from Terschelling Noord are shown in (f).

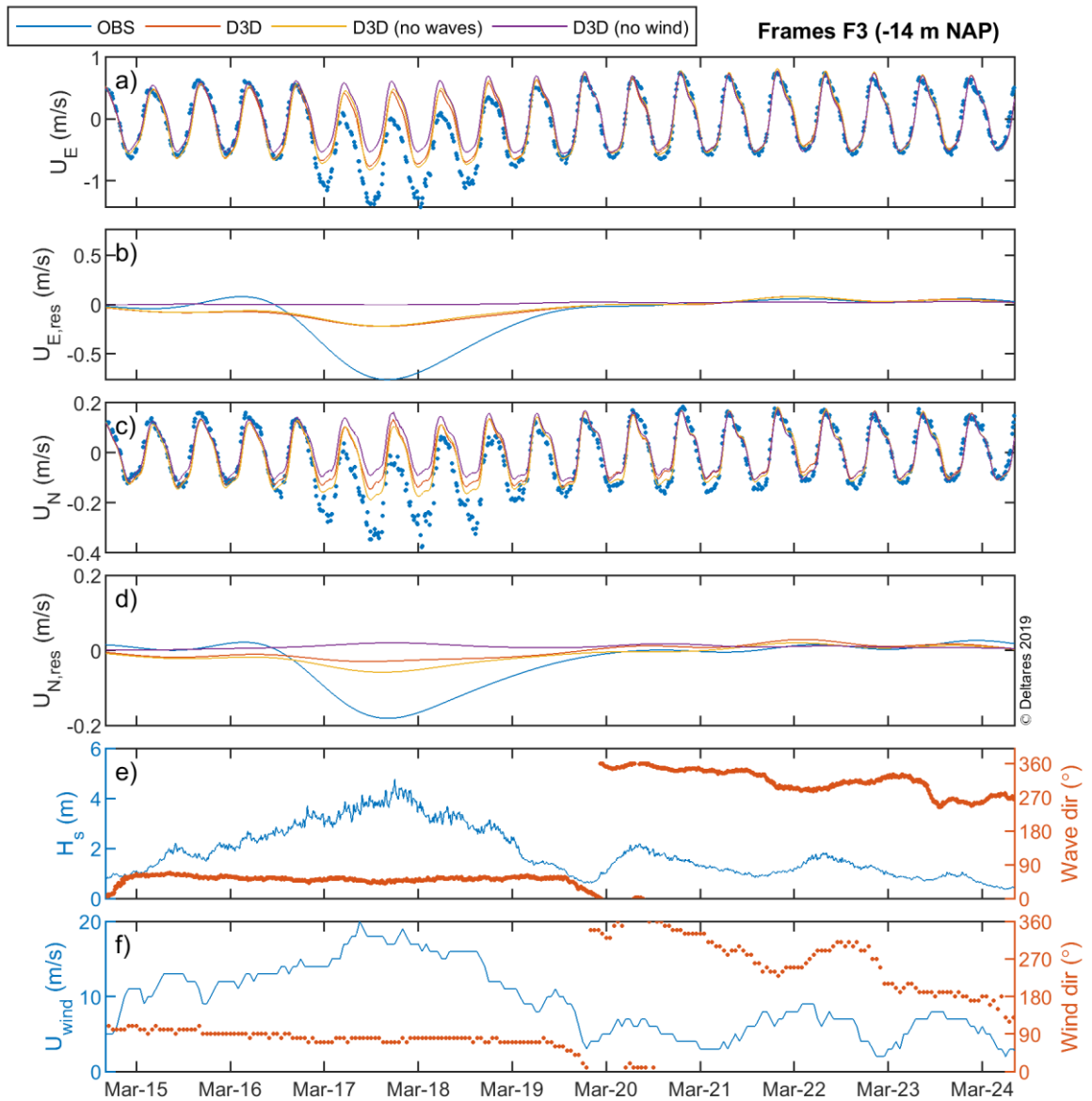


Figure 3.8 Timeseries of the depth averaged velocity signal (a) and residual flow (b) in Eastern direction, and the velocity signal (c) and residual flow (d) in Northern direction derived from observations (blue), the CGII TA model in default mode (red) without waves (yellow) and without meteorological forcing (purple). Timeseries of wave height and wave direction from wave buoy AZG-1-1 are shown in (e), timeseries of wind speed and direction from Terschelling Noord are shown in (f).

### 3.3 Conclusions

The hydrodynamic validation of the tools used for calculating sand transport at the lower shoreface is, besides the analyses shown in this report, described by Zijl et al. (2018) (DCSM-FM model), Nederhoff et al. (2019) (CGII TA model), and Grasmeijer (2018) (DCSM-FM model and wave transformation tool). Combining the analyses and the outcomes from these sources it can be concluded that:

- The wave transformation tool is an appropriate tool to derive wave parameters at the lower shoreface, indicated by a good and equal performance of the tool over the depth range studied (NAP -20 till -10 m).
- The 3D DCSM-FM and CGII TA models perform well in reproducing (depth averaged) flow velocities at the lower shoreface, indicated by bias values of less than 0.06 m/s and RMSE values less than 0.18 m/s.
- The 3D DCSM-FM and CGII TA models perform very well during normal wind and wave conditions but their performance decreases during high energetic (storm) conditions. Residual currents are underestimated under these conditions. For the annual sediment transport calculations this is an important shortcoming.
- The performance of the models decreases with decreasing water depths because the wind and wave induced residual currents become stronger at shallower depths. In quantifying annual sand transports at the Dutch lower shoreface (chapter 5), we will therefore only use the model results for water depths larger than 15 m.



## 4 Sensitivity transport modelling approaches

### 4.1 Introduction

The TSAND transport model (§2.4.4) calculates sand transport based on hydrodynamic input parameters. These input parameters can be derived from measurements and models. Here, the sensitivity of the net transport (over a relatively short period) is shown for varying configurations of this input. The analyses are focused on the locations of the measurement frames of the Coastal Genesis Lower Shoreface campaigns due to the availability of measured flow velocity profiles here, which represent the most accurate representation of flow velocities at the lower shoreface. The measurement campaigns that are focussed on in the following analyses depends on the availability of measurements, hydrodynamic conditions (storms), and the extent of the CGII TA model (only Ameland and Terschelling).

### 4.2 Wave input

Parameters for wave characteristics at the lower shoreface can be derived via the wave transformation tool (§2.4.2) and via process-based modelling with the CGII TA model (§2.3). Measurements of wave characteristics at the lower shoreface are not available. Therefore, the process-based model is considered to provide the most accurate description of waves at the lower shoreface. In §3.1 it is shown that wave characteristics from the wave transformation tool and from the CGII TA model corresponds well at the lower shoreface.

Flow velocities from the CGII TA model are used in combination with waves from the same model and the wave transformation matrix to calculate net transport over a defined period (Table 4.1). The definition of the periods is defined on the availability of measured flow velocities. Although this is not a limitation for the analysis in this paragraph, the periods are similar to the following transport analyses for consistency.

The wave parameters derived via the wave transformation matrix show in general a small overestimation of the significant wave height and peak period (Figure 3.1). The small overestimation results in increased transport rates compared to transport calculations with wave input from the process-based modelling (Figure 4.1 & Figure 4.2). The southward (cross-shore) net transport values in the Ameland inlet are, however, smaller with wave input from the matrix.

From the sensitivity analysis of wave input it can be derived that in the offline approach the effect of waves on the sand transport calculation is likely to be overestimated, except at tidal inlets where the effect is somewhat underestimated due to underestimation of the residual currents under energetic conditions here.

Table 4.1 Configurations of wave input for modelling sand transport at the lower shoreface.

Name	Flow velocities	Waves	Transport	Period analysed
D3D (SWAN)	CGII-TA	SWAN	TSAND (offline)	9 Nov 2017 – 29 Nov 2017
D3D (MATRIX)	CGII-TA	Matrix	TSAND (offline)	13 Mar 2018 – 26 Mar 2018

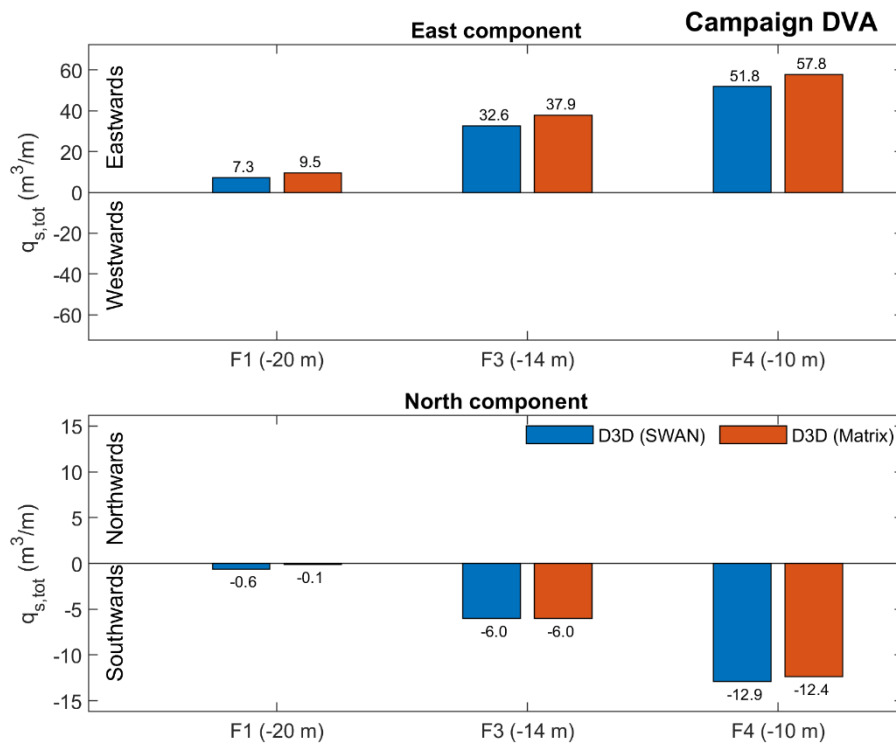


Figure 4.1 Bar plots of the TSAND calculated sand transport at the measurement frames of the Ameland Lower Shoreface campaign using velocity input from the CGII TA model in combination wave input derived from the coupled SWAN simulation (blue) and from the wave transformation matrix (red).

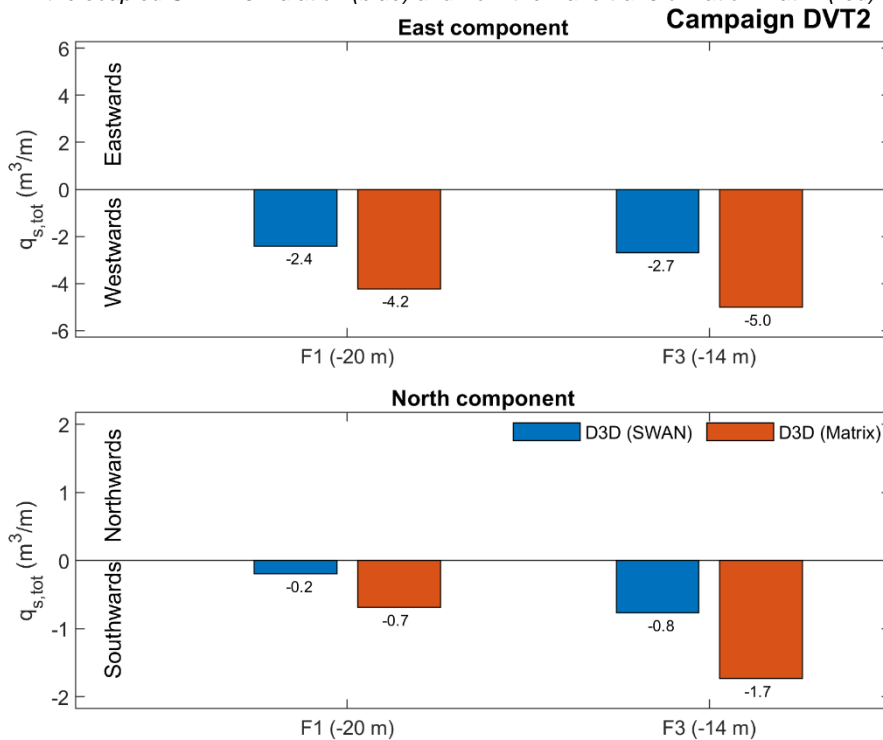


Figure 4.2 Bar plots of the TSAND calculated sand transport at the measurement frames of the March Terschelling lower shoreface campaign using velocity input from the CGII TA model in combination with wave input derived from the coupled SWAN simulation (blue) and from the wave transformation matrix (red).

### 4.3 Velocity input

The sensitivity of flow velocity input on the net transport is analysed by using the transport model with measured and modelled flow velocities and equal wave input (Table 4.2). The transport of sand is not measured directly, and the calculated transports based on the measured flow velocities is therefore considered the most accurate.

The net transport values, calculated over defined relatively short time periods, (Figure 4.3 - Figure 4.5) show that TSAND calculations with velocity input from the models underestimate the total net transport in eastward and northward direction compared to the calculations with velocity input from the measurements. Furthermore, this behaviour is equal for all sites and conditions studied, confirming the general behaviour of the models. At Ameland (Figure 4.3) the CGII TA model (D3D) performs best, which can be expected from the analysis on residual currents (§3.2.2). For the March Terschelling campaign (Figure 4.4) the offline approach shows a better performance than the CGII TA model, explained by the better performance of the 3D DCSSM-FM model to account for wind driven flow at the lower shoreface (§3.2.2). However, the model shows an underestimation of the time-integrated transport which can be attributed to the storm event around 18 March (Figure 4.6). At the Noordwijk campaign (Figure 4.5) the DSS approach shows an underestimation (factor ~2) as well. The performance of the model is, however, equal over the range of depths studied, which is not the case for the Wadden coast.

The sensitivity analysis on velocity input suggests that the net transports calculated with the offline approach tend to be underestimated. The absolute underestimation on the long term is, however, hard to determine from these analyses because it is based on relatively short measurement periods. The effect of storms is exaggerated because of this. The transport calculations presented here do not reflect the long-term net transport at the lower shoreface. This will be analysed in chapter 5.

Table 4.2 Configurations of velocity input for modelling sand transport at the lower shoreface.

Name	Flow velocities	Waves	Transport	Period analysed	Figure
OBS	Measured	Matrix	TSAND (offline)	9 Nov 2017 – 29 Nov 2017 (DVA)	Figure 4.3
DSS	DCSSM-FM	Matrix	TSAND (offline)	13 Mar 2018 – 26 Mar 2018 (DVT2)	Figure 4.4
D3D	CGII-TA	Matrix	TSAND (offline)	5 Apr 2018 12 h – 21 Apr 2018 12 h (DVN)	Figure 4.5

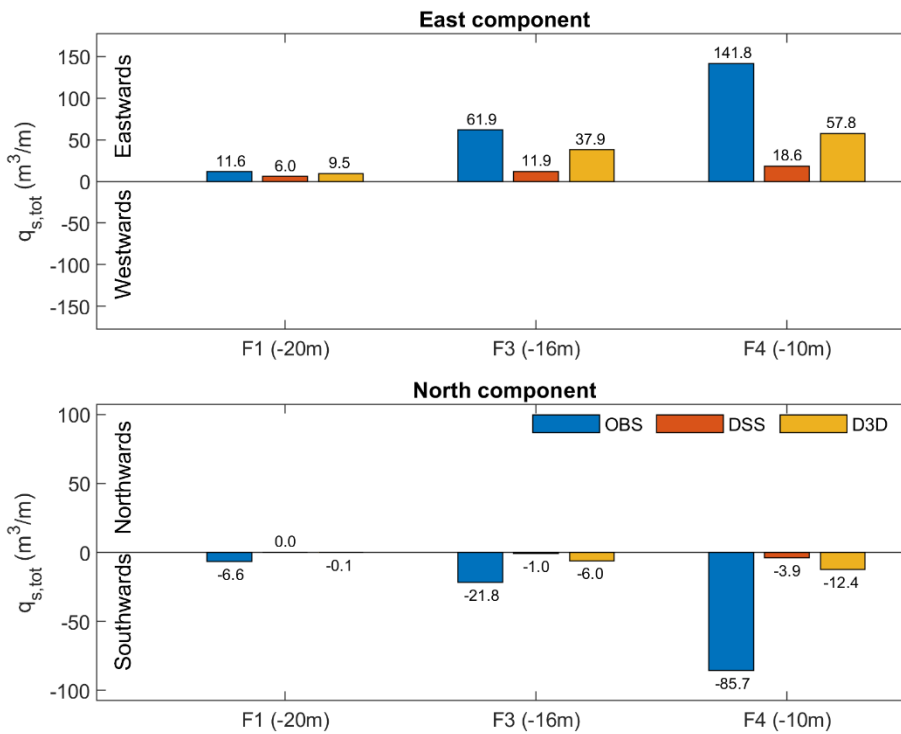


Figure 4.3 Bar plots of the TSAND calculated sand transport at the measurement frames of the Ameland Lower Shoreface campaign using velocity input from the measurements (blue), DSS model (red), and CGII TA model (yellow).

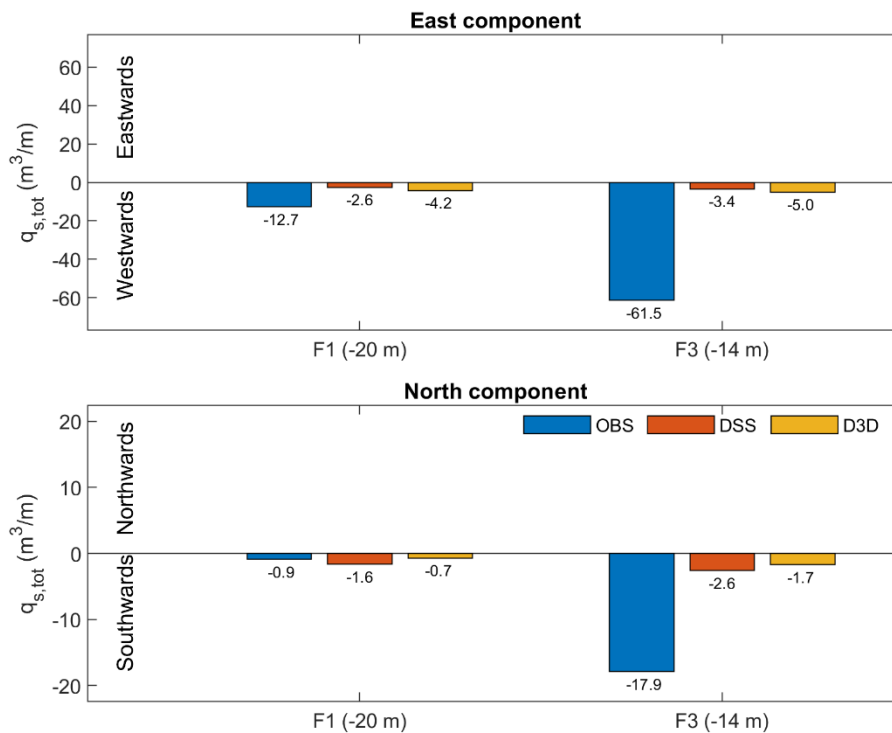


Figure 4.4 Bar plots of the TSAND calculated sand transport at the measurement frames of the Terschelling Lower Shoreface campaign using velocity input from the measurements (blue), DSS model (red), and CGII TA model (yellow).

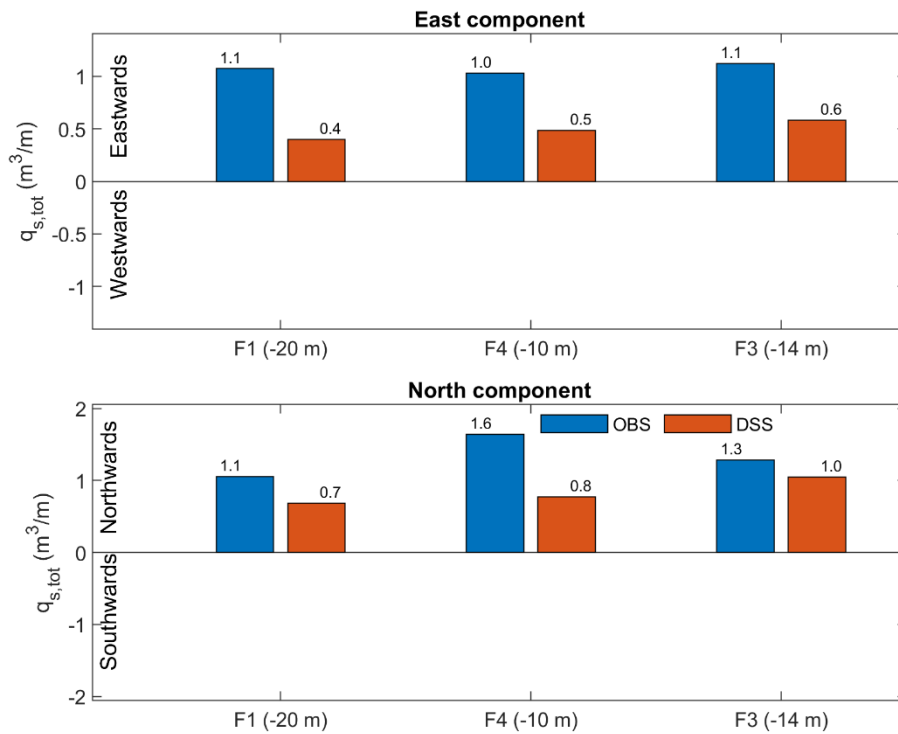


Figure 4.5 Bar plots of the TSAND calculated sand transport at the measurement frames of the Noordwijk Lower Shoreface campaign using velocity input from the measurements (blue), offline approach (DSS model, red), and CGII TA model (yellow).

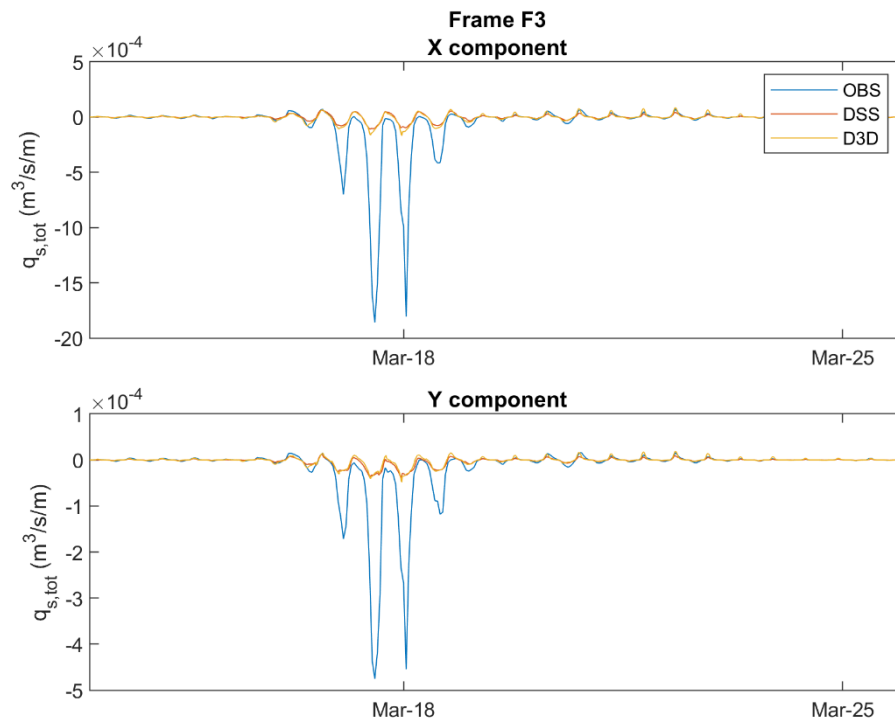


Figure 4.6 Timeseries of the TSAND calculated instantaneous sand transport at measurement frame 3 of the March Terschelling campaign using velocity input from the measurements (blue), DSS model (red), and CGII TA model (yellow).

## 4.4 Transport approach

The sensitivity of an online vs. offline transport approach can, unfortunately, not be compared directly because the differences between the two approaches consist of several aspects, like model size, model resolution, 2D/3D, density effects, transport model, etc. Nonetheless we made a comparison between the different transport models (Table 4.3). The results (Figure 4.7, campaign DVA) show that the difference between the online and offline approach is generally smaller than 50%, which is good in terms of sand transport predictions.

Table 4.3 Configurations of wave input for modelling sand transport at the lower shoreface.

Name	Flow velocities	Waves	Transport
D3D (TSAND)	CGII-TA	SWAN	TSAND (offline)
D3D (TR04)	CGII-TA	SWAN	TR2004 (online)

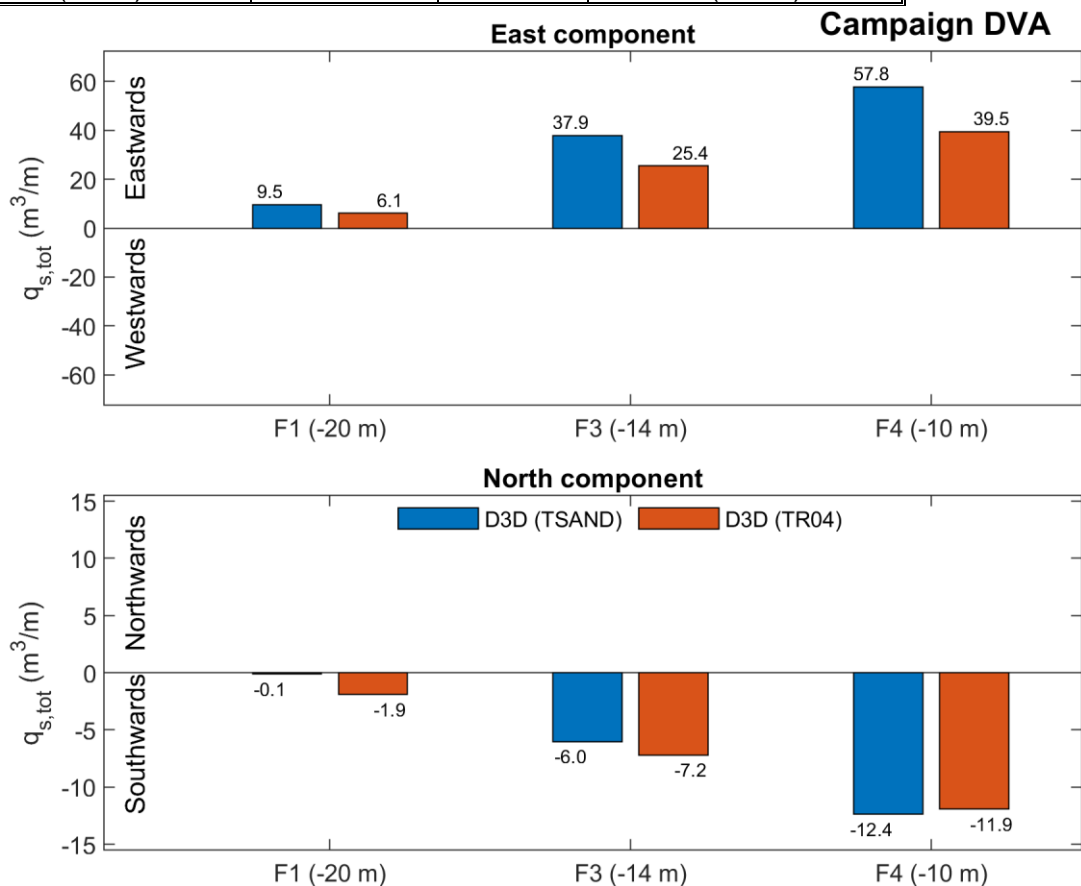


Figure 4.7 Bar plots of the TSAND calculated sand transport at the measurement frames of the Ameland Lower Shoreface campaign using the online approach with the TRANSPORT 2004 transport formulae (blue), and the offline approach with the TSAND transport formulae.

#### 4.5 Conclusions

Based on the sensitivity analyses we summarize the following:

- The sensitivity analysis on wave input suggests that the offline approach slightly overestimates the effect of waves on the net transports, except at tidal inlets where the difference is overruled by the effect of residual currents under energetic conditions.
- The sensitivity analysis on velocity input suggests that the offline approach tends to underestimate the net transports as compared to transports determined using measured velocities under high energetic conditions. The absolute underestimation on the long term is, however, hard to determine from these analyses because it is based on relatively short measurement periods.
- The difference between the online and offline approach is generally smaller than 50%, which is good in terms of sand transport predictions.





## 5 Quantifying transports at the lower shoreface

### 5.1 Introduction

As the sand transports are influenced by mean residual flows, tidal flows and waves, we will firstly discuss these hydrodynamic parameters and thereafter discuss their effect on the net annual sand transport rates. We have made flow, wave and sand transport computations for the years 2013-2017. We use the year 2016 as an illustrative example and present statistics for all five years. We present flow and wave parameters and computed transport along nine cross-shore JARKUS transects and along two contour lines i.e. the present offshore boundary of the coastal foundation at NAP-20 m and the depth contour suggested by Vermaas et al. (2015). Figure 5.1 shows the transects and contour lines.

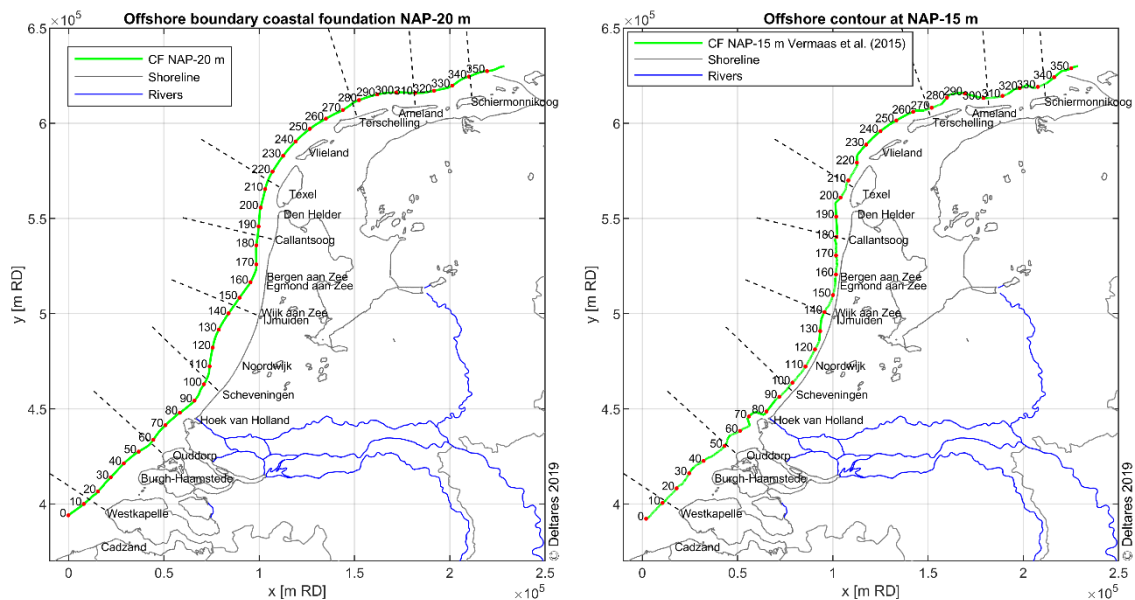


Figure 5.1 Offshore boundary of the coastal foundation at NAP-20 m (left) and the NAP-15 m contour (right) suggested by Vermaas et al. (2015). The dashed lines indicate the JARKUS transects along which the flow and wave parameters and computed transports are presented in this chapter.

Flow and transport vectors can be decomposed into an alongshore and a cross-shore component. The magnitude of the resulting alongshore and cross-shore components depends on the definition of the coast angle. Here we use two different definitions, i.e. the angle of the major component of the M2 tide and the smoothed angle based on the nine selected JARKUS transects. Figure 5.2 shows the coast angles based on these definitions.

Based on the sensitivity analysis presented in the previous chapter we consider the present modelling approach suitable for water depths  $\geq 15$  m. Therefore, we will present transports for these water depths only.

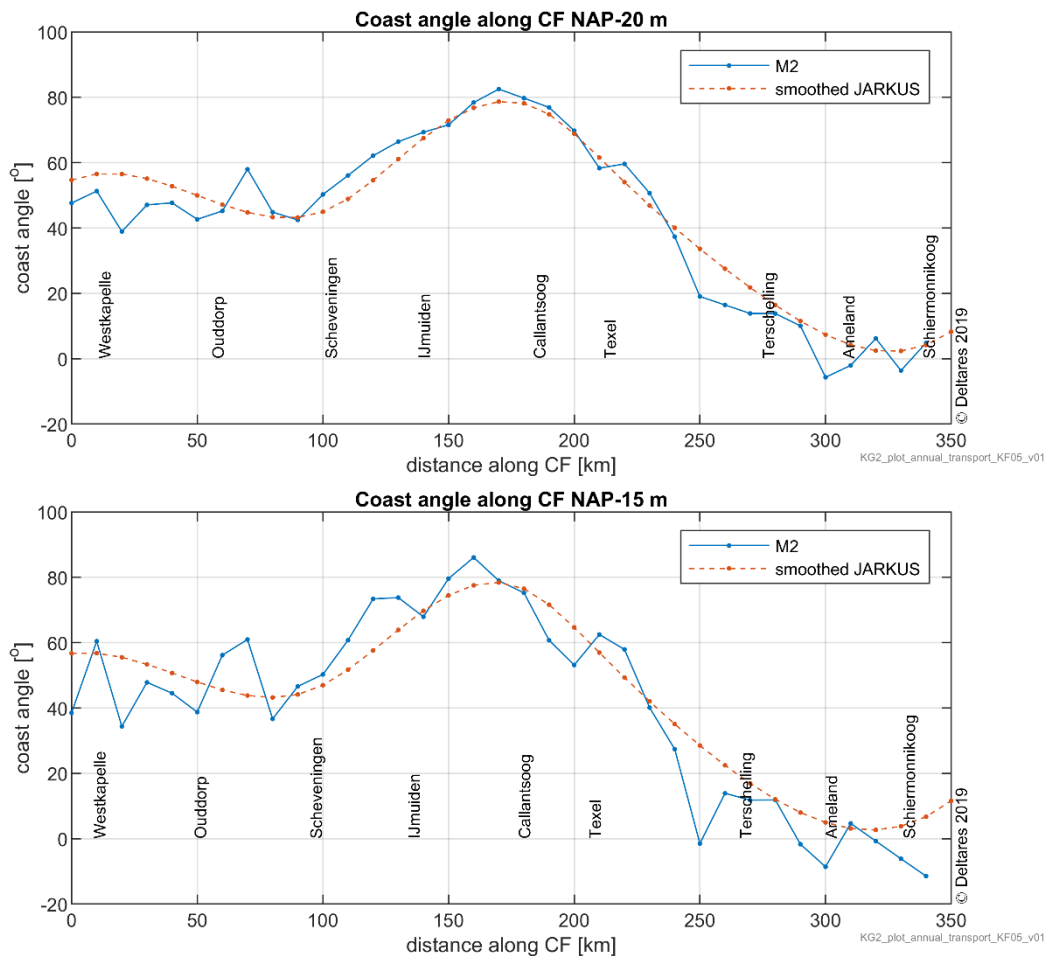


Figure 5.2 Definition of coast angle based on the major axis of the M2 tide and based on JARKUS along the offshore boundary of the present coastal foundation (top panel) and along the NAP-154 m contour suggested by Vermaas et al. (2015). Angles are measured anticlockwise from horizontal x-axis.

## 5.2 Flow velocities

### 5.2.1 Annual mean residual flow

Mean residual flows may influence the annual mean transport rates (e.g. Van Rijn, 1997). To illustrate the variation of these flows along the Dutch coast, Appendix C presents the mean annual velocity vectors near the bed, near the surface and depth-averaged as computed with the 3D DCSM-FM model using the year 2016 as an example. To illustrate the cross-shore variations, Appendix C also presents the computed annual mean residual flow velocities and directions at nine different JARKUS transects along the Dutch coast, i.e. at Ouddorp, Westkapelle, Scheveningen, IJmuiden, Callantssoog, Texel, Terschelling, Ameland and Schiermonnikoog.

The mean annual computed residual flows along the Zeeland and Holland coast show a clear effect of the wind and the fresh water outflow of the river Rhine and the Haringvliet into the saline North Sea. This causes a difference in magnitude and direction between the near-bed and near-surface flows. The near-bed velocities are more shoreward directed. The near-surface flows are clearly larger at Hoek van Holland because of the River Rhine outflow and flow contraction due to the presence of Maasvlakte II. Near-bed velocities are important for the direction of the transports because sand concentrations are largest near the bed.

Depth-averaged mean annual computed residual flow magnitudes are relatively small along the Zeeland coast at Westkapelle and Ouddorp (0.01 m/s), increase to 0.03-0.04 m/s along the Holland coast at Scheveningen and IJmuiden and increase further to 0.06-0.08 m/s at Callantsoog and Texel. The mean residual flow decreases to 0.03-0.04 m/s at Terschelling and Schiermonnikoog. The residual flows near the bed are smaller and generally have an onshore directed component. This is onshore component is less pronounced at Callantsoog and Texel.

Figure 5.3 shows the mean annual residual near-bed flows along the offshore boundary of the coastal foundation at NAP-20 m based on the near-bed velocities computed with the 3D DCSM-FM model for the years 2013-2017.

This figure shows that the alongshore directed residual near-bed flows are small between Westkapelle and Scheveningen and increase to about 0.05 m/s at the height of the tidal inlet between Callantsoog and Texel (Marsdiep). The alongshore directed residual near-bed flow reduces again to about 0.02 m/s at Schiermonnikoog.

The cross-shore directed residual near-bed flows are largest between Ouddorp and Scheveningen with onshore directed values of about 0.03 m/s and reduce to negligibly small values just south of Texel. Offshore directed residual near-bed flows (about -0.03 m/s) are present at the height of the inlet between Vlieland and Terschelling (Vliestroom). The near-bed residual flow is onshore directed between Terschelling and Schiermonnikoog with values of about 0.01 m/s.

Similar trends can be observed along the NAP-15 contour although residual near-bed velocities are smaller here (Figure 5.4).

The alongshore directed near-bed residual flow at the NAP-15 m contour are small between Westkapelle and IJmuiden and increase to about 0.04 m/s at the height of the inlet between Callantsoog and Texel (Marsdiep). The alongshore near-bed residual flow varies between 0.01 and 0.03 m/s between Texel and Schiermonnikoog.

The cross-shore directed near-bed residual flow at the NAP-15 m contour varies between -0.01 m/s (offshore directed) to +0.01 m/s (onshore directed) between Westkapelle and Ouddorp. It increases to +0.03 m/s (onshore directed) between Ouddorp and Scheveningen and decreases again to negligibly small values at Callantsoog. It is about +0.01 m/s (onshore directed) between Texel and Vlieland. The cross-shore near-bed residual flow becomes -0.01 m/s (offshore directed) between Vlieland and Terschelling and with +0.01 m/s onshore directed again between Terschelling and Schiermonnikoog.

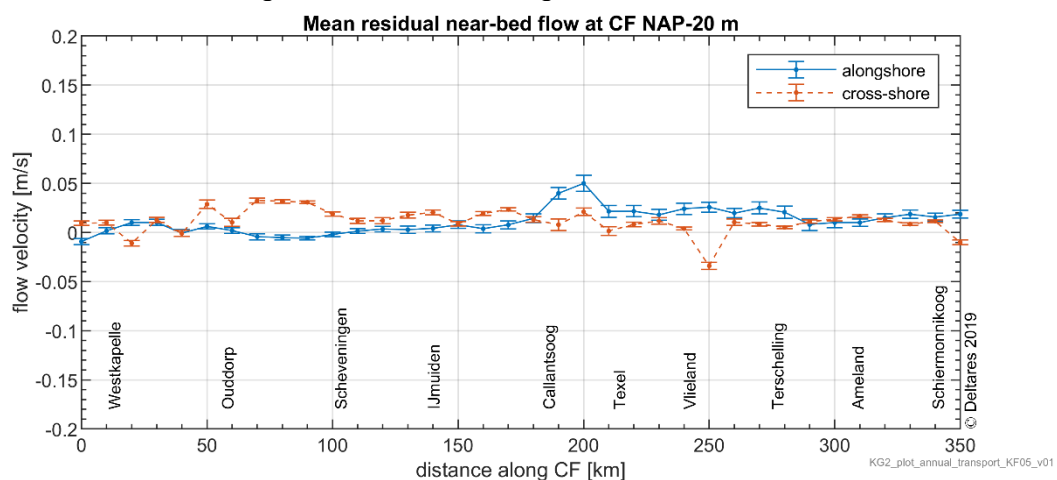


Figure 5.3 Mean annual residual near-bed flows along the offshore boundary of the coastal foundation at NAP-20 m based on near-bed velocities computed with 3D DCSM-FM model.

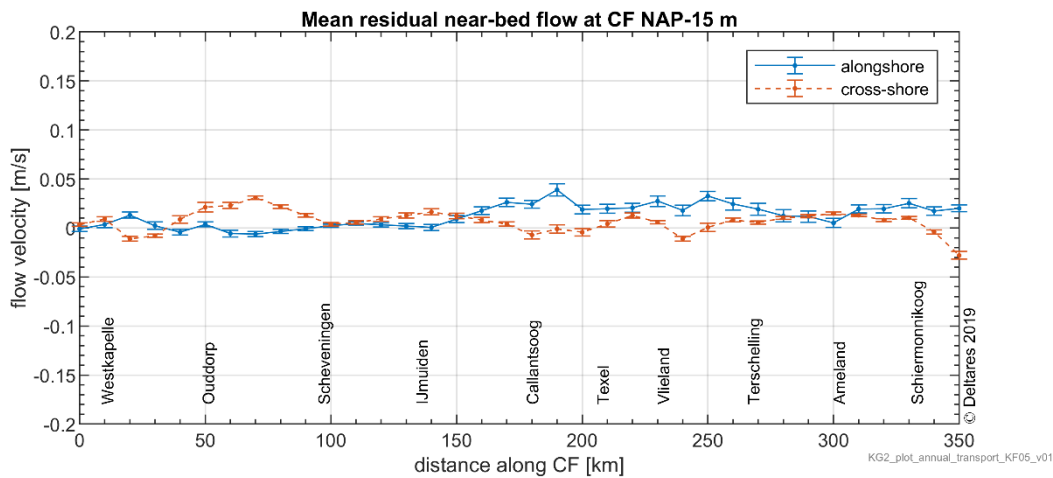


Figure 5.4 Mean annual residual near-bed flows along the NAP-15 m suggested by Vermaas et al. (2015) based on near-bed velocities computed with 3D DCSM-FM model.

### 5.2.2 Peak tidal velocities

As the tidal wave propagates from south to north along the Dutch coast it becomes increasingly distorted with shorter tidal rise than tidal fall. This is most pronounced along the central part of the Dutch coast and results in stronger flood currents than ebb currents (asymmetry in tidal currents).

To assess the variation of the tidal velocities along and across the coast, we computed the mean of all peak flood and ebb velocities from the 3D DCSM-FM model results in a year. As a year has 365 days, there are 24 hours per days and a tidal period is about 12.5 hours, this is the mean of about  $365 \cdot 24 / 12.5 \approx 700$  peak tidal velocities per year.

Appendix D plots the annual mean peak flood and ebb velocities as vector plots for five different stretches along the Dutch coast.

To illustrate the variation in peak tidal velocities along the Dutch coast, Figure 5.5 shows the annual mean peak flood and ebb velocities along the present Dutch coastal foundation (continuous NAP-20 m line). From this figure it can be seen that the peak flood velocities are generally larger than the peak ebb velocities. The alongshore variation is relatively small between Westkapelle and Ouddorp. The peak ebb velocities decrease slightly between Ouddorp and Scheveningen, whereas the peak flood velocities remain more or less the same. This results in an increase in the tidal velocity asymmetry.

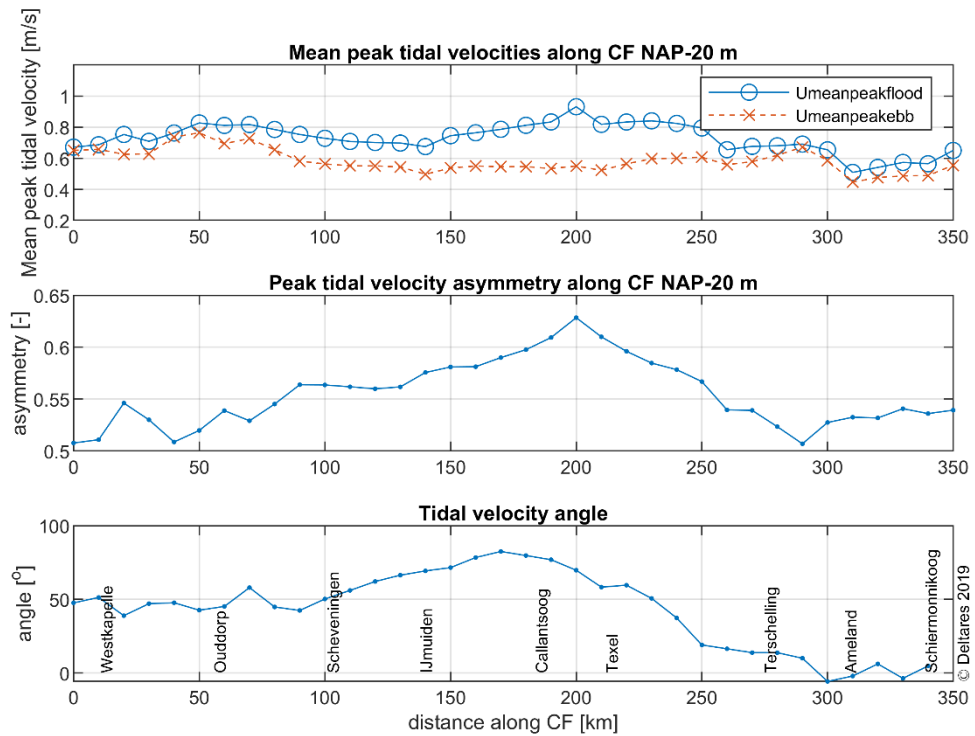
The alongshore variation in peak tidal velocities is relatively small between Scheveningen and IJmuiden. The peak flood velocities increase between IJmuiden and Callantssoog, where the peak ebb velocities remain the same. This results in an increase of the tidal velocity asymmetry. Largest flood velocities at the NAP-20 m contour occur at the height of the tidal inlet between Callantssoog and Texel and also the large tidal velocity asymmetry occurs here.

The annual mean peak flood velocities decrease between Texel and Terschelling where the peak ebb velocities remain the same. This results in a decrease of the tidal velocity asymmetry.

Both the peak flood and ebb velocities decrease along the coast from Terschelling to Ameland. The tidal velocity asymmetry stays more or less the same.

Alongshore variations between Ameland and Schiermonnikoog are small.

Figure 5.6 shows the annual mean peak flood and ebb velocities along the NAP-15 m contour line suggested by Vermaas et al. (2015). The peak flood velocities are generally about 3% smaller at the NAP-15 contour as compared to the NAP-20 m contour and the peak ebb velocities are about 6% smaller, which results in a slightly larger tidal velocity asymmetry at the NAP-15 m contour.



KG2\_plot\_annual\_transport\_KF05\_v01

Figure 5.5 Mean peak tidal velocities, tidal asymmetry and tidal velocity angle along the offshore boundary of the coastal foundation at NAP-20 m based on depth-averaged velocities computed with 3D DCSM-FM model. Angles are measured anticlockwise from horizontal x-axis.

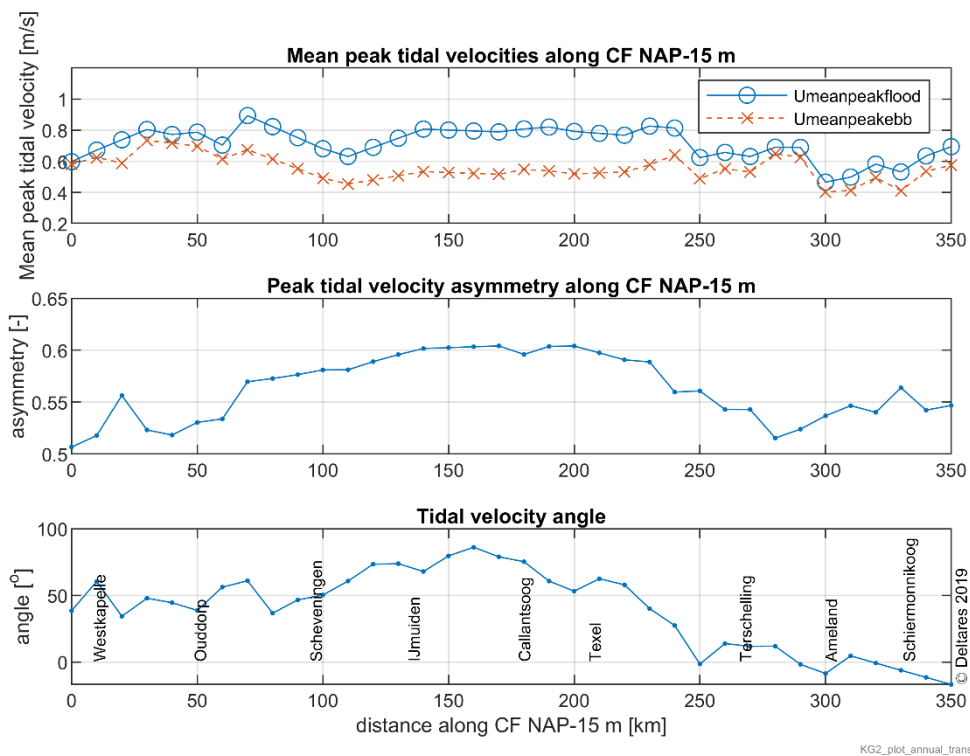


Figure 5.6 Mean peak tidal velocities, tidal asymmetry and tidal velocity angle along the contour at NAP-15 m suggested by Vermaas et al. (2015) based on depth-averaged velocities computed with 3D DCSM-FM model. Angles are measured anticlockwise from horizontal x-axis.

### 5.3 Waves

The frequency of occurrence of waves along the central Dutch coast is highest for waves from WSW and WNW. Waves are also highest from these directions (e.g. Roskam, 1988). North of Schiermonnikoog, the dominant direction is WNW to NNW. Figure 5.7 illustrates this by showing the wave roses for eight different locations along the Dutch coast for the year 2016 as obtained from the wave transformation tool. This figure also shows that waves are generally higher at the northerly stations as compared to the southerly stations along the southern and central Dutch coast.

Average annual mean wave height  $H_{m0,mean}$  at the offshore boundary of the coastal foundation is just over 1 m at Westkapelle, Ouddorp and Scheveningen (Table 5.1 and Figure 5.8). It increases to about 1.2 at IJmuiden and Callantssoog and is about 1.3 m at Texel. The mean annual significant wave height is about 1.2 m at Terschelling and Schiermonnikoog (Table 5.1 and Figure 5.8). It increases to about 2 m at IJmuiden and Callantssoog and is about 2.3 m at Texel. The 90% exceedance value  $H_{m0,90\%}$  is about 2.1-2.2 m at Terschelling and Schiermonnikoog.

The average maximum significant wave height  $H_{m0,max}$  is 4.7-5.0 m at Westkapelle, Ouddorp and Scheveningen (Table 5.1 and Figure 5.8). It increases to about 5.1-5.2 m at IJmuiden and Callantssoog and is about 5.4 m at Texel. The  $H_{m0,max}$  is about 5.3 m at Terschelling and 6.2 m at Schiermonnikoog. The maximum wave height varies from year to year with about 0.4-1.2 m.

The average annual mean wave spectrum peak period  $T_p$  varies between 5.3 and 5.7 s with longest wave periods at Callantssoog, Texel and Terschelling.

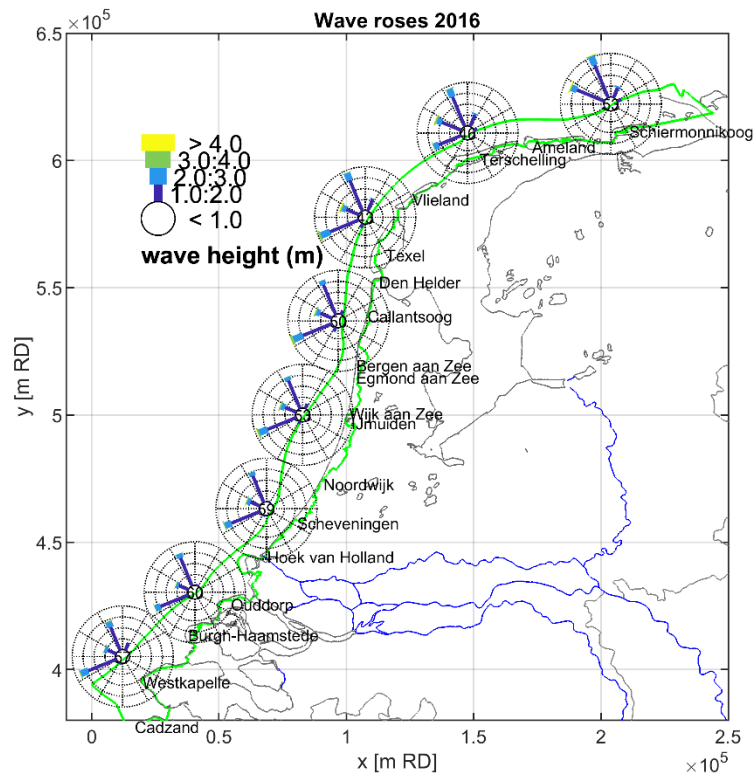


Figure 5.7 Wave roses at eight locations along the Dutch coast for the year 2016.

Table 5.1 Annual mean  $H_{m0,mean}$ ,  $H_{m0,90\%}$  and  $H_{m0,max}$  at different locations along the offshore boundary of the coastal foundation, averages of the annual means and standard deviations determined for years 2013-2017 (5 years).

	$H_{m0,mean}$		$H_{m0,90\%}$		$H_{m0,max}$		$T_p$	
	average	std	average	std	average	std	average	std
<b>Westkapelle</b>	1.09	0.05	1.99	0.13	5.01	0.38	5.3	0.1
<b>Ouddorp</b>	1.03	0.05	1.86	0.12	4.66	0.39	5.3	0.1
<b>Scheveningen</b>	1.06	0.05	1.94	0.14	4.96	0.36	5.4	0.1
<b>IJmuiden</b>	1.15	0.06	2.11	0.17	5.08	0.57	5.5	0.1
<b>Callantsoog</b>	1.19	0.06	2.19	0.17	5.21	0.52	5.6	0.1
<b>Texel</b>	1.29	0.06	2.32	0.16	5.43	0.68	5.7	0.1
<b>Terschelling</b>	1.23	0.06	2.18	0.11	5.25	0.69	5.7	0.1
<b>Schiermonnikoog</b>	1.16	0.08	2.07	0.13	6.22	1.22	5.2	0.2



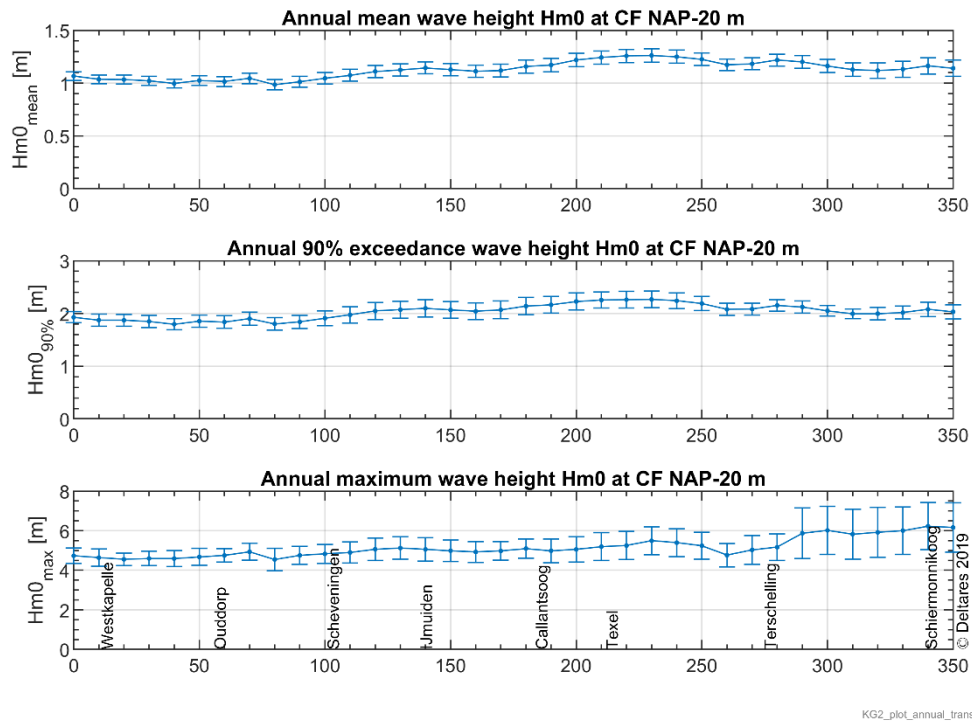


Figure 5.8 Annual mean significant wave height, 90% exceedance value and maximum significant wave height along the offshore boundary of the coastal foundation at NAP-20 m based on wave observations and wave transformation matrix.

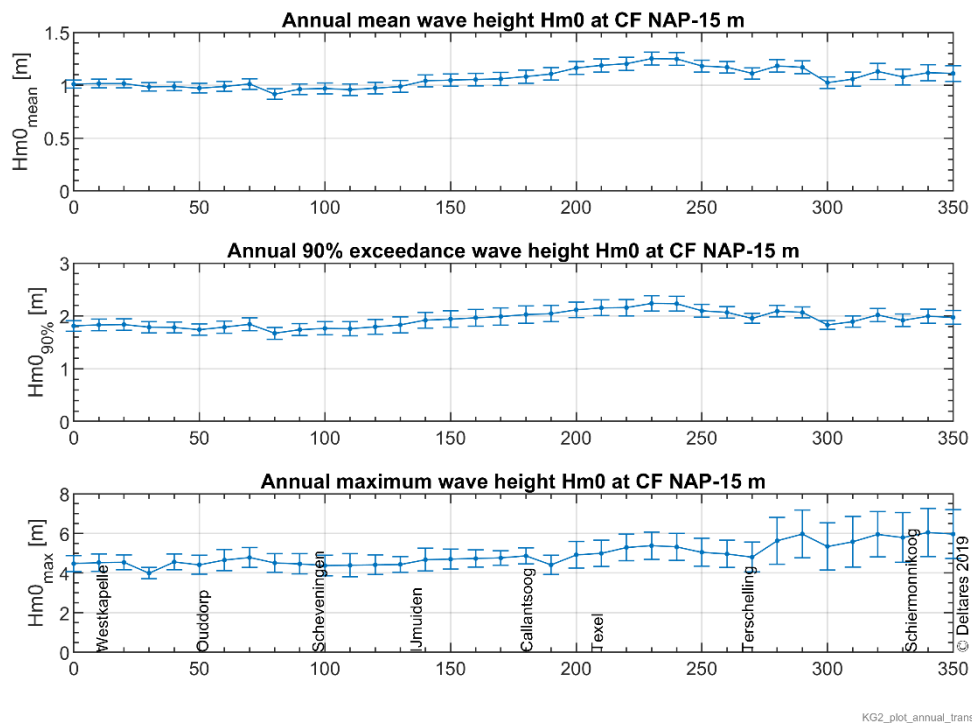


Figure 5.9 Annual mean significant wave height, 90% exceedance value and maximum significant wave height along the contour at NAP-15 m suggested by Vermaas et al. (2015) based on wave observations and wave transformation matrix.



## 5.4 Transport rates

### 5.4.1 Net annual transport rates

The tide-, wind- and density gradient driven currents calculated with the 3D DCSM-FM model combined with the waves obtained from observations using the wave transformation tool have been used as an input for a 1DV sand transport model with which the annual sand transports along the Dutch coast were computed. We applied the 1DV model by Van Rijn et al. (2018). It is an engineering approach of the Van Rijn (2007) model. We have made flow, wave and sand transport computations for the years 2013-2017 using brute force (real-time) time series which means that we have not made simplifications or schematizations to the hydrodynamic input but computed the transports based on the 'real' hydrodynamics. This is in contrast to Van Rijn (1997) who schematized the tide and waves into discrete tide and wave classes.

Here we will present the mean annual transport rates, mean transport directions and the standard deviations to illustrate the variation between the years. A median sand diameter of  $D_{50} = 250 \mu\text{m}$  was applied in all computations to be consistent with Van Rijn (1997). The transports are presented as vectors at more than 1000 locations along the Dutch coast and to cross-shore locations in eight different so-called JARKUS transects along the coast.

Figure 5.10 shows the computed annual mean transport vectors along the southwestern Dutch coast. The present coastal foundation (CF) at the NAP-20 m contour and the coastal foundation at the NAP-15 m as suggest by Vermaas (2015) is shown also as a reference. The dashed lines indicate the selected JARKUS transects. The NAP-20 m and NAP-15 contours are close to each other here and transports are comparable in magnitude and direction at these locations.

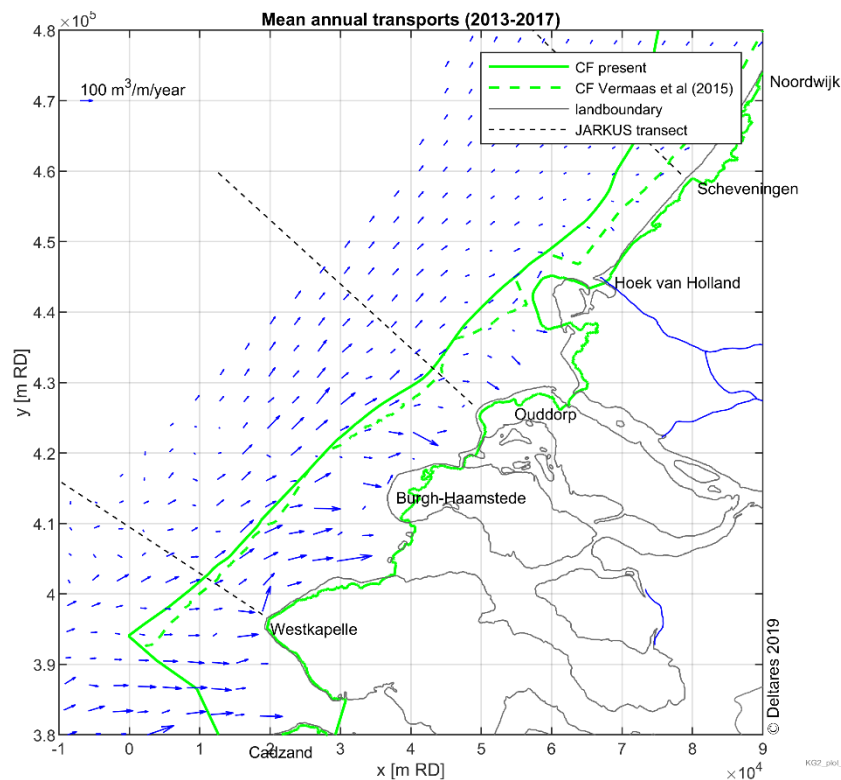


Figure 5.10 Annual mean transport rates based on computations for years 2013-2017, southwestern Dutch coast.

We decomposed the net annual transport rates along into cross-shore and longshore components with two approaches, i.e. based on the JARKUS coast angle and based on the tidal angle. We present the cross-shore and longshore transports along nine different transects along the Dutch coast. Figure 5.11 shows the computed net annual mean cross-shore and longshore transports along the Westkapelle transect. Statistics are based on annual means over years 2013-2017 and error bars indicate the standard deviation between the years. The lower panel shows the bed levels along this transect.

This figure shows that the computed alongshore transports amount to 60-70 m<sup>3</sup>/m/year at 9 km (13 m depth). The longshore transports decrease to about 50 m<sup>3</sup>/m/year at 14 km (20 m depth) and this value remains constant up to 17 km after which the longshore transports decrease to 0-5 m<sup>3</sup>/m/year transports on average at 21-22 km (23-24 m depth).

The cross-shore transports are onshore directed at 9 km (13 m depth) and amount to 30-40 m<sup>3</sup>/m/year depending on the definition of the angle. The cross-shore transport increase to nearly 50 m<sup>3</sup>/m/year at 14 km (20 m depth) and decrease to 15-20 m<sup>3</sup>/m/year at 21-22 km (23-24 m depth). This figure suggests that all sand is going shoreward, which would lead to sedimentation. However, computing and presenting transports in a cross-shore transect ignores possible alongshore transport gradients that may balance the cross-shore gradients. This is not accounted for here.

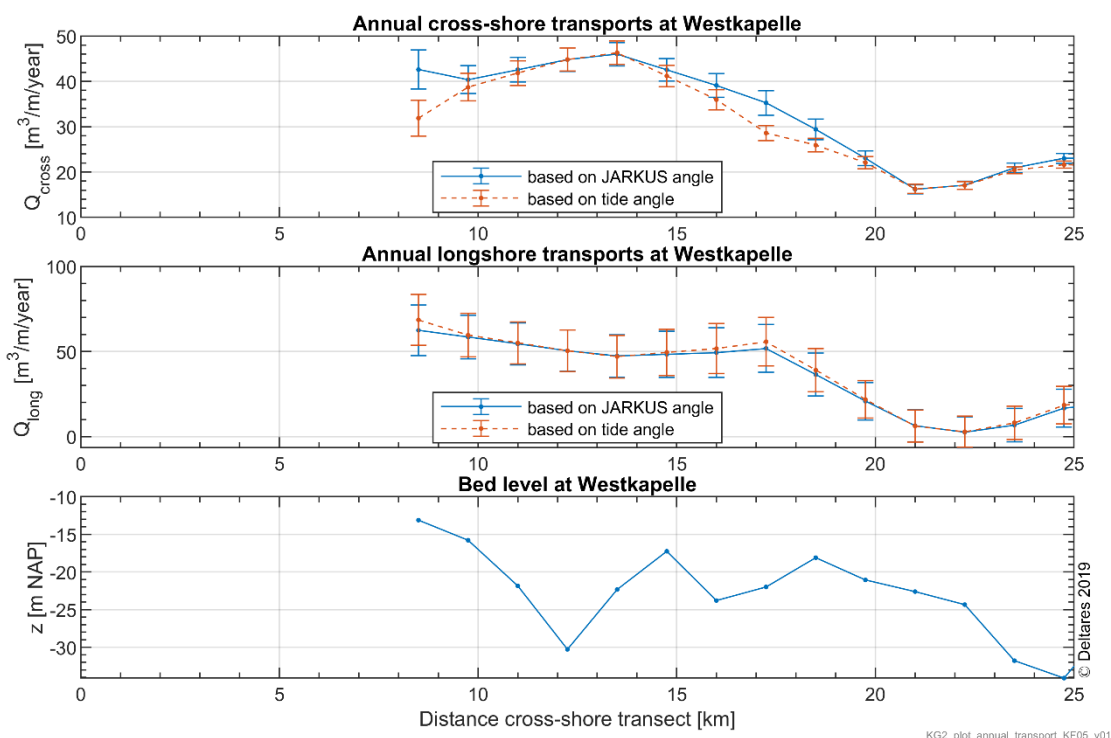


Figure 5.11 Computed net annual mean cross-shore and longshore transports along Westkapelle transect (see Figure 5.10). Statistics are based on annual means over years 2013-2017 and error bars indicate the standard deviation between the years. The lower panel shows the bed levels along this transect.

The alongshore transports along the Ouddorp transect are about 50 m<sup>3</sup>/m/year at 7 km (15 m depth) and increase to about 60 m<sup>3</sup>/m/year at 25 km (25 m depth). The cross-shore transports are onshore directed and amount to 15-20 m<sup>3</sup>/m/year at 7 km. The cross-shore transports are zero on average at 17 km (20 m depth) or 24 km (25 depth) depending on the definition of the coastal angle (JARKUS or tide).

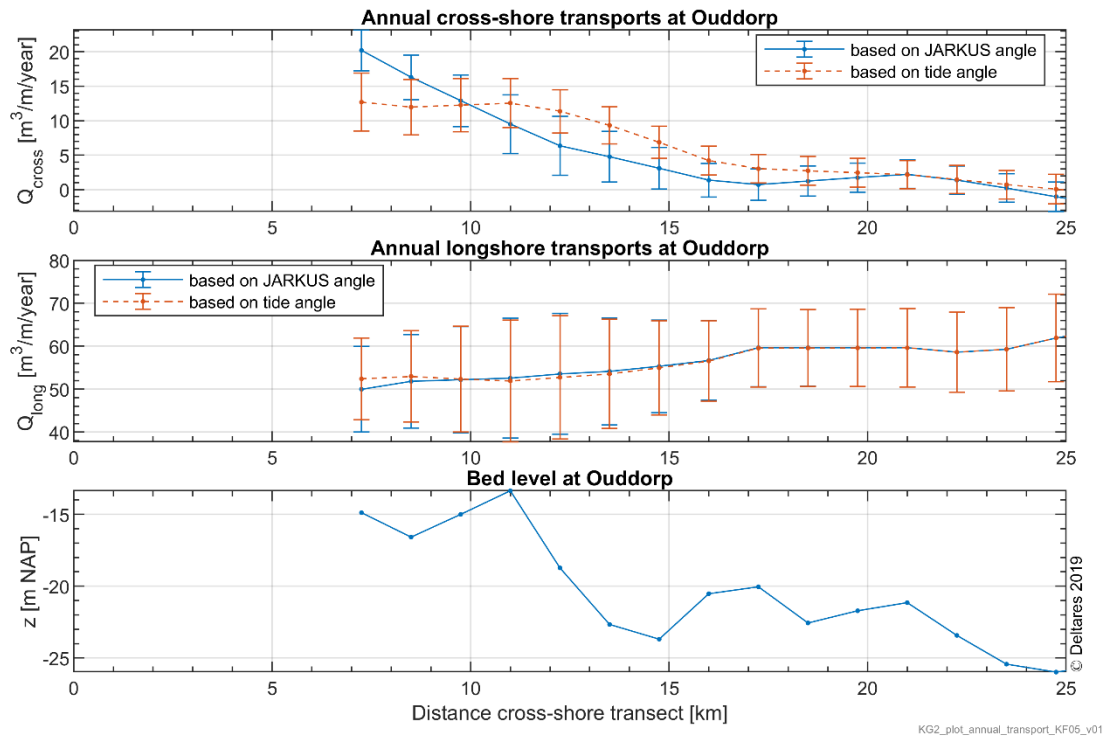


Figure 5.12 Computed net annual mean cross-shore and longshore transports along Ouddorp transect (see Figure 5.10). Statistics are based on annual means over years 2013-2017 and error bars indicate the standard deviation between the years. The lower panel shows the bed levels along this transect.

Figure 5.13 shows the computed mean annual transport vectors along the central Dutch coast between Hoek van Holland and IJmuiden. Scheveningen and IJmuiden have been selected here as representative JARKUS transects.

Figure 5.14 shows that the alongshore transports in the Scheveningen transect are about  $30 \text{ m}^3/\text{m}/\text{year}$  at 6 km (17 m depth) and decrease to  $25 \text{ m}^3/\text{m}/\text{year}$  at 10 km (20 m depth). The net longshore transports increase again to  $35 \text{ m}^3/\text{m}/\text{year}$  at 25 km (23 m depth). The cross-shore transports are onshore directed and decrease from 5-7 at 6 km to zero on average at 15 km (21 m depth) or 25 km (23 m depth) depending on the definition of the coastal angle.

Figure 5.15 shows that the longshore transports in the IJmuiden transect increase from about  $105 \text{ m}^3/\text{m}/\text{year}$  at 6 km (15 m depth) to  $135 \text{ m}^3/\text{m}/\text{year}$  at 20 km (20 m depth). The cross-shore transports are  $0\text{-}5 \text{ m}^3/\text{m}/\text{year}$  at 6 km. The cross-shore transports are zero on average at 6 km (15 m depth) or 10 km (17 m depth) depending on the definition of the coastal angle.

It is interesting to see that the cross-shore transports tend to become more onshore directed when going shallower from the present coastal foundation at NAP-20 m.

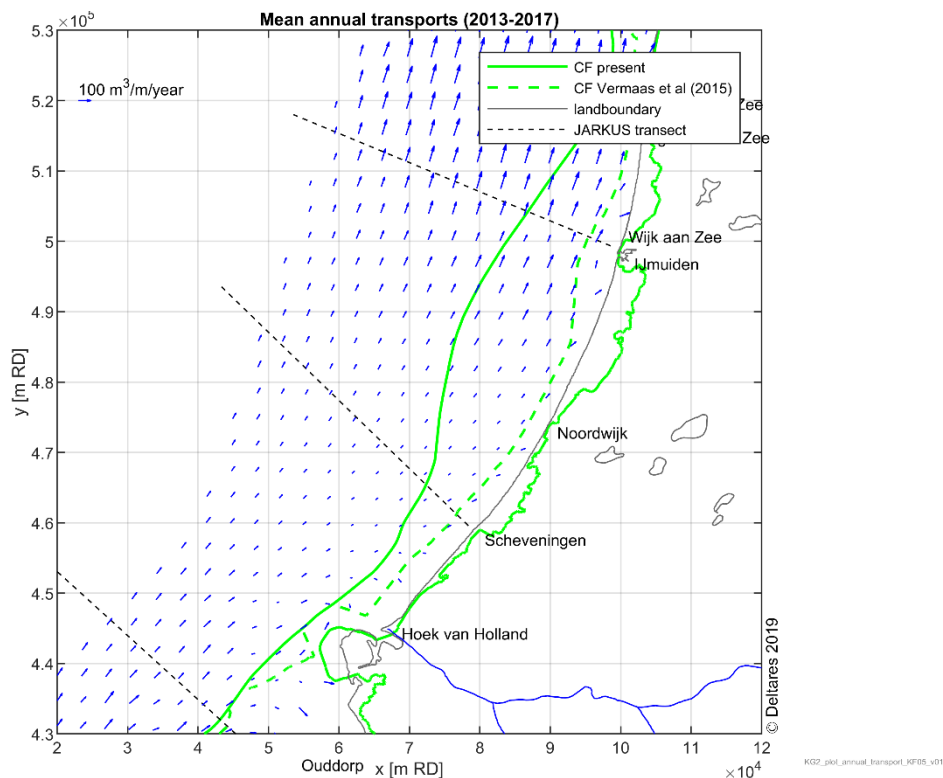


Figure 5.13 Annual mean transport rates based on computations for years 2013-2017, central Dutch coast.

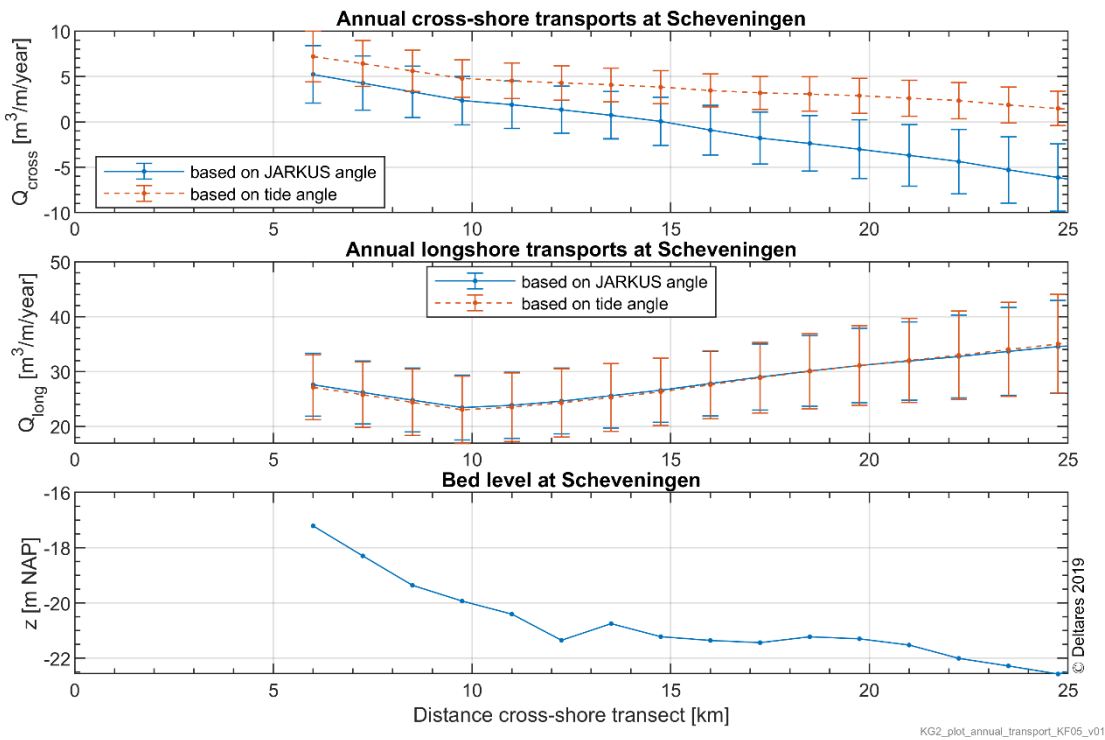


Figure 5.14 Computed net annual mean cross-shore and longshore transports along Scheveningen transect (see Figure 5.13). Statistics are based on annual means over years 2013-2017 and error bars indicate the standard deviation between the years. The lower panel shows the bed levels along this transect.

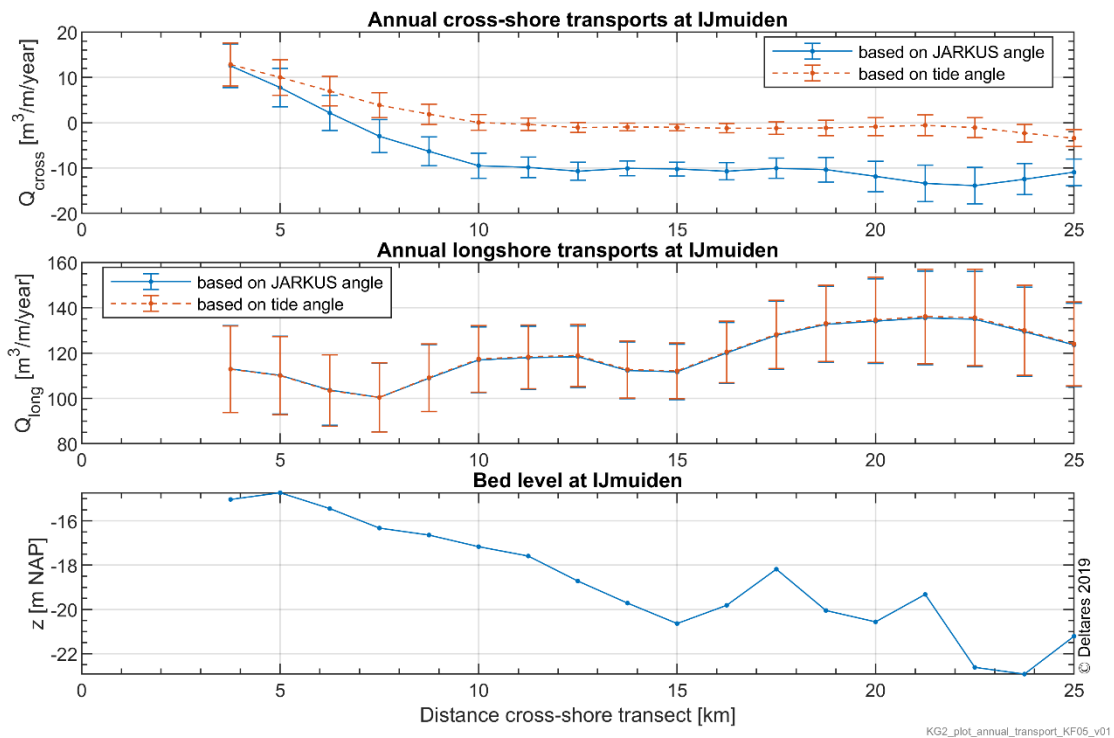


Figure 5.15 Computed net annual mean cross-shore and longshore transports along IJmuiden transect (see Figure 5.13). Statistics are based on annual means over years 2013-2017 and error bars indicate the standard deviation between the years. The lower panel shows the bed levels along this transect.

Figure 5.16 shows the computed mean annual transport vectors along the northern Dutch coast between IJmuiden and Den Helder. Alongshore transports can be clearly observed to be increasing northward along the coast and there is a relatively strong effect of the tidal inlet between Den Helder and Texel (Marsdiep). IJmuiden and Callantssoog have been selected as representative JARKUS transects along this stretch of coast.

The annual mean longshore transport is about 200 m<sup>3</sup>/m/year at 5 km (13 m depth) and 215 m<sup>3</sup>/m/year at 6 km (15 m depth) in the Callantssoog transect. This increases slightly to 230 m<sup>3</sup>/m/year at 9 km (20 m depth) and decreases slightly to 215 m<sup>3</sup>/m/year at 25 km (25 m depth).

The annual mean cross-shore transport is 0 to 5 m<sup>3</sup>/m/year at 5 km and -5 to -10 m<sup>3</sup>/m/year at 6 km and about -10 m<sup>3</sup>/m/year at 9 km. The negative sign means that the cross-shore transports are offshore directed. The exact magnitude depends on the definition of the coast angle (JARKUS or tide).

If the JARKUS coast angle would be used, the cross-shore transport become zero on average at 20 km (25 m depth). If the tide would be used as a coast angle, the cross-shore transports would always be offshore directed. In this case the offshore directed cross-shore transports would be smallest between 13 km and 21 km (21-22 m depth).

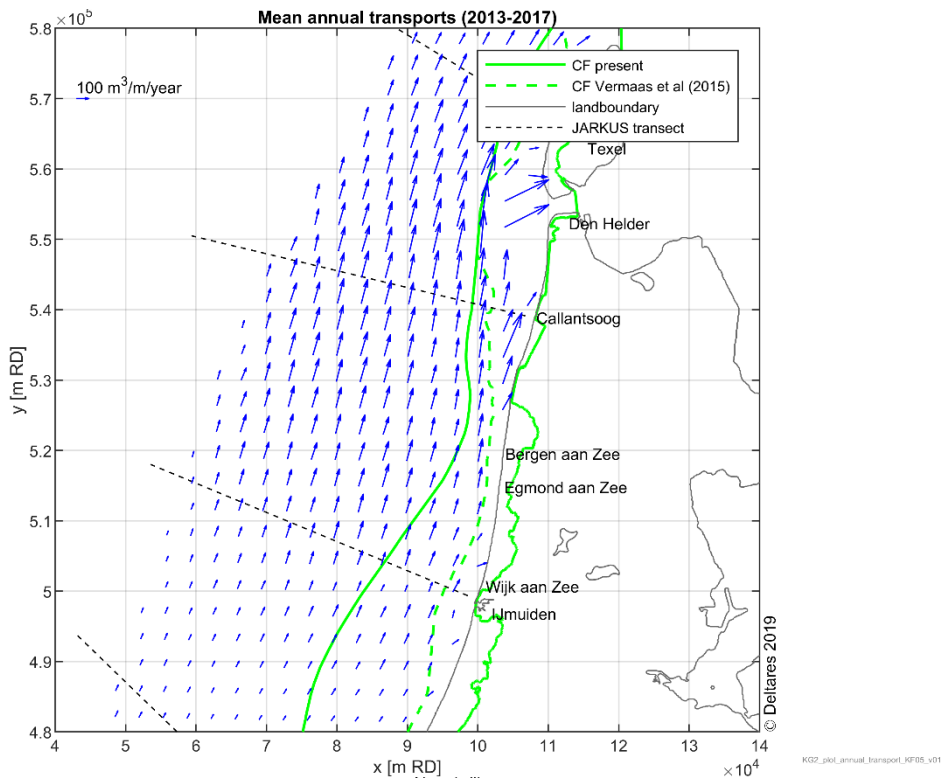


Figure 5.16 Annual mean transport rates based on computations for years 2013-2017, northern Dutch coast.

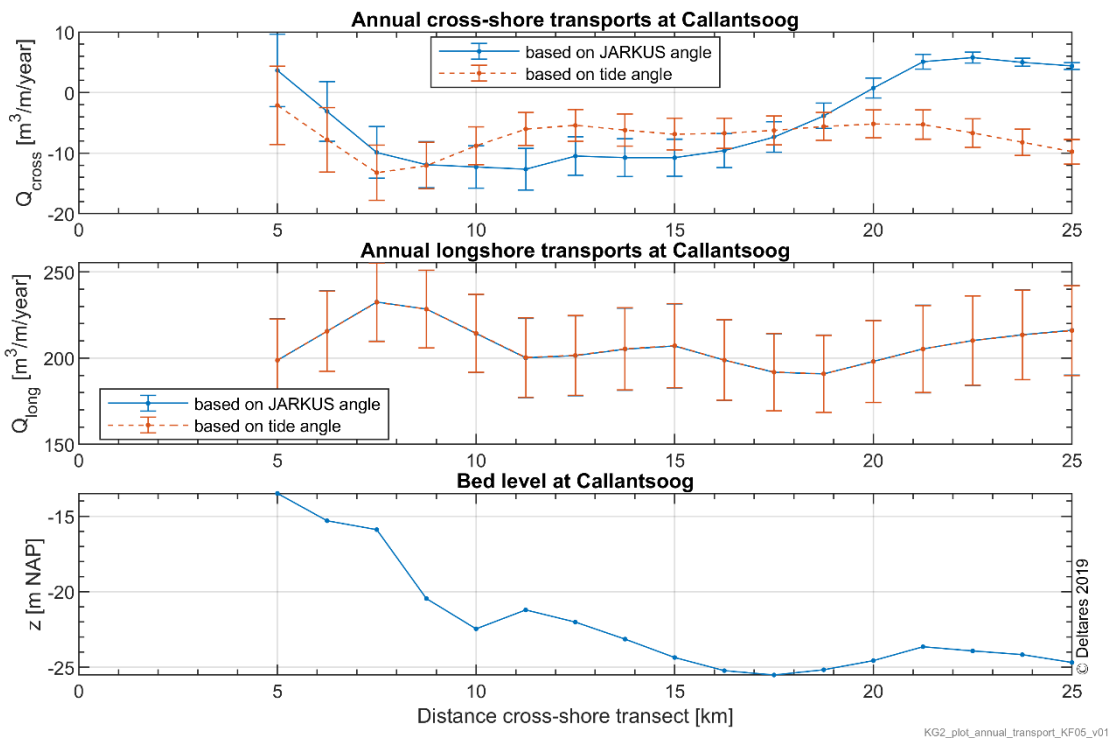


Figure 5.17 Computed net annual mean cross-shore and longshore transports along Callantssoog transect (see Figure 5.16). Statistics are based on annual means over years 2013-2017 and error bars indicate the standard deviation between the years. The lower panel shows the bed levels along this transect.

Figure 5.18 shows the computed mean annual transport rates along Texel, Vlieland and Terschelling. Transport magnitudes vary relatively strongly along this stretch of coast and the transport vectors show strong effects of the tidal inlets between Vlieland and Terschelling (Vliestroom) and also between Terschelling and Ameland.

The mean annual alongshore transport is about  $100 \text{ m}^3/\text{m}/\text{year}$  at 5 km (16 m depth) and increases to about  $190 \text{ m}^3/\text{m}/\text{year}$  at 9 km (21 m depth) along the Texel transect (Figure 5.19). The alongshore transport decreases to about  $90 \text{ m}^3/\text{m}/\text{year}$  at 25 km (30 m depth).

The mean annual cross-shore transport is  $10 \text{ m}^3/\text{m}/\text{year}$  (onshore directed) at 5 km and  $-10$  to  $-20 \text{ m}^3/\text{m}/\text{year}$  (offshore directed) at 9 km. This remains about the same along the entire transect when moving further offshore.

Along the Terschelling transect, the alongshore transports are  $55 \text{ m}^3/\text{m}/\text{year}$  at 5 km (16 m depth). This increases to  $60 \text{ m}^3/\text{m}/\text{year}$  at 9 km (20 m depth), after which it decreases to  $20 \text{ m}^3/\text{m}/\text{year}$  at 25 km (27 m depth).

The mean annual cross-shore transports are 15 to  $20 \text{ m}^3/\text{m}/\text{year}$  at 5 km. The positive sign means that the cross-shore transports are onshore directed. The magnitude depends on the definition of the coast angle. The cross-shore transports decrease to near zero on average at 12 km (22 m depth) in the Terschelling transect.

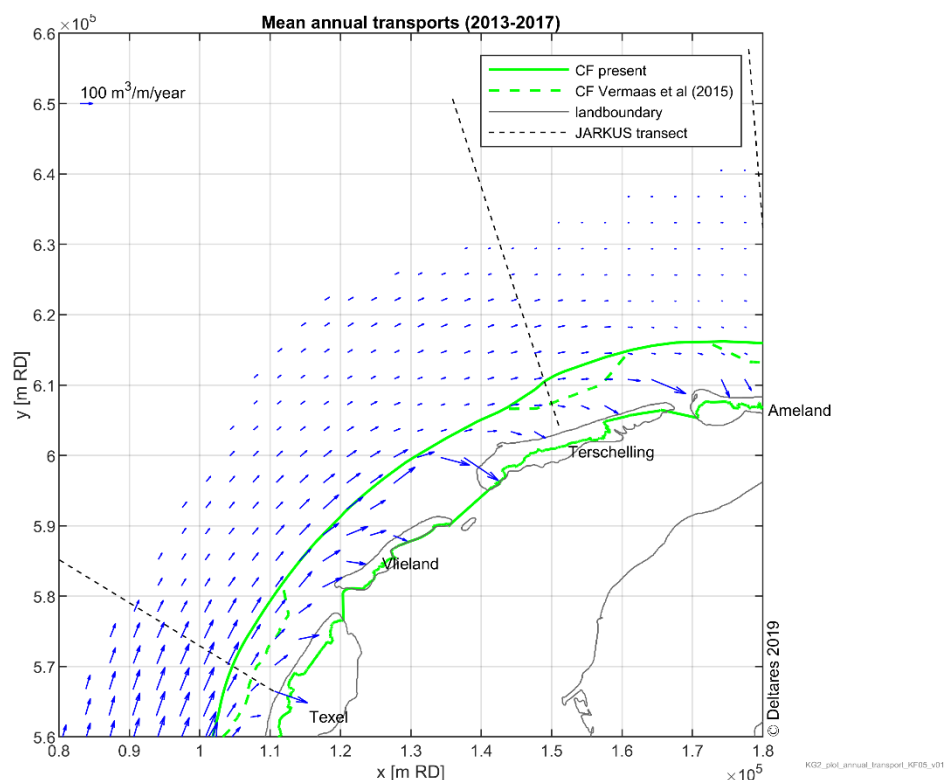


Figure 5.18 Annual mean transport rates based on computations for years 2013-2017, northwestern North Sea coast along Texel, Vlieland and Terschelling.

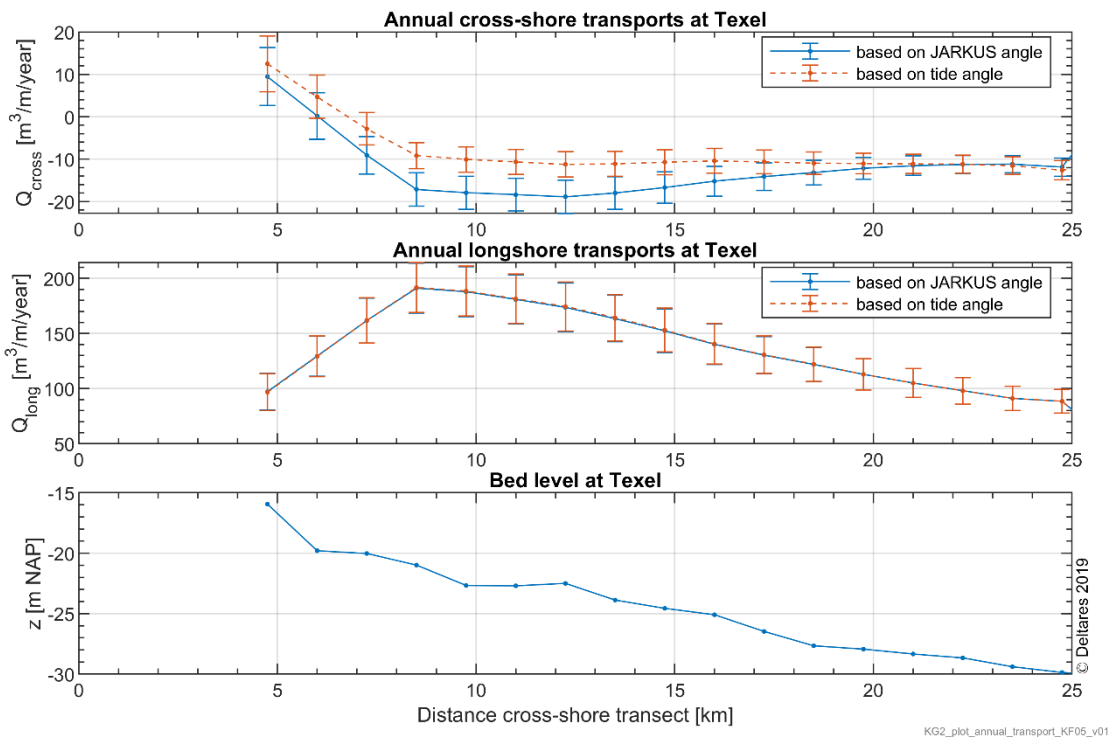


Figure 5.19 Computed net annual mean cross-shore and longshore transports along Texel transect (see Figure 5.18). Statistics are based on annual means over years 2013-2017 and error bars indicate the standard deviation between the years. The lower panel shows the bed levels along this transect.

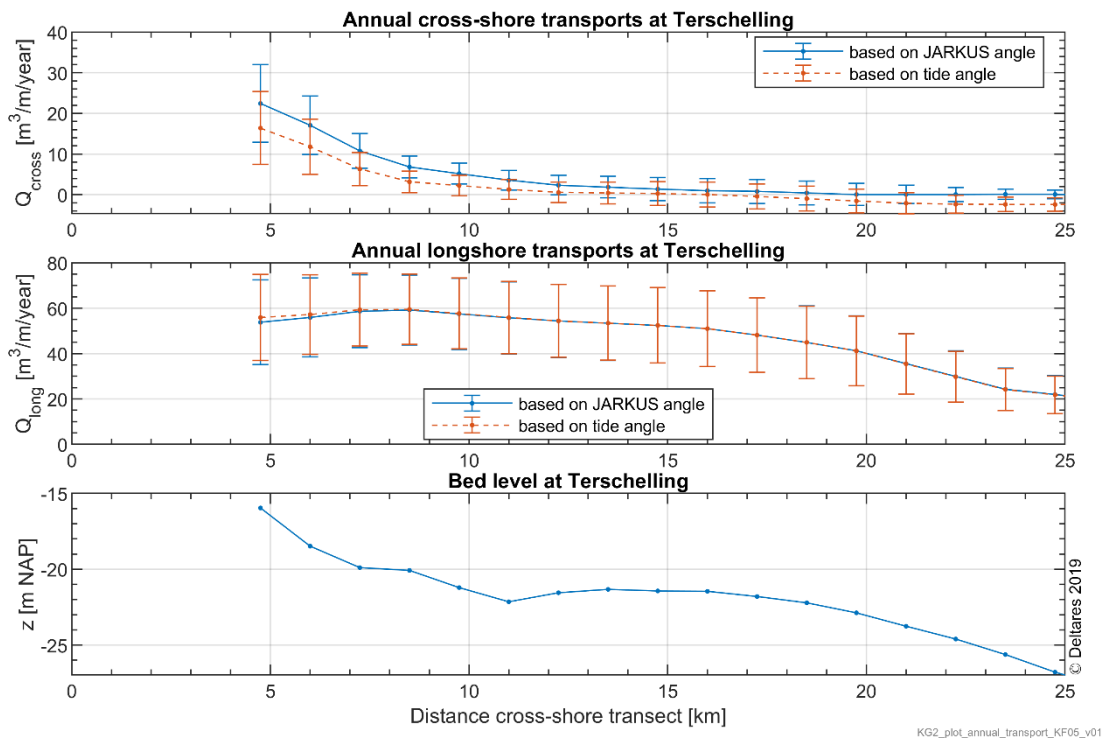


Figure 5.20 Computed net annual mean cross-shore and longshore transports along Terschelling transect (see Figure 5.18). Statistics are based on annual means over years 2013-2017 and error bars indicate the standard deviation between the years. The lower panel shows the bed levels along this transect.



Figure 5.21 shows the computed mean annual transport rates along Ameland and Schiermonnikoog. The transports are relatively small near, and offshore of the present coastal foundation at NAP -20 m (solid green line). The transports have a relatively large onshore directed component as compared to the coastal stretches described previously. This is consistent with the onshore directed components of the residual flows (par. 5.2.1) and peak tidal flows (par. 5.2.2) along this coastal stretch.

The mean annual alongshore transports are  $30 \text{ m}^3/\text{m}/\text{year}$  at 5 km (15 depth) in the Ameland transect (Figure 5.22). This decreases to  $15 \text{ m}^3/\text{m}/\text{year}$  at 6 km (18 m depth) and decreases further to about  $10 \text{ m}^3/\text{m}/\text{year}$  at 25 km (27 m depth).

The mean annual cross-shore transport in the Ameland transect is about  $30 \text{ m}^3/\text{m}/\text{year}$  at 5 km. This decreases to  $10 \text{ m}^3/\text{m}/\text{year}$  at 6 km and decreases further to nearly zero on average at 25 km.

Along the Schiermonnikoog transect, the mean annual alongshore transport is about  $90 \text{ m}^3/\text{m}/\text{year}$  at 7 km (15 m depth). This decreases to  $15 \text{ m}^3/\text{m}/\text{year}$  at 25 km (25 m depth).

The mean annual cross-shore transports are 30 to  $40 \text{ m}^3/\text{m}/\text{year}$  (onshore directed) at 7 km. The magnitude depends on the definition of the coastal angle. This decreased to zero on average at 25 km.

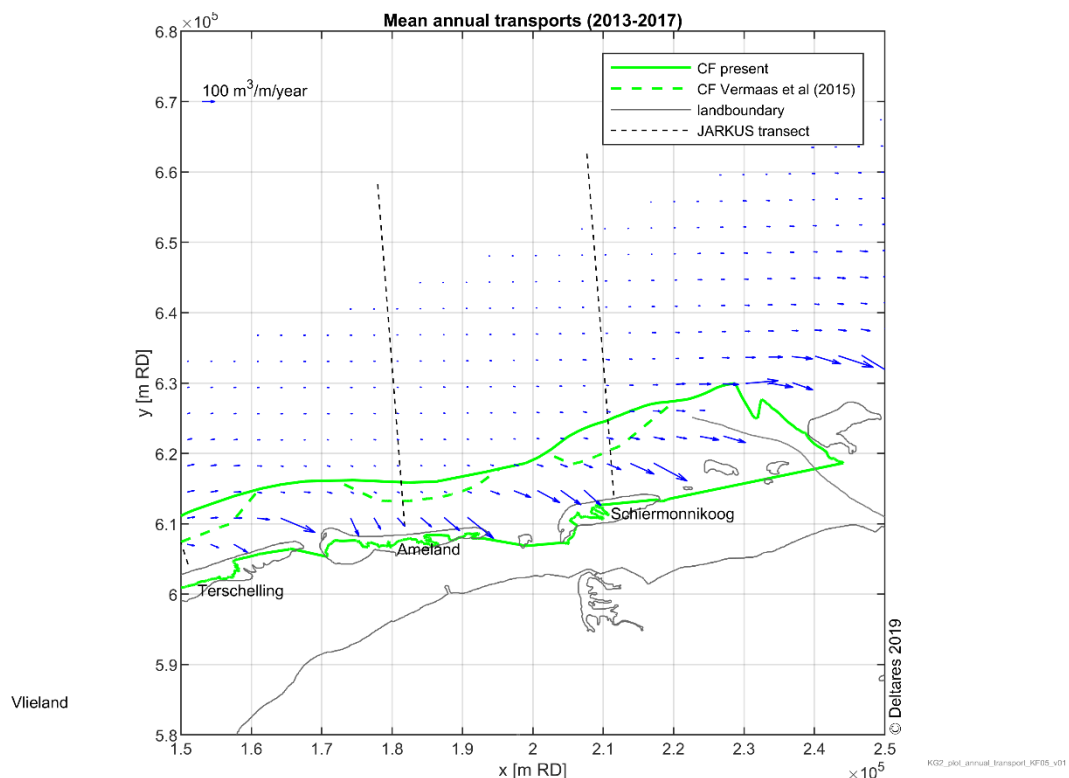


Figure 5.21 Annual mean transport rates based on computations for years 2013-2017, northeastern North Sea coast along Ameland and Schiermonnikoog

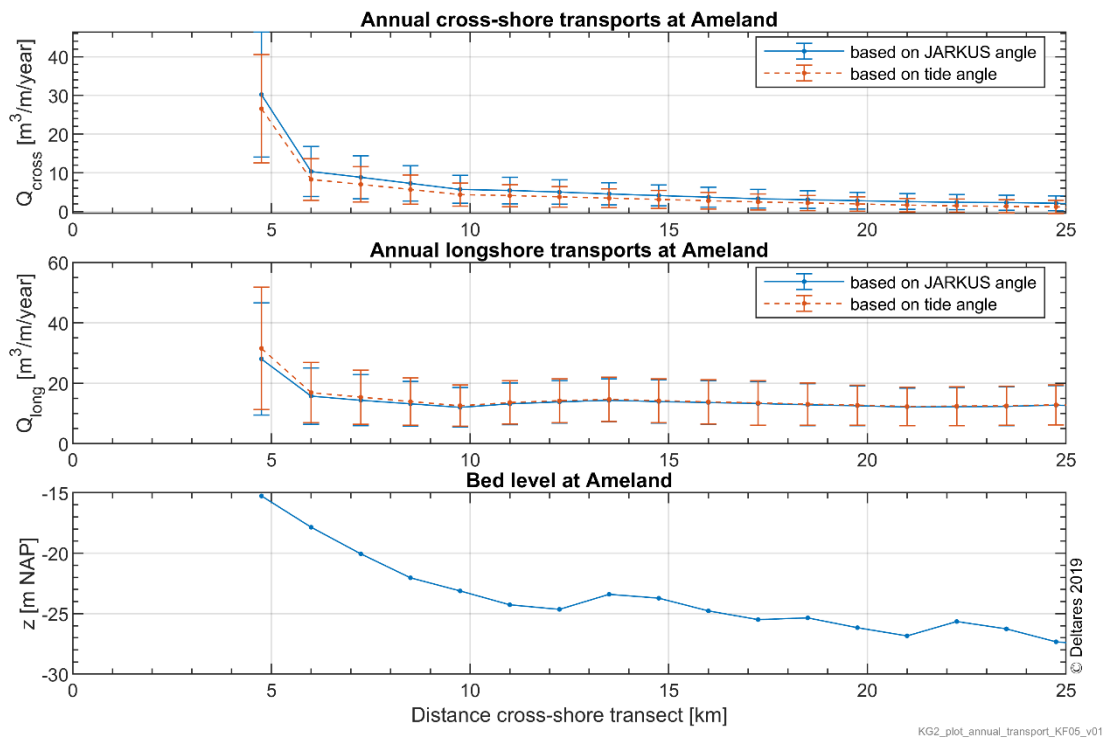


Figure 5.22 Computed net annual mean cross-shore and longshore transports along Ameland transect (see Figure 5.21). Statistics are based on annual means over years 2013-2017 and error bars indicate the standard deviation between the years. The lower panel shows the bed levels along this transect.

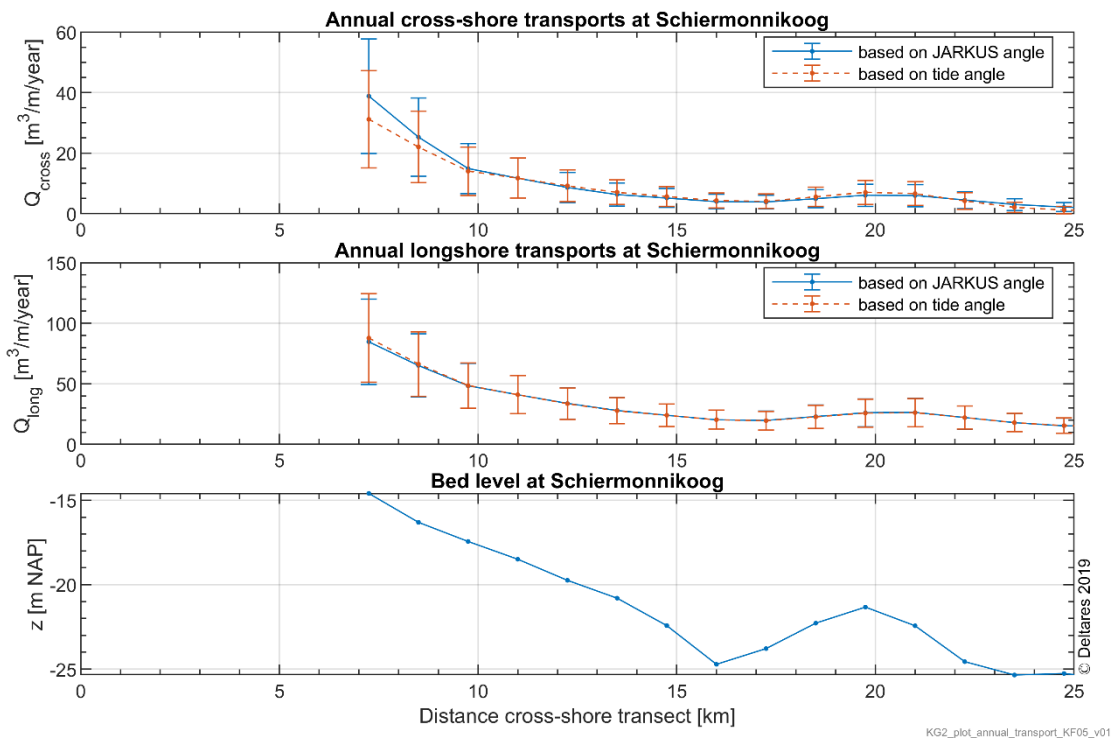


Figure 5.23 Computed net annual mean cross-shore and longshore transports along Schiermonnikoog transect (see Figure 5.21). Statistics are based on annual means over years 2013-2017 and error bars indicate the standard deviation between the years. The lower panel shows the bed levels along this transect.

Table 5.2 presents the mean annual transport rates and the transport direction at the eight selected locations along the present offshore boundary of the coastal foundation at the NAP-20 m depth contour. This table shows that transport rates decrease from Westkapelle towards Ouddorp and Scheveningen, increase again towards IJmuiden and Callantsoog and decrease towards Texel, Terschelling and Schiermonnikoog. This alongshore variation is consistent with the variation in wave height presented in Section 5.3. The third column in Table 5.2 presents the computed transport directions. The fourth column shows the coast angle based on JARKUS and the fifth column the major angle of the M2 tidal constituent. Angles are measured anticlockwise. Transports have an onshore directed component if the coast angle is larger than the transport angle. This is the case for all stations except Callantsoog and Texel, where the transport angles are larger than the coast angle and the computed annual mean transports would have an offshore directed component. The same holds when the coast angle would be defined as the major axis of the M2 tide shown in the fifth column of Table 5.2.

Table 5.3 presents the mean annual transport rates in the eight selected transects at the NAP-15 m contour. When comparing Table 5.3 with Table 5.2 it can be seen that the transport rates at the NAP-15 m contour are generally of the same order as the transports at the NAP-20 m contour, except at the Schiermonnikoog transect. At Westkapelle and Ouddorp the transports at NAP-15 m show less than 5% difference with those at NAP-20 m. At Scheveningen the transports are 20% smaller at NAP-15, at IJmuiden about 10% larger, at Callantsoog the difference is less than 5% and at Texel the transport at NAP-15 m are about 20% smaller. At Terschelling the transports at NAP-15 show less than 5% difference with those at NAP-20 m. The difference is largest at Schiermonnikoog where the NAP-15 transports are about 2 times larger than at NAP-20 m.

The mean annual transport angles (measured anticlockwise from the horizontal x-axis) are generally smaller at the NAP-15 m contour than at the NAP-20 m contour, which means that they have a tendency to be more shoreward directed (or less offshore directed).

*Table 5.2 Mean annual transport rates and directions at different locations along the offshore boundary of the present coastal foundation (NAP-20 m) based on computations for years 2013-2017. Angles are measured anticlockwise from the horizontal x-axis.*

Location	Mean annual transport magnitude (standard deviation) [m <sup>3</sup> /m/year]	Mean annual transport direction (standard deviation) [degrees]	Coast angle JARKUS [degrees]	Coast angle M2 tide [degrees]
Westkapelle	70 (11)	18 (8)	57	56
Ouddorp	55 (11)	29 (7)	48	43
Scheveningen	24 (6)	37 (13)	46	52
IJmuiden	77 (12)	66 (2)	73	70
Callantsoog	226 (25)	79 (1)	77	77
Texel	145 (20)	62 (1)	59	60
Terschelling	60 (18)	9 (4)	18	14
Schiermonnikoog	38 (17)	-10 (5)	5	5

Table 5.3 Mean annual transport rates and directions at different locations along the NAP-15 m contour suggested by Vermaas et al. (2015) based on computations for years 2013-2017. Angles are measured anticlockwise from x-axis.

Location	Mean annual transport magnitude (standard deviation) [m <sup>3</sup> /m/year]	Mean annual transport direction (standard deviation) [degrees]	Coast angle JARKUS [degrees]	Coast angle M2 tide [degrees]
Westkapelle	73 (12)	23 (7)	57	54
Ouddorp	55 (9)	25 (7)	48	39
Scheveningen	19 (3)	33 (12)	46	65
IJmuiden	83 (14)	70 (6)	73	80
Callantsoog	217 (26)	77 (2)	77	75
Texel	110 (18)	53 (5)	59	61
Terschelling	59 (22)	-7 (10)	18	11
Schiermonnikoog	89 (42)	-19 (4)	5	4

Figure 5.24 and Figure 5.25 illustrate the previously observed trends by plotting the mean annual transport magnitudes and directions along the entire offshore boundary of the present coastal foundation at NAP-20 and the offshore boundary suggested by Vermaas et al. (2015) at NAP-15 m, respectively. These figures show that the transport magnitude decreases from Westkapelle to Scheveningen, increases from Scheveningen to the inlet between Callantsoog and Texel (Marsdiep) and decreases again towards Schiermonnikoog. Transports at the NAP-15 m contour are on average 10% smaller at the NAP-15 m contour than at the NAP-20 m contour (compare Figure 5.24 and Figure 5.25). The mean annual transport angles along the NAP-20 m contour vary roughly between 0° and 40° between Westkapelle and Scheveningen, increase to 80° between Scheveningen and Callantsoog, and decrease again to 0° at Schiermonnikoog. Transport angles are on average 8° smaller at the NAP-15 m contour, which means that the transports are more shoreward directed (or less offshore directed) along this contour than along the deeper contour.

Figure 5.26 and Figure 5.27 show the transports decomposed into alongshore and cross-shore component using the major M2 axis of the tide as coast angle and also using the smoothed JARKUS angle (see Figure 5.2). These figures clearly illustrate the sensitivity of the cross-shore transports to the definition of the coast angle. But irrespective of the exact definitions, these figures also illustrate the predominant onshore transports for the coastal stretch from Westkapelle to about 10 km south of Callantsoog and at the height of the Wadden islands and the tendency to become offshore directed at the inlets between Callantsoog and Texel (Marsdiep) and between Vlieland and Terschelling (Vliestroom). The onshore directed transport component is generally larger at NAP-15 than at NAP-20 m, except near the aforementioned inlets.

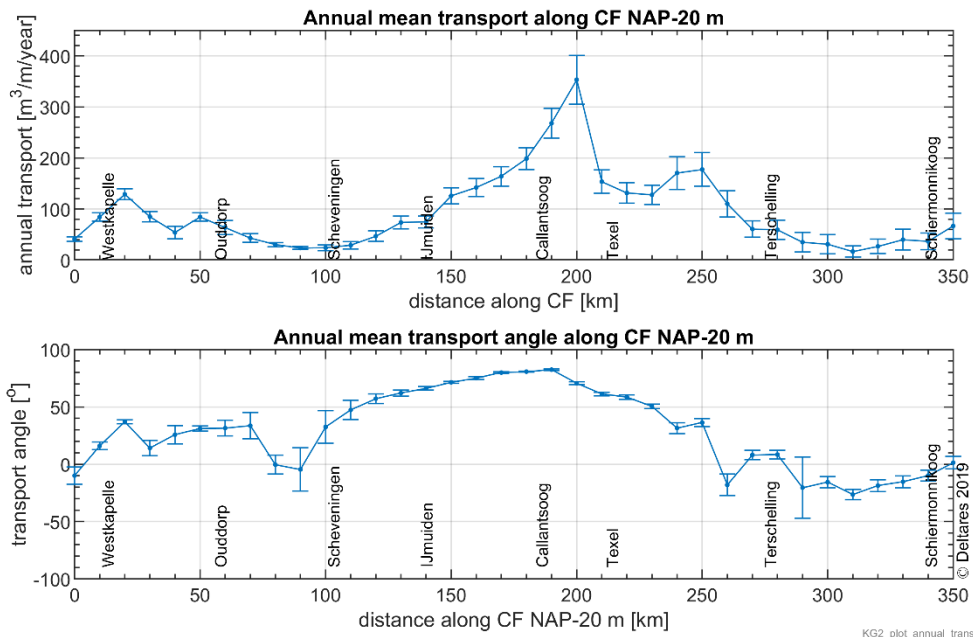


Figure 5.24 Annual mean transport rates along the offshore boundary of the present coastal foundation at the NAP-20 m based on computations for years 2013-2017.

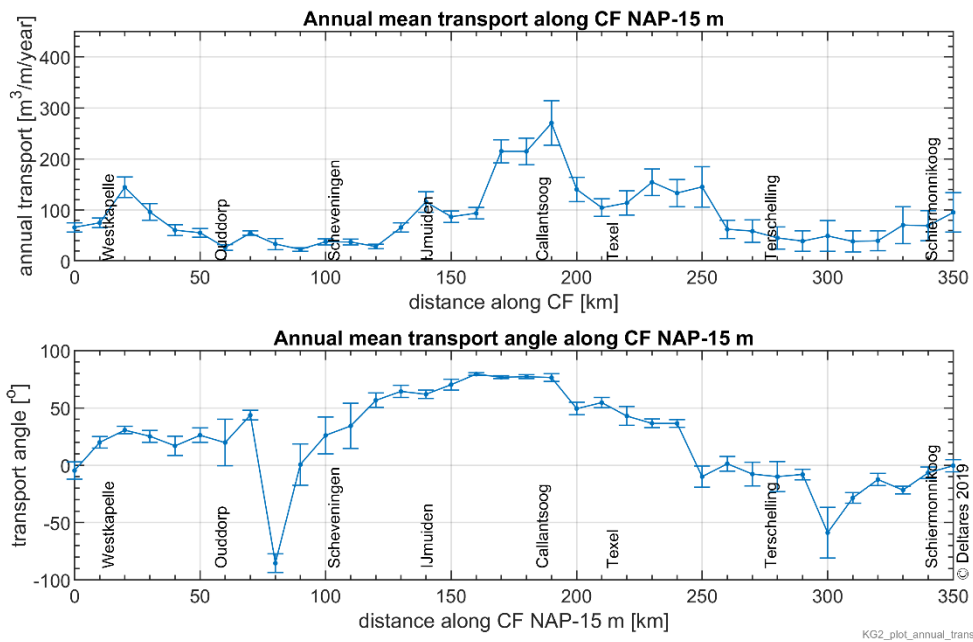
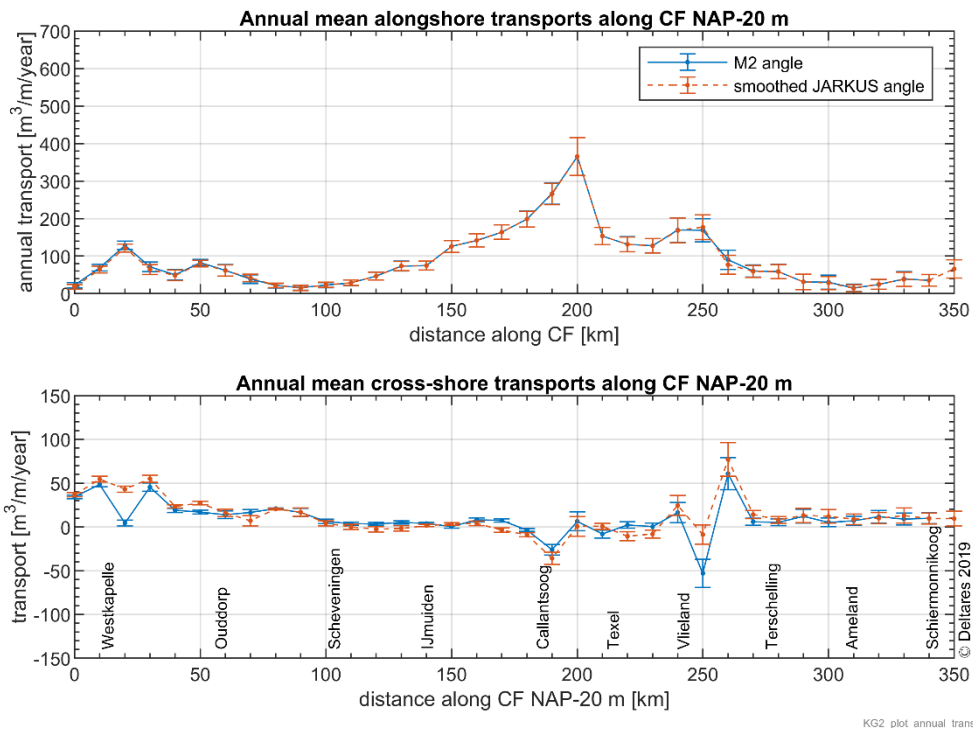


Figure 5.25 Annual mean transport rates along the NAP-20 m suggest by Vermaas et al. (2015) based on computations for years 2013-2017.



KG2 plot annual transport KF05 v01

Figure 5.26 Annual mean alongshore (top panel) and cross-shore (lower panel) transport rates along the offshore boundary of the present coastal foundation at the NAP-20 m based on computations for years 2013-2017. The blue line indicates the transport component using the major M2 axis as coast angle and the light brown dashed line using the smoothed JARKUS coast angle.

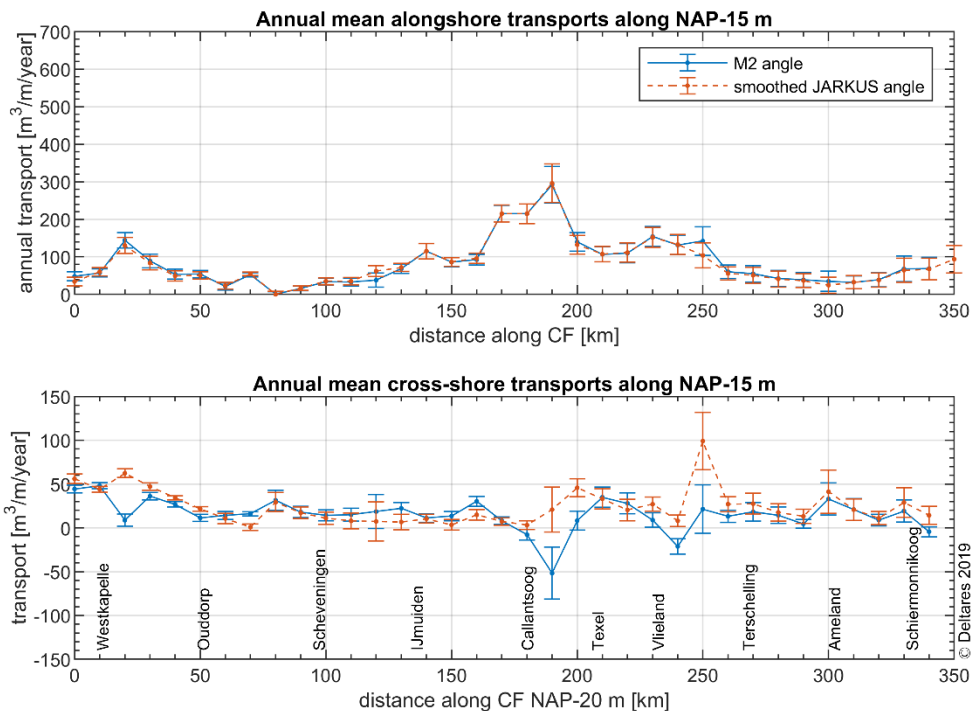


Figure 5.27 Annual mean alongshore (top panel) and cross-shore (lower panel) transport rates along the NAP-15 m suggested by Vermaas et al. (2015) based on computations for years 2013-2017. The blue line indicates the transport component using the major M2 axis as coast angle and the light brown dashed line using the smoothed JARKUS coast angle.

#### 5.4.2 Effect of density and wind

To study the effect of density and wind on the net annual transport rates and directions, we made 3D DCSM-FM model computations for the years 2013-2017 with only density turned off and both density and wind turned off, combined these with waves from the wave transformation matrix and computed sand transport with the 1DV transport model.

This is a theoretical exercise as in reality density effects will always be present due to fresh water outflow of the Rhine into the North Sea for example and waves will not be generated without wind, but it gives an impression of the relative importance of both.

We illustrate the effect of density and wind at different transects along the Dutch coast by presenting the computed mean annual cross-shore and longshore transports along the nine selected transects with wind and density and without these effects.

Effects are relatively large in the southern part of the Dutch coast. Figure 5.28 shows that in the Westkapelle transect, the longshore transport increase by about 5-15% and the cross-shore transports reduce by 10-20% in water depths of 15-20 m when turning off density. The longshore transports are strongly reduced by turning off wind and may even become southward directed.

In the Ouddorp transect, turning off density results in an increase of the longshore transports of 40-60% and a decrease in cross-shore transports of 30-100% (Figure 5.29). The longshore transports are strongly reduced (up to a factor 3) when turning off wind also.

Further north, in the Scheveningen transect, turning off the effects of density leads to 10-50% larger longshore transports and 100% reduction or offshore directed cross-shore transports (Figure 5.30). Turning off wind also appears to counteract this effect.

In the IJmuiden transect, turning off density leads to 20-80% increase in longshore transports and cross-shore transport to be always offshore directed where they are onshore directed near the coast with the effect of density (Figure 5.31). Turning off wind also counteracts this effect to a certain extent.

Relatively large effects of turning off density can be observed in the Callantssoog transect also where the longshore transports increase by 5-50% and the cross-shore transport that were already offshore directed with density effect, now the offshore directed transports increase up to a factor 3 (Figure 5.32). Turning off wind counteracts this here also to a certain extent.

At Texel, turning off density effects results in an increase of the longshore transports by 5-35% and larger offshore directed cross-shore transports with an increase of the offshore directed cross-shore transports up to a factor of 2 (Figure 5.33). Turning off wind counteracts this here also.

Effects of density are less pronounced in the Terschelling transect. Here, turning off density results in a decrease of the longshore transports by 5-10% at 15-20 m depth but an increase of 5-10 in deeper waters. It results in a decrease of the cross-shore transports of 10-40% (Figure 5.34) but the cross-shore transports remain onshore directed. Turning off wind strongly decreases the alongshore transports here and slightly increases the onshore directed cross-shore transports.

In the Ameland transect the longshore transports are hardly affected by turning off density (Figure 5.35). The cross-shore transports are reduced by 10-30%. Cross-shore transport remain onshore directed here. Turning strongly decreases the alongshore transports and slightly increases the onshore directed cross-shore transports.

In the Schiermonnikoog transect, longshore transports are reduced by about 10% and cross-shore transports by 10-30% by turning off density. Cross-shore transport remain onshore

directed here also. Turning off wind reduces the longshore transports and increases the onshore directed cross-shore transports.

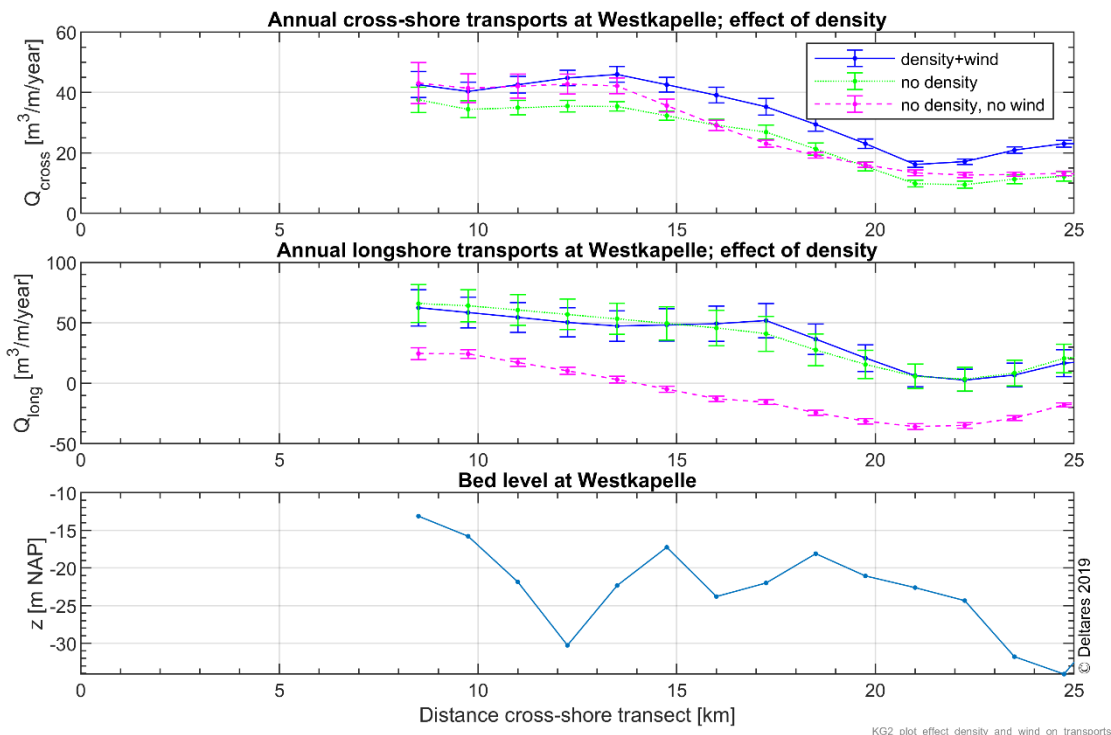


Figure 5.28 Effect of density on the cross-shore and alongshore transport rates in the Westkapelle transect based on computations for years 2013-2017.

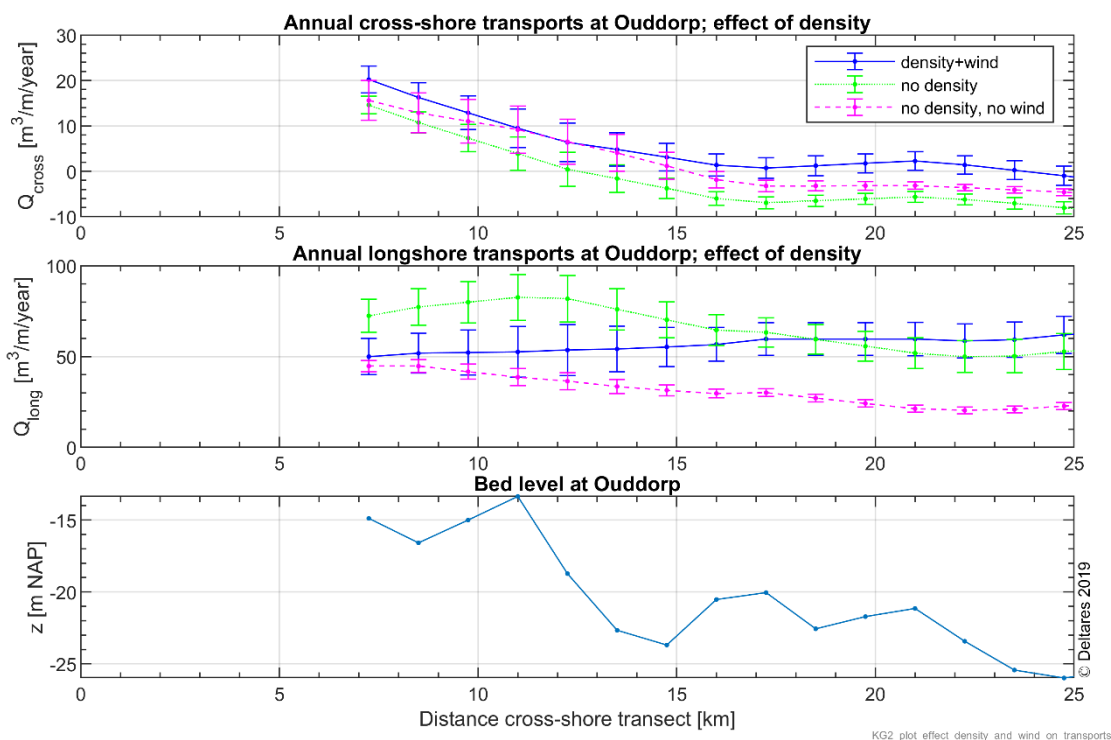


Figure 5.29 Effect of density on the cross-shore and alongshore transport rates in the Ouddorp transect based on computations for years 2013-2017.



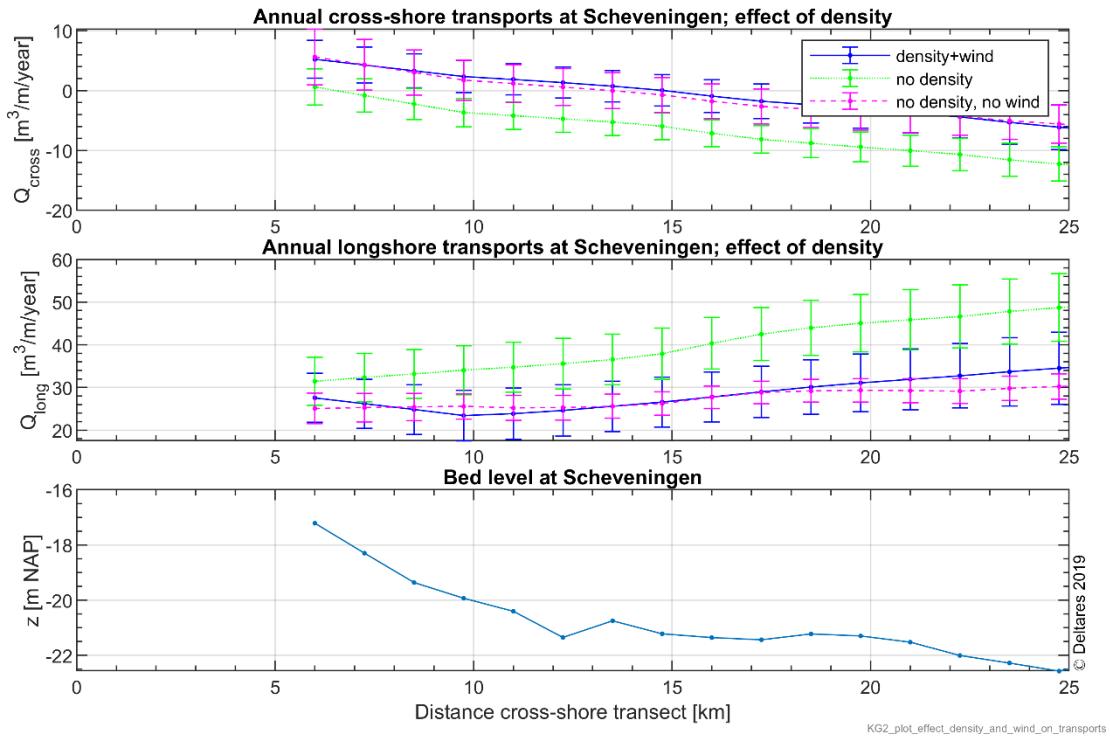


Figure 5.30 Effect of density on the cross-shore and alongshore transport rates in the Scheveningen transect based on computations for years 2013-2017.

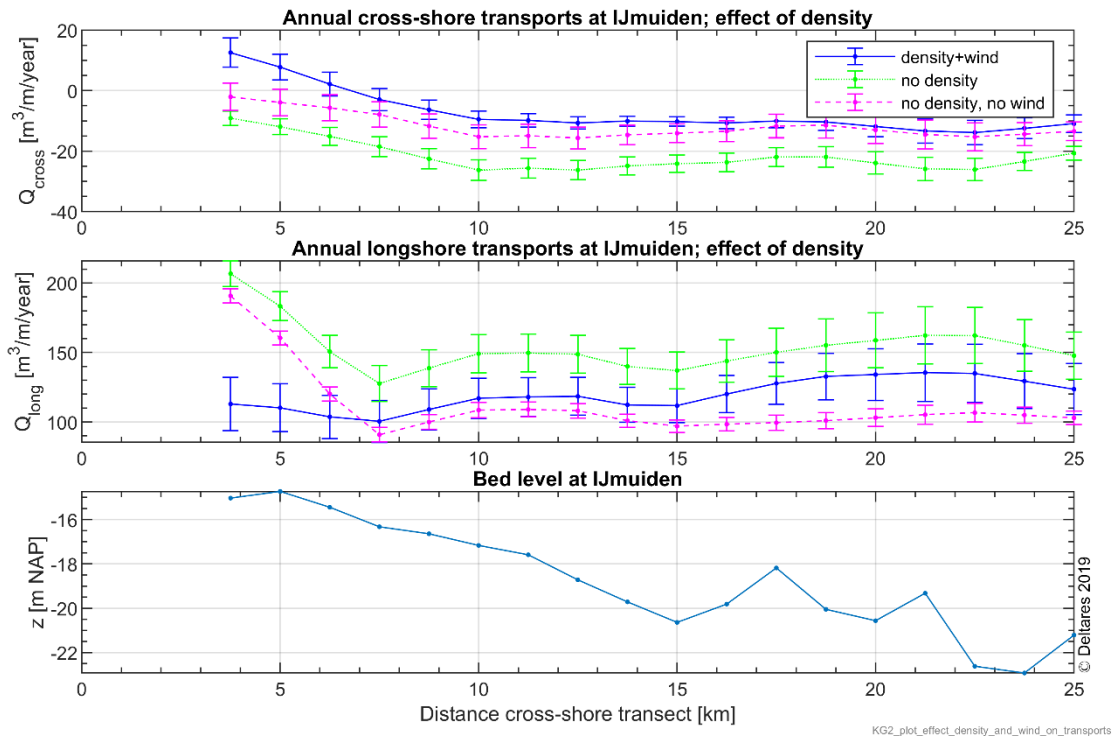


Figure 5.31 Effect of density on the cross-shore and alongshore transport rates in the IJmuiden transect based on computations for years 2013-2017.

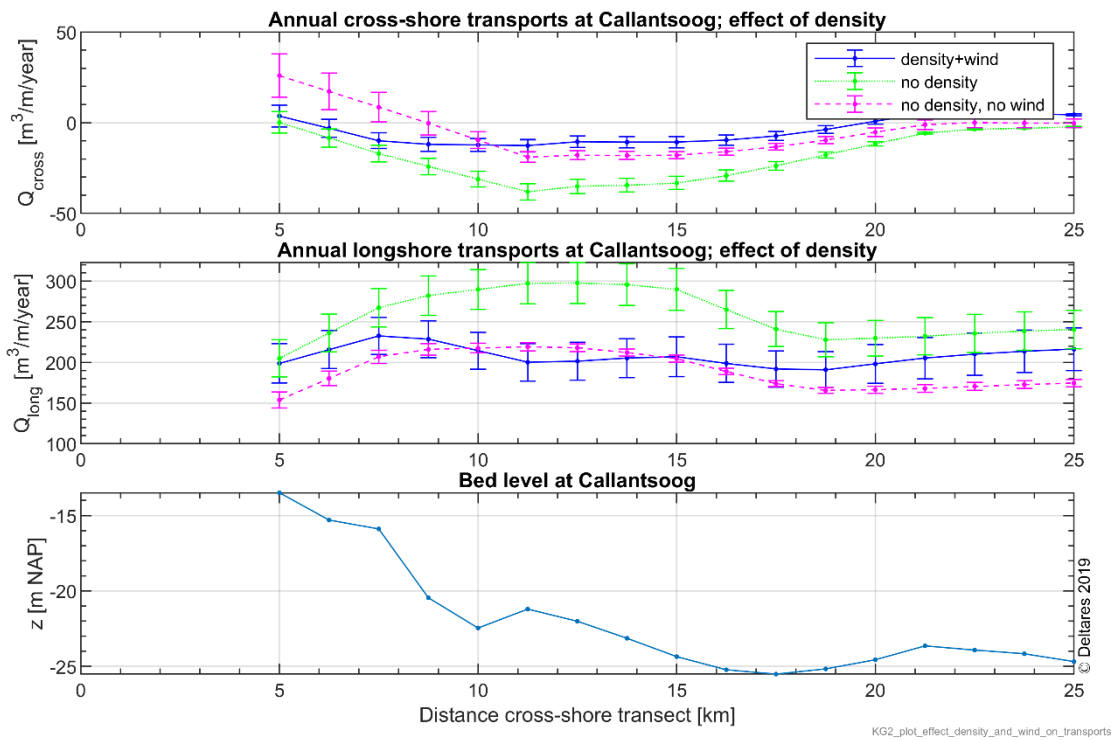


Figure 5.32 Effect of density on the cross-shore and alongshore transport rates in the Callantsoog transect based on computations for years 2013-2017.

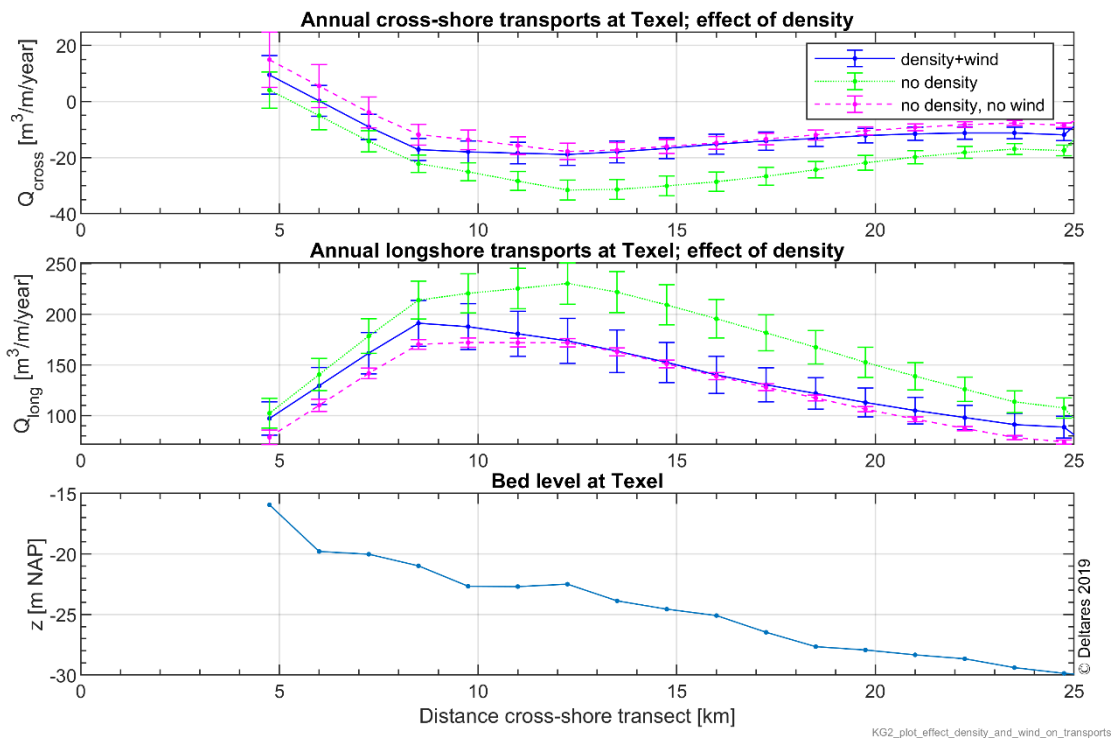


Figure 5.33 Effect of density on the cross-shore and alongshore transport rates in the Texel transect based on computations for years 2013-2017.

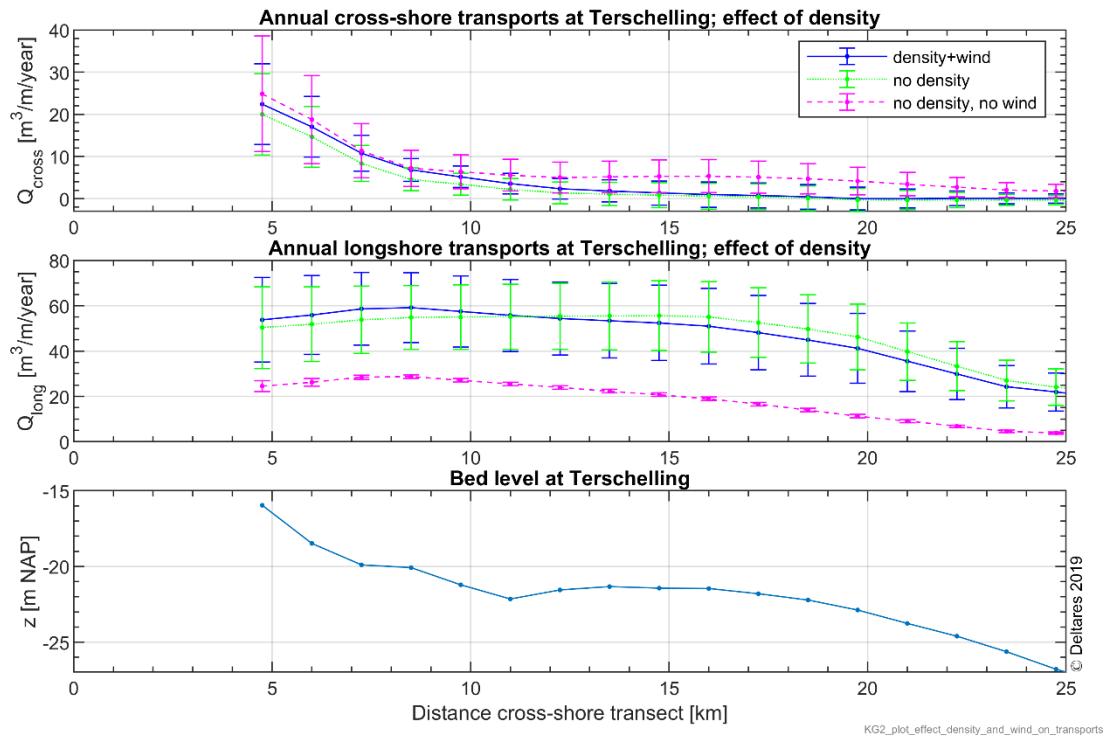


Figure 5.34 Effect of density on the cross-shore and alongshore transport rates in the Terschelling transect based on computations for years 2013-2017.

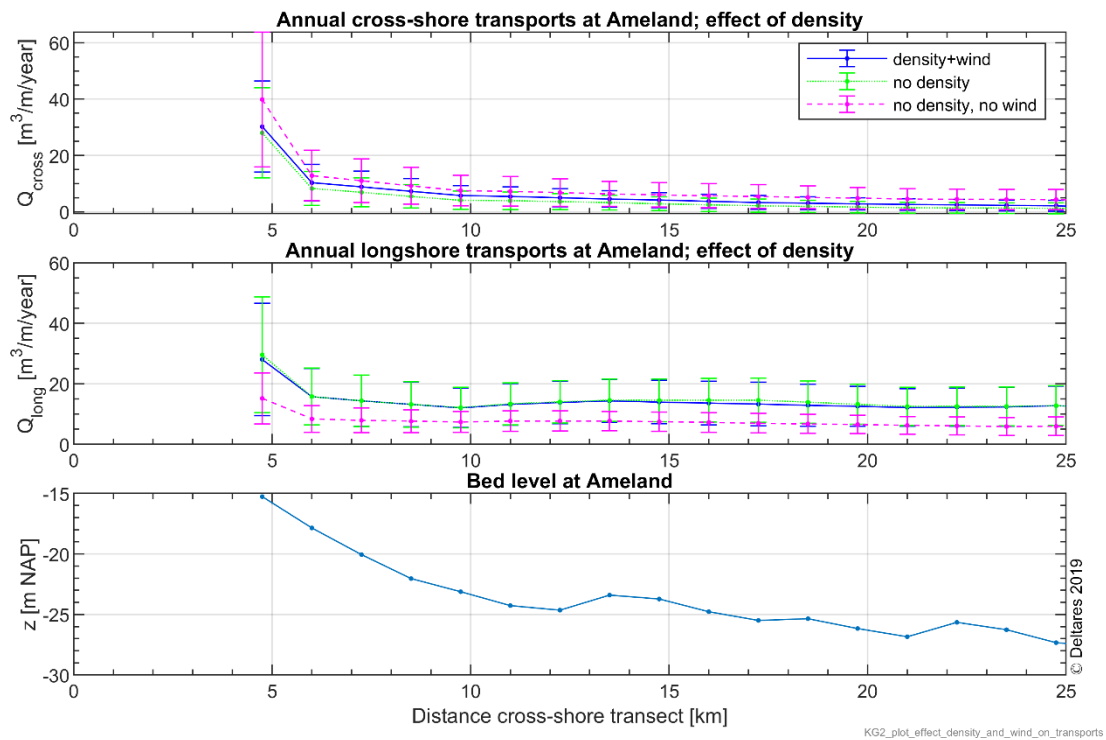


Figure 5.35 Effect of density on the cross-shore and alongshore transport rates in the Ameland transect based on computations for years 2013-2017.

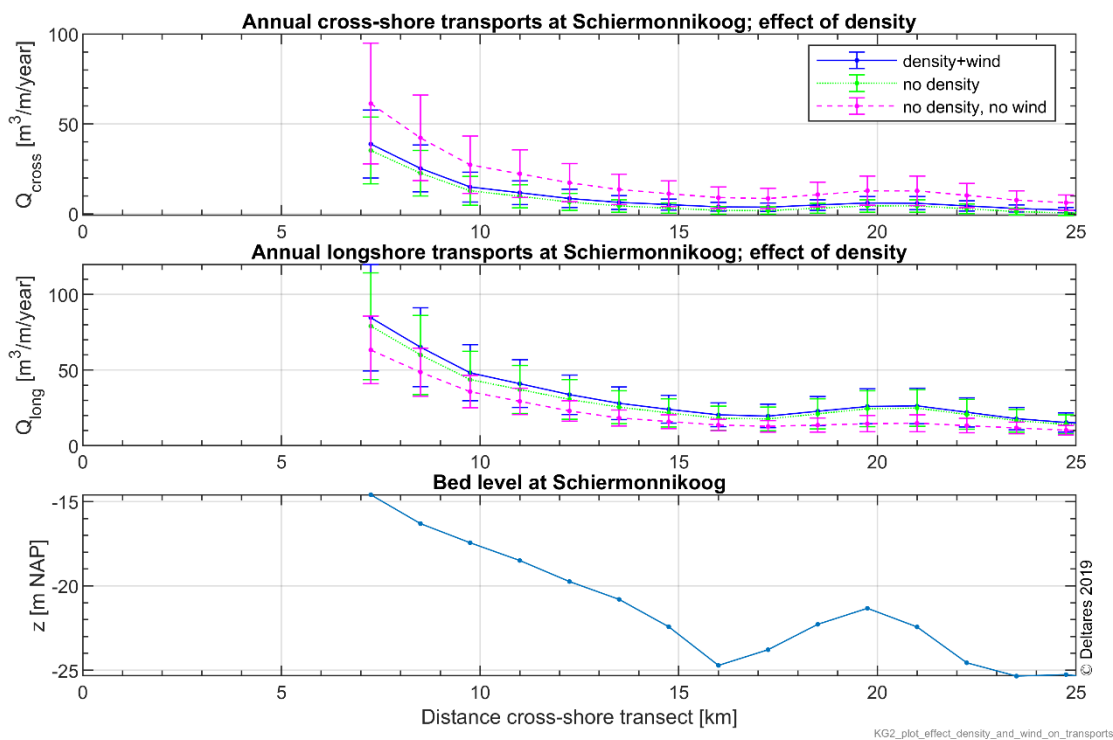


Figure 5.36 Effect of density on the cross-shore and alongshore transport rates in the Schiermonnikoog transect based on computations for years 2013-2017.

Figure 5.37 and Figure 5.38 show the transports without effect of density decomposed into alongshore and cross-hore component along the NAP-20 and NAP-15 contour, respectively. Comparing these with Figure 5.26 and Figure 5.27 (including effects of density) it can be seen that the alongshore transport are generally larger when turning off density effects. In cross-shore direction, the onshore directed transports are generally much smaller (or negligibly small) and the offshore directed transport are larger when turning off the effect of density. This is most pronounced along the Zeeland and Holland coast between Westkapelle and Texel.

Figure 5.39 and Figure 5.40 show the transports without effect of density and without wind decomposed into alongshore and cross-hore component along the NAP-20 and NAP-15 contour, respectively. Comparing these with the previous figures (without only density) it can be seen that also turning off wind partly compensates for turning off density alone. The offshore directed transports are smaller when turning off wind. In contrast to density effects, wind not only plays an important role along the Zeeland and Holland coasts but also along the Wadden island coasts.

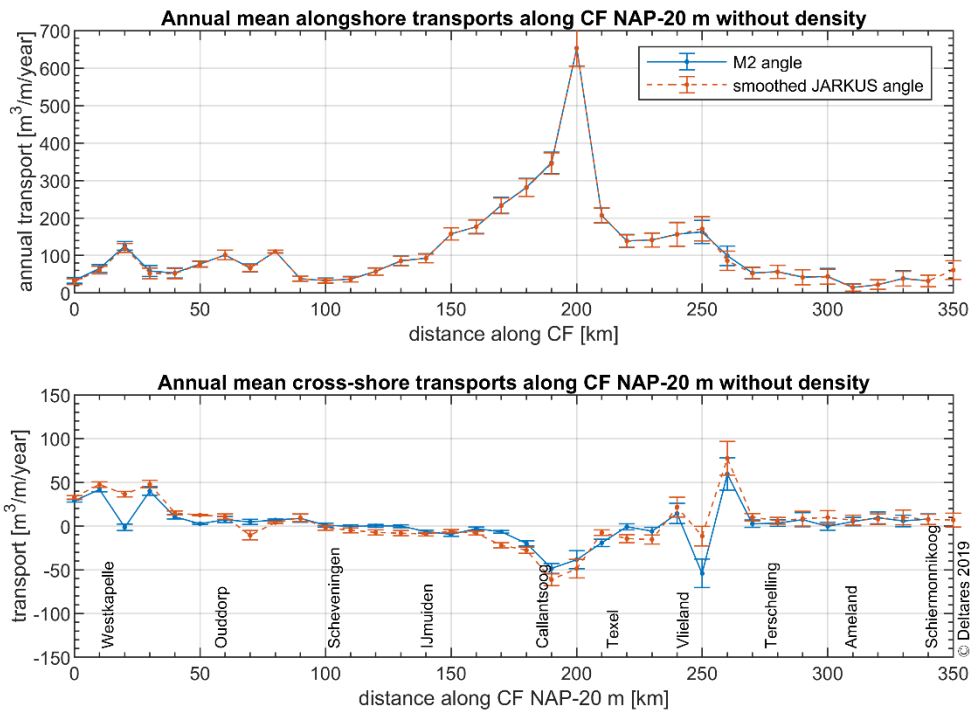


Figure 5.37 Annual mean alongshore (top panel ) and cross-shore (lower panel) transport rates along the offshore boundary of the present coastal foundation at the NAP-20 m based on computations for years 2013-2017 **without effect of density**. The blue line indicates the transport component using the major M2 axis as coast angle and the light brown dashed line using the smoothed JARKUS coast angle.

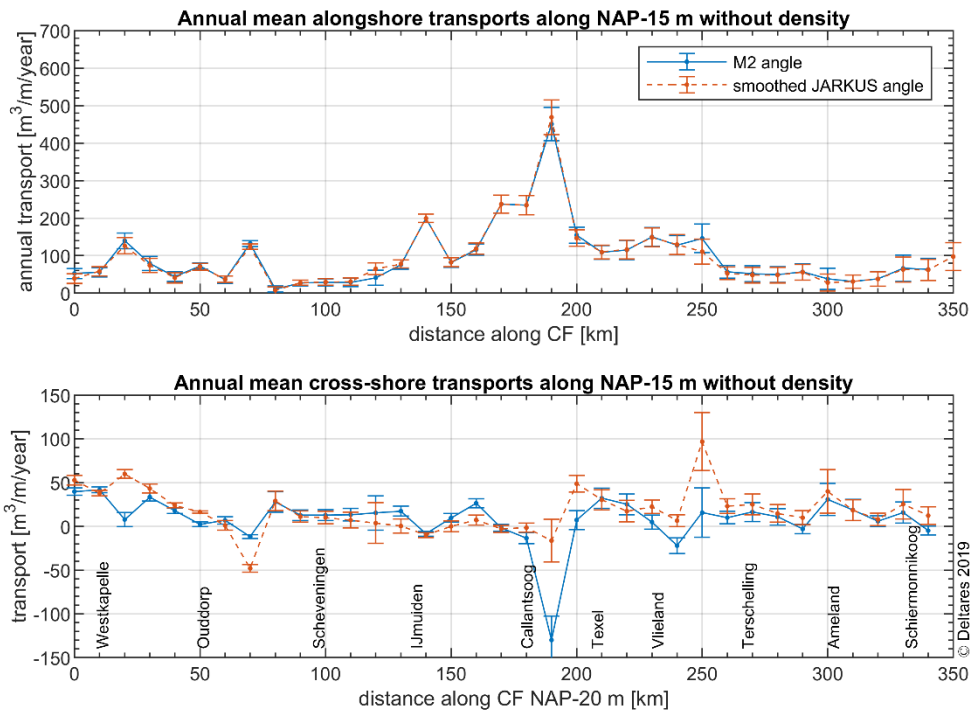


Figure 5.38 Annual mean alongshore (top panel ) and cross-shore (lower panel) transport rates along the NAP-15 m suggested by Vermaas et al. (2015) based on computations for years 2013-2017 **without effect of density**. The blue line indicates the transport component using the major M2 axis as coast angle and the light brown dashed line using the smoothed JARKUS coast angle.

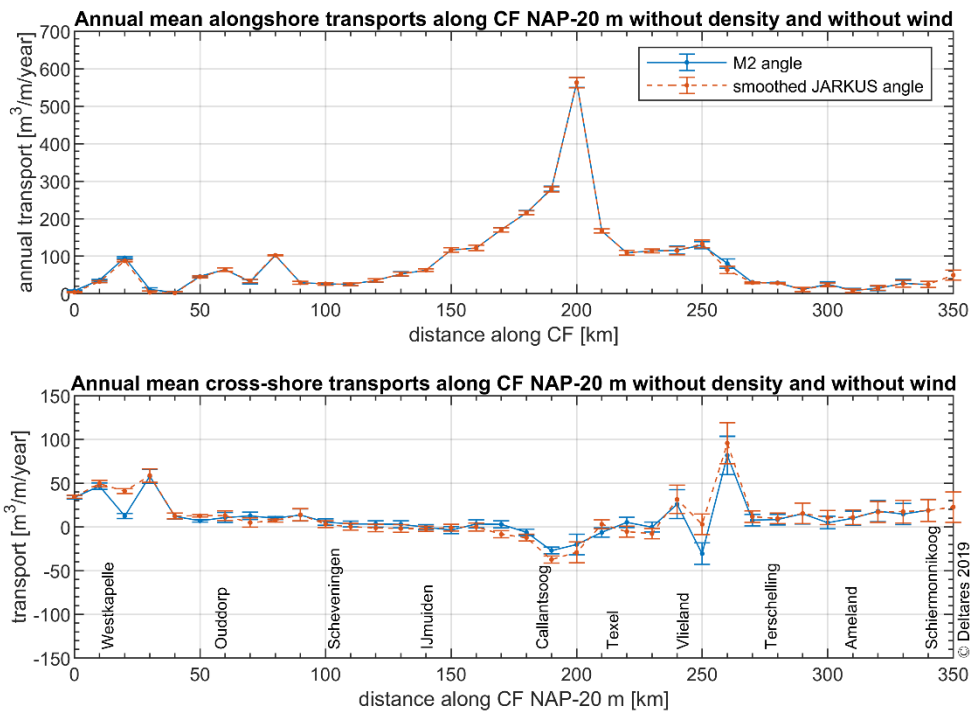


Figure 5.39 Annual mean alongshore (top panel ) and cross-shore (lower panel) transport rates along the offshore boundary of the present coastal foundation at the NAP-20 m based on computations for years 2013-2017 **without effect of density and without wind**. The blue line indicates the transport component using the major M2 axis as coast angle and the light brown dashed line using the smoothed JARKUS coast angle.

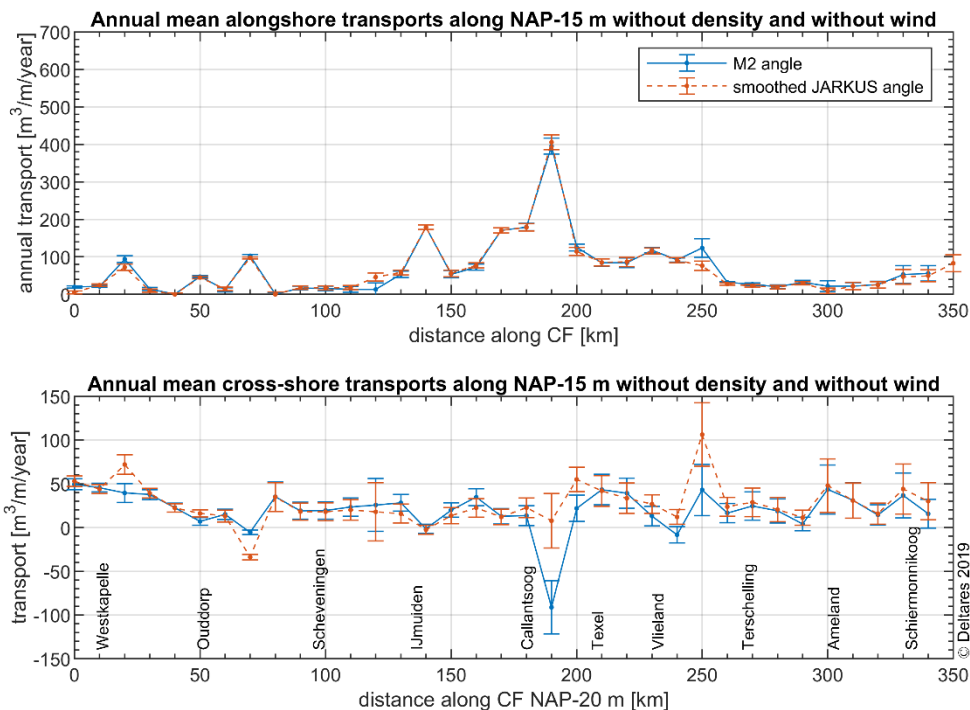


Figure 5.40 Annual mean alongshore (top panel ) and cross-shore (lower panel) transport rates along the NAP-15 m suggested by Vermaas et al. (2015) based on computations for years 2013-2017 **without effect of density and without wind**. The blue line indicates the transport component using the major M2 axis as coast angle and the light brown dashed line using the smoothed JARKUS coast angle.

#### 5.4.3 Contribution of storm events to the annual transports

To study the relative importance of different wave heights on the cross-shore transports, we clustered the computed cross-shore transports into different wave height classes and determined the relative contribution of each wave height class to the total cross-shore transport rate. This we performed for six different locations, i.e. Westkapelle, Scheveningen, IJmuiden, Callantsoog, Terschelling and Schiermonnikoog, along the offshore boundary of the present coastal foundation.

Figure 5.41 shows the cross-shore transports as a function of wave height, the probability of different wave height classes and the relative contribution of each wave height class to the total cross-shore transport rate for the six selected locations.

This figure illustrates that larger transports generally occur for larger wave heights. However, negligibly small transports may also occur for large wave heights if the flow velocities are small. Figure 5.41 also shows that significant wave heights of 0.5-1.0 m occur most frequently along the Dutch coast.

Although it can hardly be seen from Figure 5.41, the probability of occurrence of the highest waves of 4 to 6 m is higher at Terschelling and especially Schiermonnikoog than at the other locations (see also par. 5.3). This results in a higher contribution to the cross-shore transports for these wave classes at these locations.

Figure 5.41 also shows that the net cross-shore transport is sometimes determined by a delicate balance between an onshore and offshore directed component. If the net cross-shore transport during normal conditions is negligibly small because onshore and offshore components are equal in magnitude, a storm may push the balance to one direction. In Figure 5.41 this can most clearly be observed for the computed transports at Terschelling and Schiermonnikoog.

These results suggest that storm conditions play an important role for the transport rates at the lower shoreface. We should note that our modelling approach underestimates the residual flow under high energetic conditions (see Chapter 4). This requires further investigation.

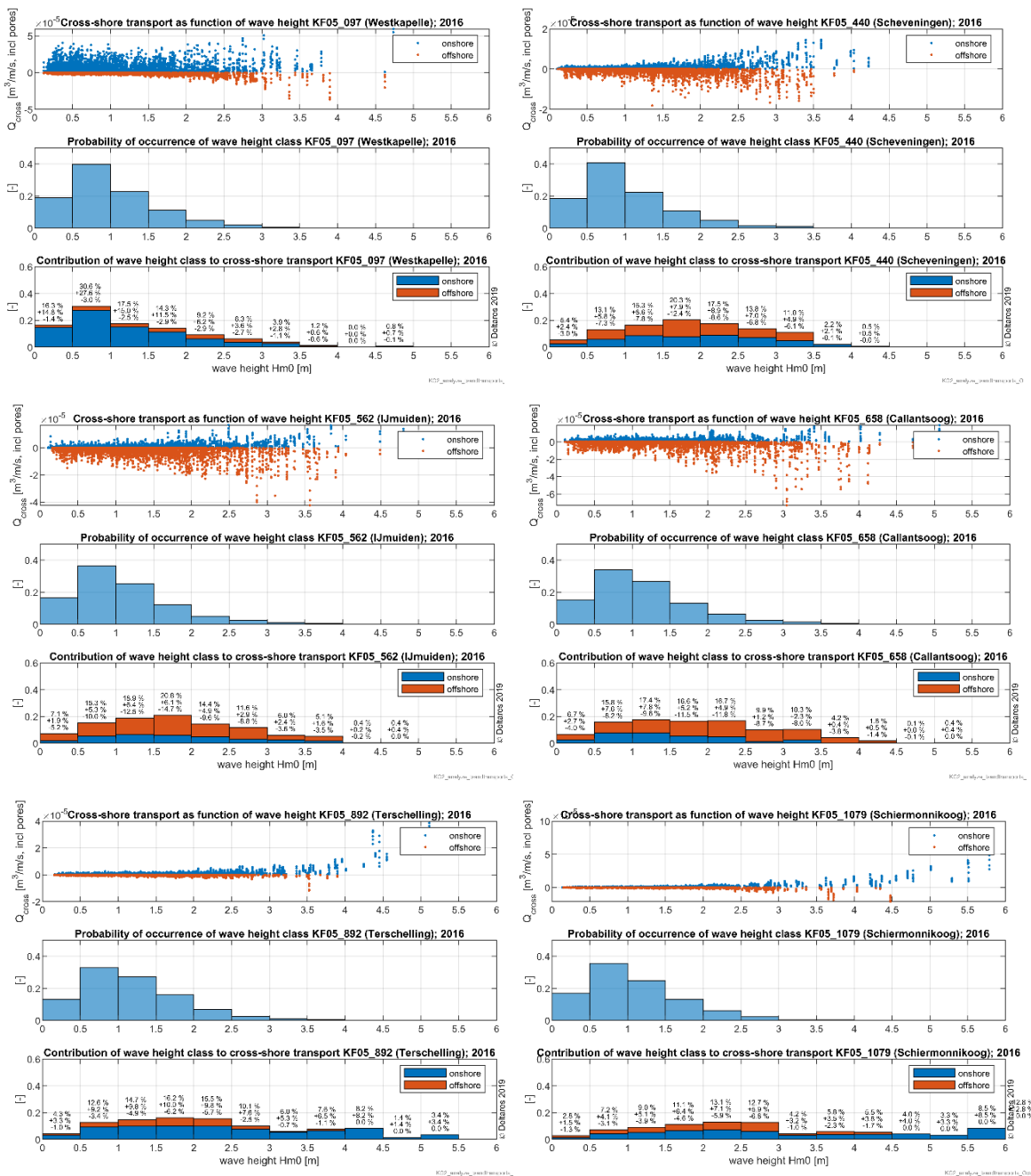


Figure 5.41 Transports as a function of wave height, probability of different wave height classes and relative contribution of each wave height class to the total cross-shore transport rate.



## 6 Discussion, conclusions and recommendations

### 6.1 Discussion

The annual transport rates at the lower shoreface computed here are comparable to those presented by Van Rijn (1997) for the southern part of the central Dutch coast (between Scheveningen and Egmond aan Zee). However, for the northern part of the central Dutch coast (from Egmond to Callantsoog) the transport rates are a factor of 3-5 larger. This difference is likely caused by the difference in methodology. Van Rijn (1997) applied schematized tide, wind and wave conditions whereas here the transports are based on brute force computations (real time series).

Decomposing the transports into alongshore and cross-shore components using two different definitions of the coast angle illustrates the sensitivity of the cross-shore transports to the definition of the coast angle. For many parts of the coast the difference between both methods is small but near inlets such as the Marsdiep inlet the difference can be large.

The modelling approaches applied here underestimates the measured residual flows during high wave events. This results in an underestimation of the transport rates under these conditions and the relative contribution of these conditions to the net annual mean transport rate. In case of the Delft3D model of Ameland and Terschelling this may be caused by the limited size of the model due to which residual flow over a larger domain is not captured. In case of the 3D DCSM-FM model this may be caused to the limited model resolution due to which exchange between the North Sea and the tidal basins is insufficiently captured.

### 6.2 Conclusions

Dutch coastal policy aims for a safe, economically strong and attractive coast. This is achieved by maintaining the part of the coast that support these functions; the coastal foundation. The coastal foundation is maintained by means of sand nourishments.

Up to now, it has been assumed that transports across the coastal foundation's offshore boundary at the 20 m depth contour are negligibly small. In the framework of the Coastal Genesis 2.0 program we investigated sand transports across this boundary and across other depth contours at the lower shoreface. Based on this, possibilities for an alternative offshore boundary of the coastal foundation will be discussed in a synthesis report. The lower shoreface is the zone where the mixed action of shoreface currents (tide-, wind- and density gradient driven) and shoaling and refracting waves is predominant. Transport rates are relatively small and hence the bed levels in the lower shoreface undergo relatively slow adaptations.

Earlier work has mainly focused on the central Dutch coast between Hoek van Holland and Den Helder without the effects of tidal inlets or estuaries. The computations were based on cross-shore profile models (2DV) or horizontal depth-averaged models (2DH). This required schematizing wave and current conditions based on results from large scale models or excluding effects such as salinity and 3D circulation in order to keep the computation time limited. However, 3D circulation patterns by e.g. fluid density gradients play an important role for the total cross-shore transport rate at water depths deeper than about 8 m.

So far, process-based 3D modelling to study the transport processes along the entire Dutch coast has not been carried out.

We developed an efficient approach to compute the annual sand transport rates at the Dutch lower shoreface, based on the 3D Dutch Continental Shelf Model with Flexible Mesh (3D DCSM-FM), a wave transformation tool and a 1DV sand transport module. We have made flow,

wave and sand transport computations for the years 2013-2017 using brute force (real-time) time series which means that we have not made simplifications or schematizations to the hydrodynamic input but computed the transports based on the 'real' hydrodynamics.

In the following paragraphs we present conclusions of the hydrodynamic validation and sensitivity analysis after which we will answer the main research questions.

### 6.2.1 Hydrodynamic validation

The following conclusions can be drawn from the hydrodynamic validation:

- The wave transformation tool is an appropriate tool to derive wave parameters at the lower shoreface, indicated by a good and equal performance of the tool over the depth range studied (NAP -20 till -10 m).
- The 3D DSCM-FM and CGII TA models perform well in reproducing (depth averaged) flow velocities at the lower shoreface, indicated by bias values of less than 0.06 m/s and RMSE values less than 0.18 m/s.
- The 3D DSCM-FM and CGII TA models perform very well during normal wind and wave conditions but their performance decreases during high energetic conditions. Residual currents are underestimated under these conditions.

The performance of the models decreases with decreasing water depths because the wind and wave induced residual currents become stronger at shallower depths. In quantifying annual sand transports at the Dutch lower shoreface the model results have therefore only been applied for water depths larger than 15 m.

### 6.2.2 Sensitivity analysis

Conclusions from the sensitivity analyses are summarized as follows:

- The sensitivity analysis on wave input suggests that the offline approach slightly overestimates the effect of waves on the net transports, except at tidal inlets where the difference is overruled by the effect of residual currents under energetic conditions.
- The sensitivity analysis on velocity input suggests that the offline approach tends to underestimate the net transports as compared to transports determined using measured velocities under high energetic conditions. The absolute underestimation on the long term is, however, hard to determine from these analyses because it is based on relatively short measurement periods.
- The difference between the online and offline approach is generally smaller than 50%, which is good in terms of sand transport predictions.

### 6.2.3 Main research questions

The main research questions are described as follows:

1. How do the hydrodynamics conditions vary along and across the Dutch Lower Shoreface?
  - a) Peak tidal velocities
  - b) Residual flow
  - c) Waves
2. What are typical net sand transport rates on the Dutch lower shoreface?
  - a) Which physical processes determine lower shoreface net sand transport?
  - b) How does net transport vary across and along the Dutch lower shoreface?
  - c) What is the effect of storms?

The first research question helps in understanding the variation of the transports along and across the lower shoreface in the second question. The answers to these questions are described in the following paragraphs

### 6.2.3.1 How do the hydrodynamics conditions vary along and across the Dutch Lower Shoreface?

#### 1a: Peak tidal velocities

The peak flood velocities vary between 0.6 and 0.8 m/s along the NAP-20 m contour. The computations show a small increasing trend between Westkapelle and Ouddorp, a decreasing trend between Ouddorp and Scheveningen and an increasing trend again between Scheveningen and Texel. The peak flood velocities decrease from Texel towards Schiermonnikoog.

The peak ebb velocities vary between 0.5 and 0.7 m/s with more or less the same trends as the peak flood velocities along the coast. However, the difference between the peak flood and ebb velocities, reflecting tidal asymmetry, increases from Westkapelle towards Texel (increasing tidal asymmetry) and decreases again from Texel to Terschelling and Schiermonnikoog (decreasing tidal asymmetry).

The peak flood velocities are generally slightly smaller (about 3%) when moving from the NAP-20 m contour to the NAP-15 contour. The peak ebb velocities are about 6% smaller, which results in a slightly larger tidal velocity asymmetry at smaller water depths.

The year-to-year variation of the annual mean peak tidal velocities is small ( $\leq 0.01$  m/s).

#### 1b: Annual mean residual flow

The mean annual computed residual flows along the Zeeland and Holland coast show a clear effect of the wind and the fresh water outflow of the river Rhine and the Haringvliet into the saline North Sea. This causes a difference in magnitude and direction between the near-bed and near-surface flows. The near-bed velocities are more shoreward directed. The near-surface flows are clearly larger at Hoek van Holland because of the River Rhine outflow and flow contraction due to the presence of Maasvlakte II. Near-bed velocities are important for the direction of the transports because sand concentrations are largest near the bed.

Depth-averaged mean annual computed residual flow magnitudes are relatively small along the Zeeland coast at Westkapelle and Ouddorp (0.01 m/s), increase to 0.03-0.04 m/s along the Holland coast at Scheveningen and IJmuiden and increase further to 0.06-0.08 m/s at Callantsoog and Texel. The mean residual flow decreases to 0.03-0.04 m/s at Terschelling and Schiermonnikoog. The residual flows near the bed are smaller and generally have an onshore directed component. This is onshore component is less pronounced at Callantsoog and Texel.

#### 1c: Waves

Average annual mean significant wave height at NAP-20 m is just over 1 m at Westkapelle, Ouddorp and Scheveningen. It increases to about 1.2 at IJmuiden and Callantsoog and is about 1.3 m at Texel. The mean annual wave height is about 1.2 m at Terschelling and Schiermonnikoog.

The average 90% exceedance value of  $H_{m0}$  at NAP-20 m is 1.7-1.9 m at Westkapelle, Ouddorp and Scheveningen. It increases to about 2 m at IJmuiden and Callantsoog and is about 2.3 m at Texel. The 90% exceedance value of  $H_{m0}$  is about 2.1-2.2 m at Terschelling and Schiermonnikoog.

The maximum significant wave height is 4.7-5.0 m at Westkapelle, Ouddorp and Scheveningen. It increases to about 5.1-5.2 m at IJmuiden and Callantsoog and is about 5.4 m at Texel. The maximum is about 5.3 m at Terschelling and 6.2 m at Schiermonnikoog. The maximum wave height varies from year to year with about 0.4-1.0 m.

### 6.2.3.2 What are typical net sand transport rates on the Dutch lower shoreface?

#### 2a: Which physical processes determine lower shoreface net sand transport?

Sand transport at the Dutch lower shoreface is determined by tide, wind and density driven currents and by waves. Variations in the net annual transport rates are determined by variations in peak tidal velocities (and asymmetry thereof), density driven residual flow, wind driven residual flow and waves. The effect of density difference and wind on the 3D structure of the flow cannot be neglected along the Dutch lower shoreface.

To study the effect of density and wind on the net annual transport rates and directions, we made 3D DCSM-FM model computations for the years 2013-2017 with only density turned off and both density and wind turned off, combined these with waves from the wave transformation matrix and computed sand transport with the 1DV transport model.

Density driven flow shows a tendency to be onshore directed near the bed because saline sea water flows towards the coast near the bed and fresh water river water spreads out into the North Sea near the surface. If this effect is turned off, the onshore directed density driven flow near the bed is switched off. Turning off density therefore reduces the onshore directed transport or enhances the offshore directed transport.

Wind driven flow has a strong onshore directed component near the surface because of the predominant wind directions along the Dutch coast and the shape of the coast with respect to the wind directions. The onshore wind driven flow near the surface is generally balance by a more offshore directed wind driven component near the bed (because of mass balance, otherwise all water would pile up at the coast). If wind is turned off, the offshore directed wind driven component near the bed is turned off. Turning off wind therefore enhances the onshore directed transport or reduces the offshore directed transport. This is in contrast to turning off density.

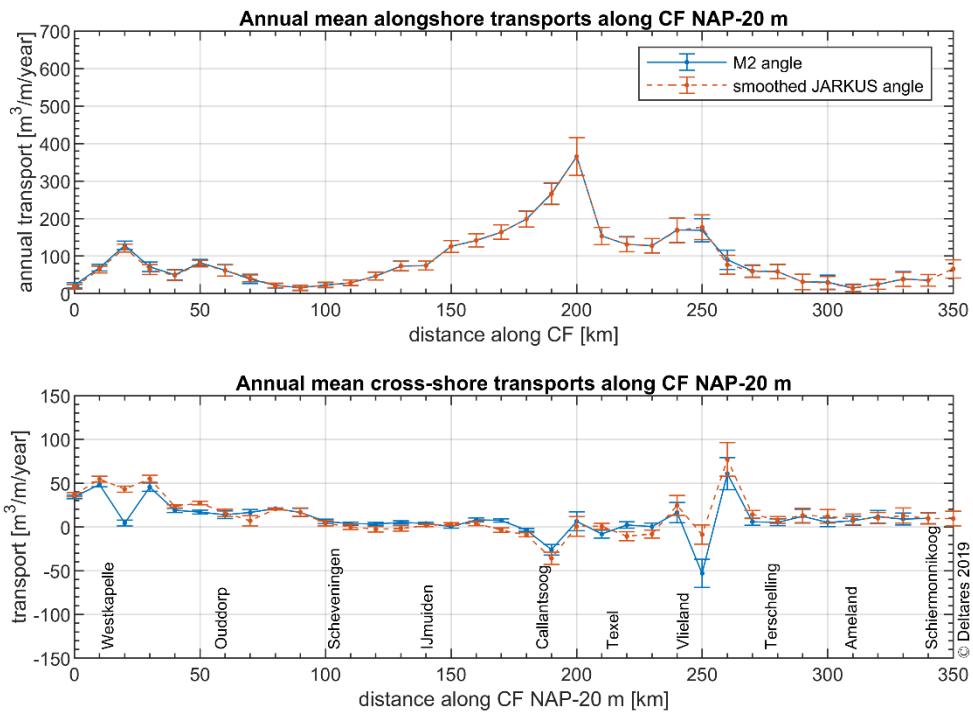
So, the general influence of the density-driven currents is that it enhances an onshore directed transport component. This effect is strongest along the Zeeland and Holland coast.

The general influence of the wind is that it enhances an offshore directed transport component. This effect plays a role along the entire Dutch coast but is less pronounced than the density effect.

#### 2b: How does net transport vary across and along the Dutch lower shoreface?

Our computations show decreasing annual mean alongshore transports from Westkapelle to Scheveningen, increasing from Scheveningen to the inlet between Callantsoog and Texel (Marsdiep) and decreasing again towards Schiermonnikoog at the NAP-20 contour (top panel Figure 6.1). Alongshore transports at the NAP-15 m contour were on average 10% smaller than at the NAP-20 m contour (compare top panels Figure 6.2 and Figure 6.1).

The lower panels in Figure 6.1 and Figure 6.2 illustrate the sensitivity to the definition of the coast angle to the cross-shore transports. However, irrespective of the exact definition of the coast angle, our analysis shows predominantly onshore directed transports for the coastal stretch from Westkapelle to about 10 km south of Callantsoog and at the Wadden islands. The computed transports show a tendency to become offshore directed at the inlets between Callantsoog and Texel (Marsdiep) and between Vlieland and Terschelling (Vliestroom). The onshore directed transport component was generally larger for smaller water depths closer to the shore, except near the aforementioned inlets.



KG2 plot annual transport KF05 v01

Figure 6.1 Annual mean alongshore (top panel ) and cross-shore (lower panel) transport rates along the offshore boundary of the present coastal foundation at the NAP-20 m based on computations for years 2013-2017. The blue line indicates the transport component using the major M2 axis as coast angle and the light brown dashed line using the smoothed JARKUS coast angle.

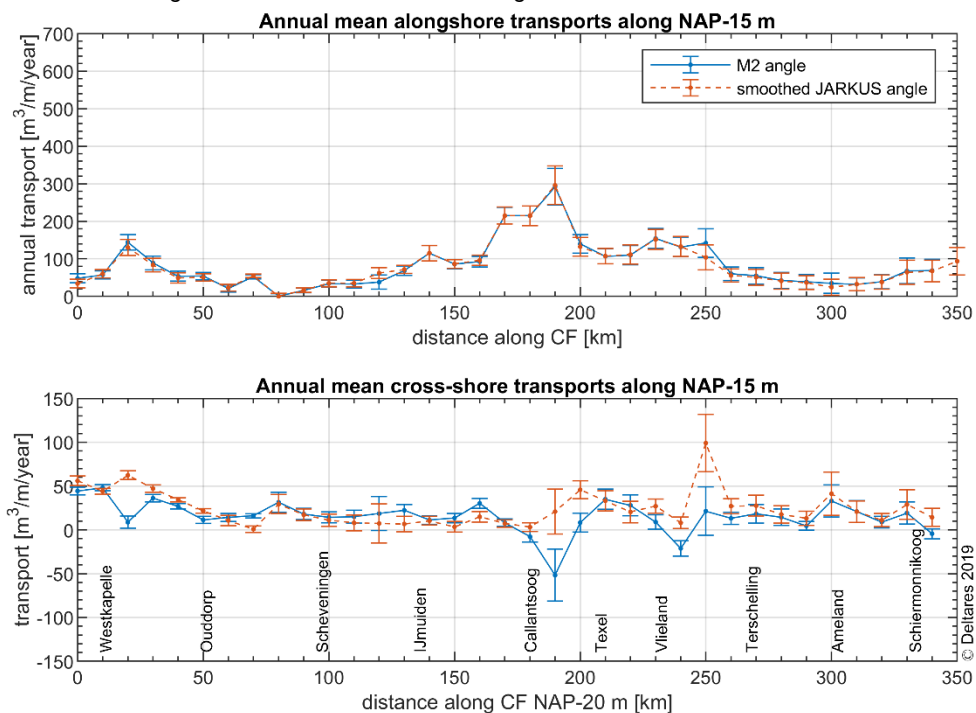


Figure 6.2 Annual mean alongshore (top panel ) and cross-shore (lower panel) transport rates along the NAP-15 m suggested by Vermaas et al. (2015) based on computations for years 2013-2017. The blue line indicates the transport component using the major M2 axis as coast angle and the light brown dashed line using the smoothed JARKUS coast angle.

### 2c: What is the effect of storms?

Larger transports generally occur for larger wave heights. However, negligibly small transports may also occur for large wave heights if the flow velocities are small. Significant wave heights of 0.5-1.0 m occur most frequently along the Dutch coast.

The probability of occurrence of the highest waves of 4 to 6 m is higher along the North Sea coast of the eastern Wadden islands (Terschelling and especially Schiermonnikoog) than at the other locations along the Dutch coast. This results in a higher contribution to the cross-shore transports for these wave classes at these locations.

The net cross-shore transport is sometimes determined by a delicate balance between an onshore and offshore directed component. If the net cross-shore transport during normal conditions is negligibly small because onshore and offshore components are equal in magnitude, a storm may push the balance to one direction. Our results suggest that storm conditions play an important role for the transport rates at the lower shoreface. We should note however that our modelling approach underestimates the residual flow under high energetic conditions. This requires further investigation.

## 6.3 Recommendations

The following recommendations are made:

- Because of the underestimation of residual currents in the North Sea along the Wadden islands under high wave conditions:
  - increase the 3D DCSM-FM model resolution around tidal inlets and within the Wadden Sea to improve representation of the exchange between the North Sea and the Wadden Sea
- Because of the difference between the transport computed here and those computed by Van Rijn (1997) transports for the northern part of the central Dutch coast (from Egmond to Callantsoog):
  - Compare the schematized hydrodynamic input data used by Van Rijn (1997) with the brute force conditions applied here and analyse the relative contribution of the different conditions in flood and ebb direction to assess the exact reason for the mismatch
- Because of the relatively strong increase in the computed residual currents and tidal velocities from IJmuiden to Callantsoog and lack of validation data:
  - make measurements in the Callantsoog transect at 15 and 20 m water depth
  - validate the models with these measurements
- Because the offline approach as applied here is only valid for water depths > 15 m:
  - Make model computations with a detailed 3D nearshore model for the years 2013-2017 to cover the entire profile from the lower shoreface to beach and dunes
- Assess sensitivity to sand size ( $D_{50}$ ), bed roughness, wave skewness, Longuet-Higgins streaming, Stokes drift and undertow.
- Derive analytical expressions to account for the currently missing wave-driven currents.

## 7 References

- Battjes, J.A., Janssen, J.P.F.M., 1978. Energy loss and set-up due to breaking of random waves. Proc. 6th Int. Conf. on Coastal Engineering. ASCE, New York, pp. 570–587.
- Battjes, J.A., Stive, M.J.F., 1985. Calibration and verification of a dissipation model for random breaking waves. J. Geophys. Res. 90, 9159–9167.
- Bijker, E.W., 1986. Scour around structures. Proc. on the 20th Intern. Conf. on Coastal Engineering, Taipei, Taiwan, 1986, Vol.11, pp.1754-1768.
- Boers, M., 2005. Surf zone turbulence. Ph.D. thesis, Delft University of Technology, The Netherlands.
- De Fockert, A., & Luijendijk, A. (2011). Wave look-up table: Building with Nature. Delft, The Netherlands.
- Grasmeijer, B.T., 2018. Method for Calculating Sediment Transport on the Dutch Lower Shoreface. Deltares report 1220339-000. 25 p.
- Grasmeijer, B.T., 2019. Method for calculating annual sand transports on the Dutch lower shoreface to assess the offshore boundary of the Dutch coastal foundation. Proceedings of the 9<sup>th</sup> International Conference Coastal Sediments Conference 2019. Tampa/St. Petersburg, Florida, USA. World Scientific Publishing
- Hop, M. (2017). The impact of the Rhine ROFI on the alongshore variability of cross-shore sediment transport of the Holland coast. MSc. Thesis, Delft University of Technology.
- Hulscher, S.J.M.H., Ribberink, J.S., Knaapen, M.A.F., 2002. Syllabus Marine Dynamics II. Civil Engineering & Management, University of Twente, The Netherlands.
- Isobe, M., and Horikawa, K., 1982. Study on water particle velocities of shoaling and breaking waves. Coastal Engineering in Japan, 25, 109–123
- Knook, P.P., 2013. Sediment transport on various depth contours of the 'Holland Coast' shoreface. MSc. thesis, 82 pages, Delft University of Technology, Delft, The Netherlands.
- Lesser, G. R., Roelvink, J. A., van Kester, J. a. T. M., & Stelling, G. S. (2004). Development and validation of a three-dimensional morphological model. Coastal Engineering, 51(8–9), 883–915. <https://doi.org/10.1016/j.coastaleng.2004.07.014>
- Leummens, M. (2018). Hydrodynamics and sand transport on the lower shoreface of the Ameland tidal inlet. Retrieved from <https://www.utwente.nl/en/et/wem/education/msc-thesis/2018/leummens.pdf>
- Miche, M. 1944. Mouvement ondulatoires de la mer. Annales des ponts et chaussee, 114, 25-78, 131-164, 270-292, 369-406. (in French)
- Nederhoff, C. M., Schrijvershof, R. A., Tonnon, P. K., & van der Werf, J. J., 2019. The Coastal Genesis II Terschelling - Ameland inlet (CGII-TA) model.
- Roelvink, J.A., Stive, M.J.F., 1990. Sand transport on the shoreface of the Holland coast, in: Proceedings of the 22nd International Conference on Coastal Engineering. Delft, The Netherlands, pp. 1909–1922.
- Ruessink, B.G., Walstra, D. J. R., Southgate, H. N., 2003. Calibration and verification of a parametric wave model on barred beaches. Coastal Engineering, 48: 139-149.
- Roscoe, K. (2009). Extreme Offshore Wave Statistics in the North Sea, Extension of the measurement time series and comparison of methodologies. Report 1200103-042-HYE-0002, Deltares, The Netherlands.
- Svendsen, I.A., 1984, Mass flux and undertow in a surf zone. Coast. Eng. 8, 347–365.
- Svendsen, I.A., 2005. Advanced Series on Ocean Engineering, Introduction to Nearshore Hydrodynamics Volume 24, World Scientific, Singapore
- Van der Hout, C.M., Tonnon, P.K., De Ronde, J.G., 2009. Morphological effects of mega nourishment (No. 1200659-000). Deltares, Delft, The Netherlands.

- Van der Spek, A., Elias, E., Lodder, Q., Hoogland, R., 2015. Toekomstige suppletievolumes - Eindrapport. Rapport 1208140-005-ZKS-000 1. Deltares, Nederland. (in Dutch)
- Van der Werf, J.J., Giardino, A., 2009. Effect van zeer grootschalige zandwinning langs de Nederlandse kust op de waterbeweging, zandtransporten en morfologie (No. 1200996-000-NaN-0010). Deltares, Delft, The Netherlands.
- Van der Werf, J.J., Grasmeyer, B.T., Hendriks, E., Van der Spek A., Vermaas, T., 2017. Literature study Dutch lower shoreface. Report 1220339-004-ZKS-00001. Deltares, Delft, The Netherlands.
- Van Rijn, L.C. (1997). Sediment transport and budget on the central coastal zone of Holland. *Coastal Engineering*, 32, 61–90.
- Van Rijn, L. C. (2007). Unified View of Sediment Transport by Currents and Waves: part I and II. *Journal of Hydraulic Engineering*, (June), 649–667.
- Van Rijn, L.C. (2013). Principles of fluid flow and surface waves in rivers, estuaries, seas and oceans. Aqua Publications, The Netherlands.
- Van Rijn, L.C., Grasmeyer, B.T and Perk, L., 2018 Effect of channel deepening on tidal flow and sediment transport; Part I: sandy channels. *Ocean Dynamics*
- Walstra, D.J.R., Roelvink, J.A., Groeneweg, J., 2000. Calculation of wave-driven currents in a 3D mean flow model. *Edge, B. Coastal Engineering vol. 2. ASCE, New York*, pp. 1050–1063.
- Zijl, F., Veenstra, J., 2018. The 3D Dutch Continental Shelf Model - Flexible Mesh (3D DCMSM-FM). Setup and validation. Report 1220339-005-ZKS-0003. Deltares, Delft, The Netherlands.
- Zijl, F., Verlaan, M., & Gerritsen, H. (2013). Improved water-level forecasting for the Northwest European Shelf and North Sea through direct modelling of tide, surge and non-linear interaction Topical Collection on the 16th biennial workshop of the Joint Numerical Sea Modelling Group (JONSMOD) in Bre. *Ocean Dynamics*, 63(7), 823–847. <https://doi.org/10.1007/s10236-013-0624-2>



## A Wave driven currents

### A.1 Wave breaking

Wave breaking is an important driving mechanism for wave-driven currents, especially in the alongshore direction.

For irregular (random) waves there is no well-defined breakpoint. The largest waves break furthest offshore, and the smallest closest to the shoreline. A mean breaker line can be defined as where the wave height (significant wave height or root-mean-square wave height  $H_{rms} = H_s/\sqrt{2}$ ) is highest. Based on field data, Van Rijn (2013) suggested  $(H_s/h)_{max} \sim 0.4$  for a (nearly) horizontal bed with  $h$  the water depth. This corresponds for water depths of 20 m and 12 m to maximum (local) wave significant heights of  $\sim 8$  m and  $\sim 5$  m.

There are two important types of wave breaking. At deep water (large  $kh$ , with  $k = 2\pi/L$  the wave number, with  $L$  the wave length), waves can break when they become very steep (“white capping”). Miche (1944) proposed the following expression for the maximum wave steepness:

$$\left(\frac{H}{L}\right)_{max} = 0.14 \tanh(kh) \quad (1.1)$$

In shallow water depth-induced wave breaking occurs. Both breaker processes are captured in the expression of Battjes & Janssen (1978):

$$H_{max} = \frac{0.88}{k} \tanh\left(\frac{\gamma kh}{0.88}\right) \quad (1.2)$$

with  $\gamma$  the breaker criterion. In shallow water ( $kh \rightarrow 0$ ) this reduces to  $H_{max} = \gamma^* h$ . In deep water ( $kh \rightarrow \infty$ ),  $H_{max} = 0.88/k$ , which corresponds to  $(H/L)_{max} = 0.14$ ; in line with Eq. (1.1). Based on field data, Ruessink et al. (2003) derived the following expression for the gamma-parameter:

$$\gamma = 0.76kh + 0.29 \quad (1.3)$$

which was based on field data with  $0.25 < kh < 0.75$ . Eq. (1.1) - (1.3) are visualised in Figure A.1, with  $\gamma = 0.86$  beyond  $kh = 0.75$  and  $\gamma = 0.48$  below  $kh = 0.25$ . It is shown that the depth-induced breaking criterion of Ruessink et al. (2003) is stricter in shallow water than the Miche (1944) steepness criterion. Both criteria converge at deep water.

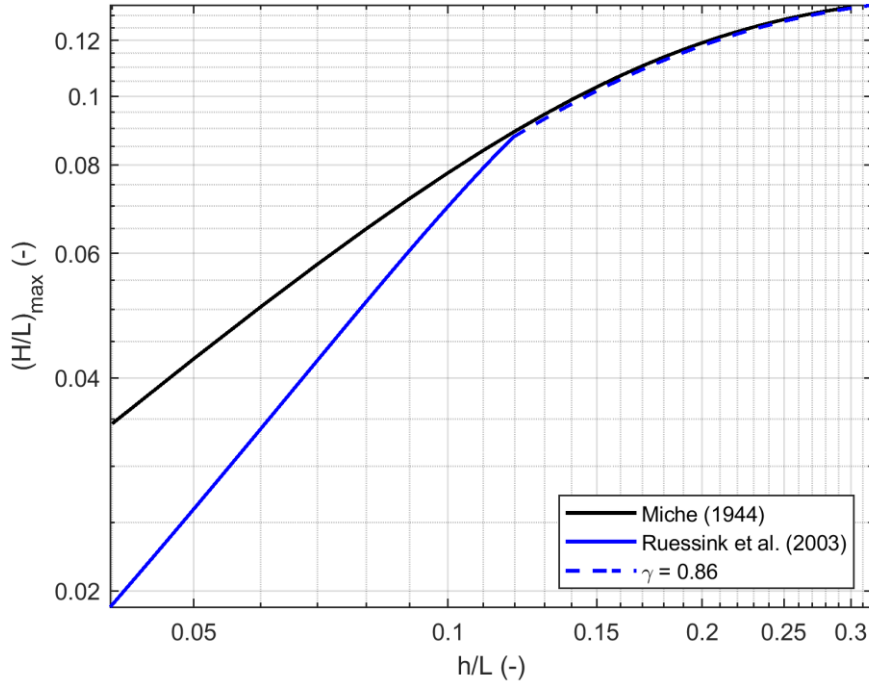


Figure A.1 Wave breaking diagram.

Assuming the commonly-used Rayleigh distribution, the fraction of breaking waves,  $Q_b$ , can be computed with (Battjes & Stive, 1985):

$$\frac{(1-Q_b)}{\ln Q_b} = -\left(\frac{H_{rms}}{H_{max}}\right)^2 \quad (1.4)$$

The wave breaking energy dissipation can then be computed with, for example, the expression of Battjes & Janssen (1978):

$$D_b = \frac{1}{4} \alpha \rho g f_p Q_b H_{max}^2 \quad (1.5)$$

with coefficient  $\alpha \approx 1$  and  $f_p$  the peak frequency. This expression can be used to compute wave transformation from the steady wave energy balance:

$$\frac{\partial(Enc \cos \theta)}{\partial x} = -D_b \quad (1.6)$$

assuming alongshore uniformity and neglecting wave energy dissipation due to bed friction.

As an example, Figure A.2 shows the wave transformation using this simple wave energy balance for a normal incident wave, constant bed slope (1:500) and constant wave period for different offshore (30 m water depth) wave conditions, respectively. The significant wave period was computed from the significant wave height,  $T_{1/3} = 6 \cdot H_s^{0.33}$ , following Van Rijn (2013), and it was assumed that  $f_p = f_{1/3}$ .

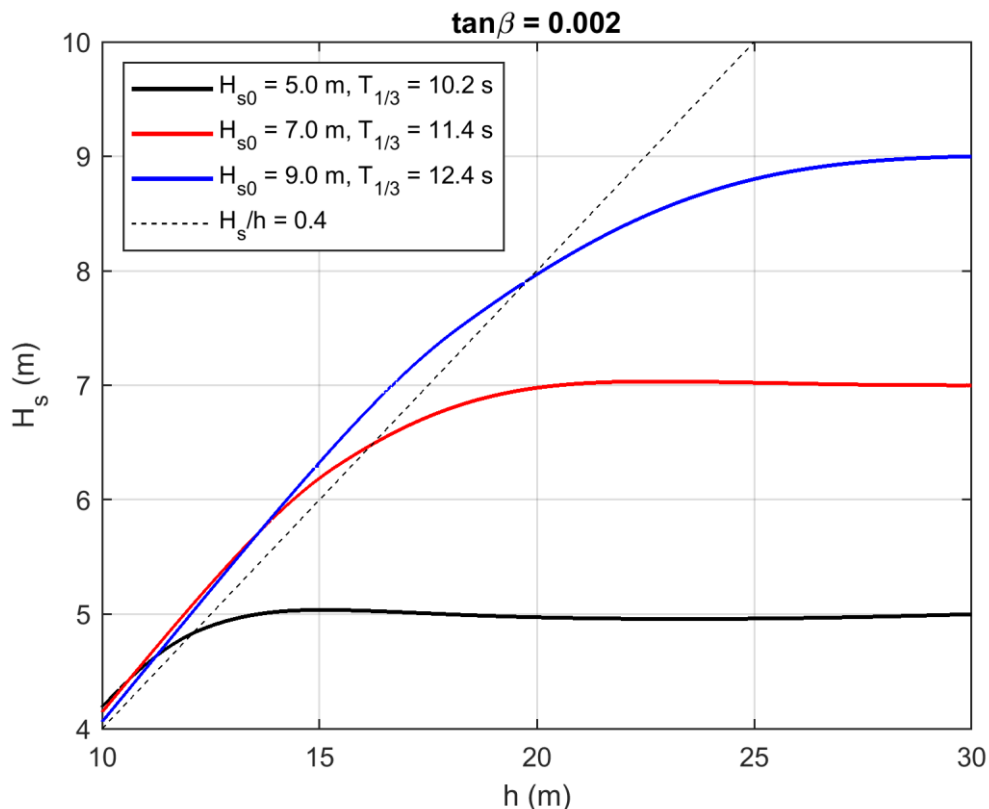


Figure A.2 Wave transformation using a simple wave energy balance for a normal incident wave, constant bed slope and constant wave period.

This figure shows that wave breaking becomes important, defined through  $H_s/h = 0.4$  according to Van Rijn (2013), at water depths of about 12, 16 and 20 m for the 5, 7 and 9 m offshore wave heights.

The offshore significant wave heights of 5, 7 and 9 m correspond to return periods about 0.5, 6 and 300 years for the Schiermonnikoog-Noord wave buoy (see Roscoe, 2009). The return periods are much longer for the milder Holland coast with  $\sim 1.5$  years for the 5 m wave height and  $\sim 1000$  years for the 7 m wave height (at Meetpost Noordwijk). These return periods indicate that wave breaking is not expected to play a role at water depths of 20 m. At 16 m water depth, wave breaking can be important at the Wadden Coast (return period of  $\sim 6$  years), but not along the Holland Coast. At the 12 m water depth, a storm with a return period of  $\sim 0.5$  year (Wadden Coast) and  $\sim 1.5$  years (Holland Coast) is probably sufficient to have an important impact on hydrodynamics.

## A.2 Wave-driven currents from a force perspective

Short waves exert a wave-averaged force on the fluid mass in which they propagate. This wave force can lead to additional water level variations (set-up/set-down) and/or wave-driven currents. The additional force is the result of horizontal gradients in the total mean momentum flux induced by waves:

$$R_x = -\frac{\partial S_{xx}}{\partial x} - \frac{\partial S_{xy}}{\partial y} \quad (1.7)$$

$$R_y = -\frac{\partial S_{yx}}{\partial x} - \frac{\partial S_{yy}}{\partial y} \quad (1.8)$$

in cross-shore ( $x$ , positive = onshore) and along-shore ( $y$ ) direction. In case of alongshore uniformity ( $d/dy = 0$ ) this reduces to:

$$R_x = -\frac{\partial S_{xx}}{\partial x} \quad (1.9)$$

$$R_y = -\frac{\partial S_{yx}}{\partial x} \quad (1.10)$$

The mean momentum flux due to waves is known as radiation stress. Using linear wave theory, the following expression can be derived for the radiation stress tensor:

$$S_{xx} = \left( n - \frac{1}{2} + n \cos^2 \theta \right) E \quad (1.11)$$

$$S_{xy} = S_{yx} = n \sin \theta \cos \theta E \quad (1.12)$$

$$S_{yy} = \left( n - \frac{1}{2} + n \sin^2 \theta \right) E \quad (1.13)$$

where the first index indicates the direction of the flux and the second the direction of momentum.  $n$  is the ratio of the group and wave celerity (0.5 for deep water, 1 for shallow water),  $\theta$  is the direction of wave advance ( $0^\circ =$  coast normal,  $90^\circ =$  coast parallel), and  $E = 1/8 \cdot \rho \cdot g \cdot H_{rms}^2$  is the wave energy with  $g$  the acceleration due to gravity and  $\rho$  the water density.

These wave forces can be added to the 2DH wave-averaged equation (neglecting the generally-small advection terms):

$$g \frac{\partial \bar{\zeta}}{\partial x} = \frac{R_x}{\rho h} - \frac{\bar{\tau}_{bx}}{\rho h} \quad (1.14)$$

$$g \frac{\partial \bar{\zeta}}{\partial y} = \frac{R_y}{\rho h} - \frac{\bar{\tau}_{by}}{\rho h} \quad (1.15)$$

where  $\bar{\zeta}$  the mean water level and  $\bar{\tau}_b$  the mean bed shear stress. The bed shear stress in  $x$ -direction is usually small ( $O(5\%)$ , see Svendsen, 2005) and ignored, and alongshore uniformity is generally assumed, which reduces these equations to:

$$g \frac{\partial \bar{\zeta}}{\partial x} = \frac{R_x}{\rho h} \quad (1.16)$$

$$0 = \frac{R_y}{\rho h} - \frac{\overline{\tau_{by}}}{\rho h} \quad (1.17)$$

The wave forces are different outside and inside the surfzone. Outside the surfzone the wave energy increases due to shoaling, and inside the wave energy decreases to wave breaking. This means that outside the surfzone  $S_{xx}$  increases in the onshore direction driving an offshore-directed wave force ( $R_x$ ), as a result of which the water level gradient is negative (Eq. 1.16). This is called wave-set down. The opposite occurs within the surfzone resulting in wave set-up.

There is thus no cross-shore depth-mean current according to this. However, there is a cross-shore circulation because of the vertical variation of the forces over the water depth. In the surfzone the radiation stress gradient is generally not uniformly distributed over the water depth. It has its highest value near the surface and lowest near the bed (see e.g. Svendsen, 2005). The water level gradient due to wave set-up is the same at all vertical levels. As a result, there is an offshore current near the bed (“undertow”) and an onshore-directed current near the surface.

Using Snell’s law the wave force in y-direction can be expressed as follows (combining Eq. 1.10 and 1.12):

$$R_y = -\frac{\sin \theta_0}{c_0} \frac{\partial}{\partial x} (Enc \cos \theta) \quad (1.18)$$

where the subscript “0” indicates the offshore wave angle and celerity. Outside the surfzone the wave energy flux is constant and no net force in y-direction is generated. Inside the surfzone the wave energy flux decreases due to dissipation and so  $R_y > 0$  and the bed shear stress  $> 0$  (Eq. 1.17), driving an alongshore current. Using the wave energy balance and dominant wave energy dissipation in x-direction and due to wave breaking (Eq. 1.6), Eq. (1.18) can be written into:

$$R_y = \frac{\sin \theta_0}{c_0} D_b \quad (1.19)$$

According to this, radiation stress gradients do not generate depth-averaged cross-shore currents. This is in line with a closed-coast situation and alongshore uniformity, e.g. more or less the Holland coast. However, this situation might be different in front of a tidal inlet, e.g. offshore the Ameland Inlet, where water can flow into the Wadden Sea and diverge in the alongshore direction. The wave set-up is then potentially not well developed and the bed shear stress compensates mainly for the cross-shore force (Eq. 1.14), driving a cross-shore current in a similar way as the alongshore current.

### A.3 Wave-driven currents from a continuity perspective

#### A.3.1 Mass flux

Under progressive waves, water particles move along elliptic orbits that are generally not completely closed, as the particle under the wave crest moves faster than under the wave trough, because it is higher above the bed. Using linear wave theory this wave-averaged mass flux or Stokes drift can be estimated:

$$M = \frac{E}{c} \quad (1.20)$$

And an associated depth-mean velocity:

$$\langle U_s \rangle = \frac{E}{c\rho h} \quad (1.21)$$

From an Eulerian perspective the Stokes drift takes place between the wave crest and trough (Van Rijn, 2013), i.e. for  $-0.5H < z < 0.5H$  ( $H = H_{rms}$  for irregular waves):

$$U_{S,E} = \frac{g \left[ (0.5H)^2 - z^2 \right]^{0.5}}{\pi c} \quad (1.22)$$

From a Lagrangian perspective the Stokes drift increases from the bed to reach a maximum at the wave-mean water level (Van Rijn, 2013):

$$U_{S,L} = \frac{1}{8} \omega k H^2 \frac{\cosh[2k(z+h)]}{\sin^2(kh)} \quad (1.23)$$

with  $\omega = 2\pi/T$  the angular frequency. Both correspond to the mass flux expressed in Eq. (1.20). In the surfzone rollers generate an onshore mass flux too (Boers, 2005):

$$M_r = \frac{2E_r}{c} \quad (1.24)$$

With  $E_r$  the roller energy. The roller energy can be estimated as follows (Svendsen, 1984; Boers, 2005):

$$E_r = \frac{1}{2} \rho c \frac{A_r}{T} Q_b = \frac{1}{2} \rho c \frac{0.9H_{max}^2}{T} Q_b \quad (1.25)$$

with  $A_r$  the roller surface area.

### A.3.2 Cross-shore currents

For a closed-coast situation and alongshore uniformity the depth-averaged cross-shore velocity should be zero for reasons of continuity. The return flow is generally not uniformly distributed over the water depth. Van Rijn (2013) schematized the undertow velocity as follows:

Near-bed layer:

$$U_r = \alpha_r \frac{U_{r,\delta}}{\ln\left(\frac{\delta_m}{z_0}\right)} \ln\left(\frac{z}{z_0}\right) \quad z_0 < z \leq \delta_m \quad (1.26)$$

Intermediate layer:

$$U_r = \alpha_r \frac{\overline{U}_r}{\left[-1 + \ln\left(\frac{h}{z_a}\right)\right]} \ln\left(\frac{z}{z_a}\right) \quad \delta_m < z \leq 0.5h \quad (1.27)$$

Upper layer:

$$U_r = U_{r,mid} \left[1 - \left(\frac{z - 0.5h}{0.5h}\right)^3\right] \quad 0.5h < z \leq h \quad (1.28)$$

In which

$$\alpha_r = \frac{C_1}{(C_3 + 0.375C_2)}$$

$$C_1 = -1 + \ln\left(\frac{h}{z_a}\right)$$

$$C_2 = \ln\left(\frac{0.5h}{z_a}\right) \quad (1.29)$$

$$C_3 = \left(\frac{\delta_m}{h} - 0.5\right) + 0.5 \ln\left(\frac{0.5h}{z_a}\right) - \frac{\delta_m}{h} \ln\left(\frac{\delta_m}{z_a}\right)$$

$$U_{r,\delta} = \frac{\overline{U}_r}{\left[-1 + \ln\left(\frac{30h}{k_a}\right)\right]} \ln\left(\frac{30\delta_m}{k_a}\right) \quad (1.30)$$

$$\overline{U}_r = \frac{M}{h} \quad (1.31)$$

$$\delta_m = 0.216A \left(\frac{A}{k_{sw}}\right)^{-0.25} \quad (1.32)$$

$$U_{r,mid} = \alpha_r \frac{\overline{U}_r}{\left[-1 + \ln\left(\frac{h}{z_a}\right)\right]} \ln\left(\frac{0.5h}{z_a}\right) \quad (1.33)$$

where  $z_0 = k_{sc}/30$ ,  $k_{sc}$  is the current-related roughness,  $k_a$  is the apparent roughness,  $z_a = k_a/30$ ,  $k_{sw}$  the wave-related roughness and  $A$  the orbital excursion amplitude.

Figure A.3 shows an example calculation of the return flow using these expressions with  $k_{sc} = k_{sw} = 0.02$  m and  $k_a = 0.08$  m. The total mass flux was computed using Eqs. (1.19), (1.23) and (1.24). The figure shows that the Van Rijn (2013) model gives lower near-bed undertow velocities than the depth-uniform approach, which is important for sand transport modelling as sand transport mainly takes place near the bed.

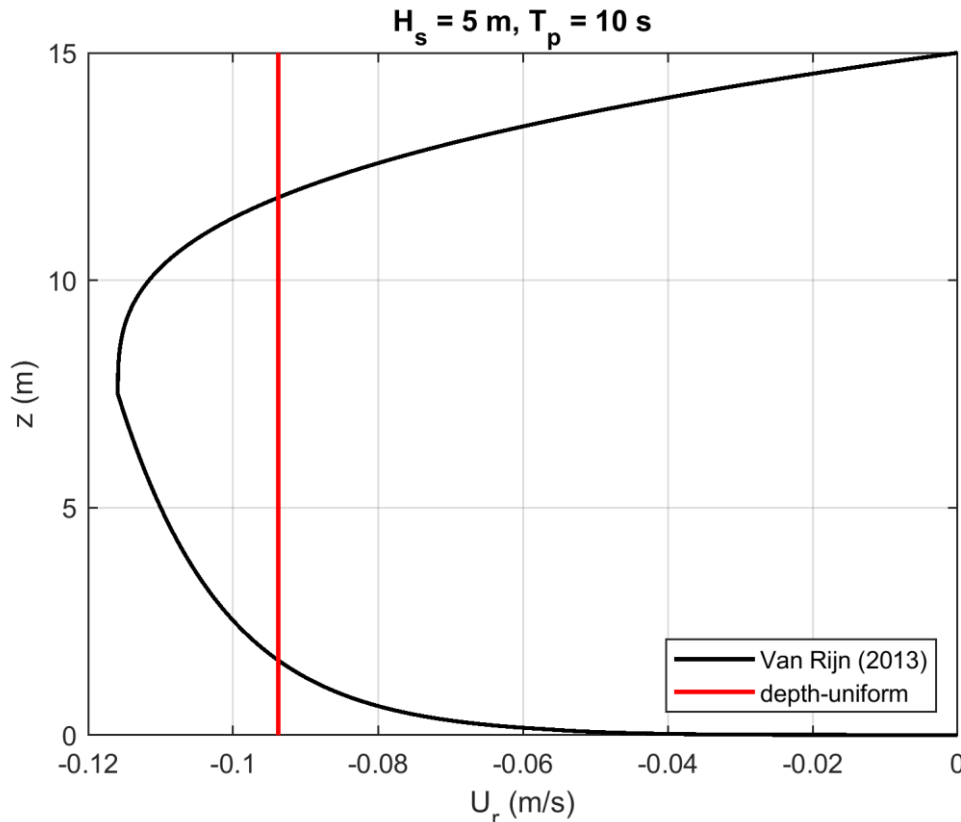


Figure A.3 Examples of Eulerian return flow.

It can be argued that suspended sand particles are not only advected by the Eulerian velocity, but by the Lagrangian velocity as well. At least to a certain degree. It is expected that the sand grains do not fully follow the same path as the water particles, as it has a fall velocity of typically  $\sim 0.02$  m/s for grain size of  $\sim 0.2$  mm, typical for the Dutch coast. Delft3D computes the Generalized Lagrangian Mean (GLM) velocity which is related to the Eulerian mean velocity and Stokes drift as follows (see Walstra et al, 2000):

$$U_{GLM} = U_E + U_s \tag{1.34}$$

With  $U_s$  from Eq. (1.22). The Eulerian mean velocity is used to compute the bed shear stress, bedload transport and sediment pick-up. The Delft3D user has the option to use either  $U_{GLM}$  or  $U_E$  in the sediment advection-diffusion equation, the latter option leads by definition to more offshore-directed suspended load as  $U_s$  is onshore-directed. Figure A.4 shows the Eulerian mean velocity profile according to Van Rijn (2013) (same as in Figure A.3), the Stokes drift according to Eq. (1.22), and a GLM velocity from this using Eq. (1.33). The GLM velocity will lead to less offshore-directed suspended load than when using the Eulerian mean velocity.



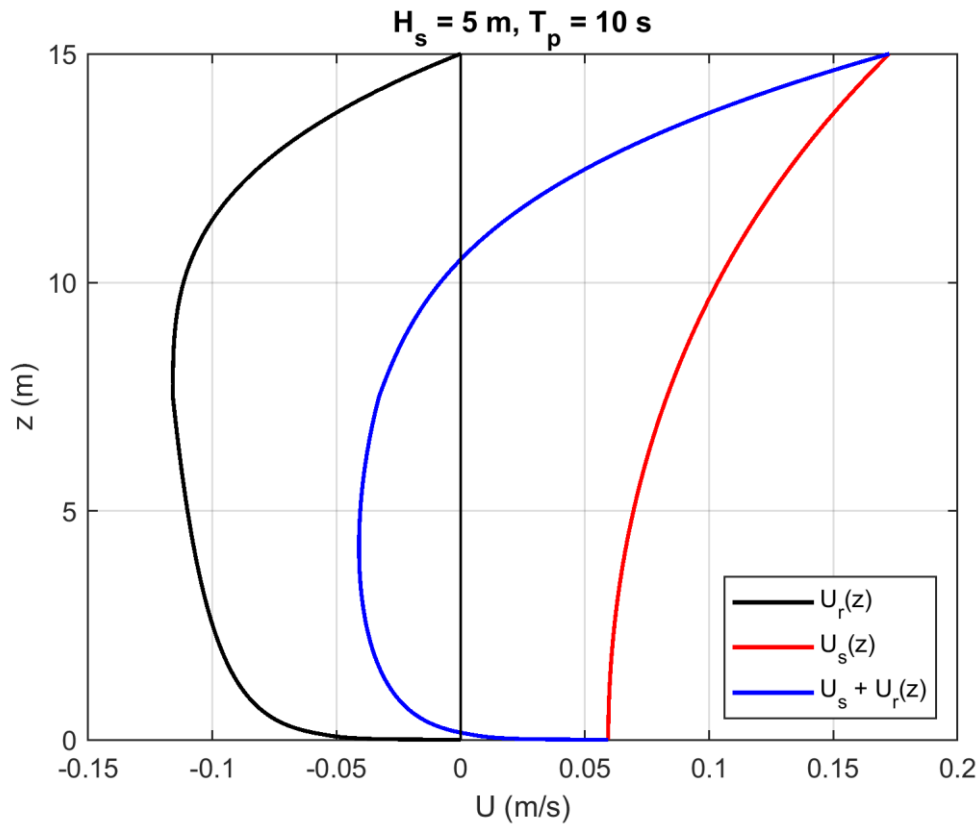


Figure A.4 Eulerian mean velocity (return flow,  $U_r$ ) according to Van Rijn (2013), Stokes drift ( $U_s$ ), and a GLM velocity which is the sum of these two.

### A.3.3 Alongshore currents

The bed shear stress term in the momentum equation in  $y$ -direction (Eq. 1.15) can be written as:

$$\tau_{b,y} = \alpha_1 \rho f U \bar{V} \quad (1.35)$$

with coefficient  $\alpha_1$  equals 0.15 according to Bijker (1986),  $1/\pi = 0.3$  following Svendsen (2005), 0.5 according to Van Rijn (2013) to get realistic results for the longshore current near Egmond, The Netherlands, and is (among other things) related to the shape of the longshore current profile  $\alpha_1 = \frac{V_b}{\pi \bar{V}}$  with  $V_b$  the near-bed alongshore current (Hulscher et al., 2002),  $f$  is the friction coefficient ( $= (f_c * f_w)^{0.5}$  according to Van Rijn, 2013 with  $f_c$ ,  $f_w$  the current and wave friction coefficient, respectively), and the orbital velocity amplitude from linear wave theory in shallow water:

$$U = \frac{g^{0.5} H}{2h^{0.5}} = \frac{1}{2} (gh)^{0.5} \gamma \quad (1.36)$$

Under the assumption of near-coast normal incoming shallow water waves ( $\cos \theta \approx 1$ ,  $n = 1$ ,  $H = \gamma h$ ), the depth-averaged longshore current in the surfzone can be computed in the following way (see e.g. Van Rijn, 2013) by combining Eqs. (1.15), (1.16), (1.34) and (1.35):

$$\bar{V} = \frac{5}{8\alpha_1} \frac{\gamma \sqrt{g} h \sin \theta_{br}}{(f_c f_w)^{0.5} \sqrt{h_{br}}} \tan \beta \quad (1.37)$$

$\theta_{br}$  is the wave height at the breaker line and  $h_{br}$  the water depth at the breaker line. With Snell's the latter two can be taken at any water depth. This equation shows that the alongshore current is largest at deep water and increases with bed slope.

The alongshore current can also be computed from the wave breaking dissipation (Eq. 1.18):

$$\bar{V} = \frac{1}{\alpha_1} \frac{\sin \theta}{\rho (f_c f_w)^{0.5} U c} D_b \quad (1.38)$$

Both approaches ignore the lateral mixing that spreads the longshore current in cross-shore direction, making the peak smaller and inducing currents at somewhat deeper water than the surfzone (see e.g. Svendsen, 2005; Van Rijn, 2013).

Figure A.5 shows the computed alongshore current using Eq. (1.36) (Van Rijn) and based on the wave breaking dissipation (Eq. 1.37). The Van Rijn predictions are clipped to 0 at deeper water where  $H_s/h < 0.4$  (blue dashed line in Figure 8). The offshore wave direction and celerity were used.

The “ $D_b$ -approach” gives a smoother trend in the alongshore current with also small alongshore currents offshore from  $H_s/h = 0.4$ . Inside “the breaker zone”, the alongshore currents by the two methods are similar. The predicted currents are generally not so large for this case, with a typical value of ~0.1 m/s at 10-12 m water depths.

The differences between the two methods as well as the alongshore current become larger for an 8 m offshore (20 m water depth) wave height (Figure A.6).

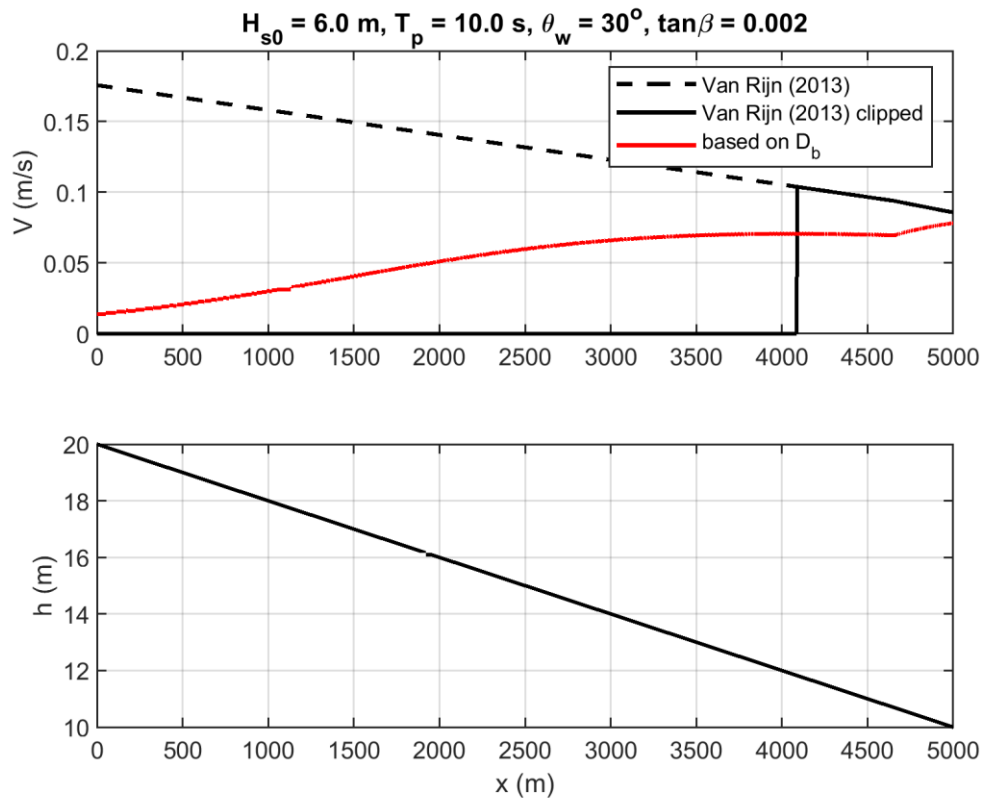


Figure A.5 Alongshore current computed in different ways for an offshore wave height of 6.0 m.

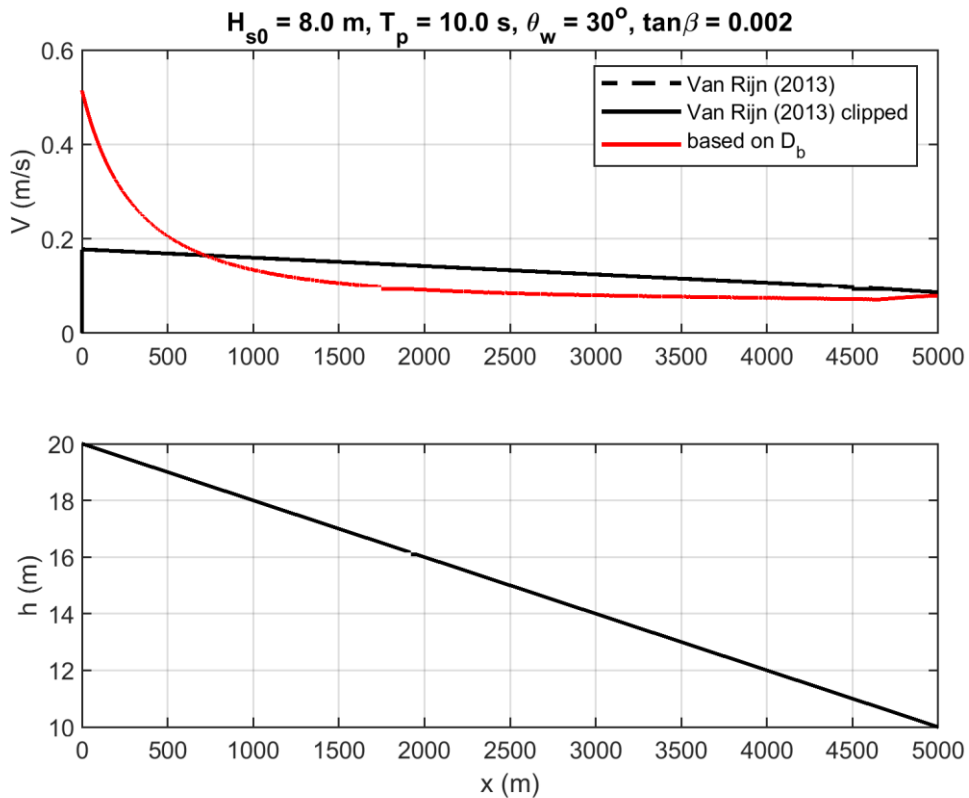


Figure A.6 Alongshore current computed in different ways for an offshore wave height of 8.0 m.

#### A.4 Discussion

Wave breaking criteria suggest that wave breaking and associated currents are not important at water depths of 20 m. Wave breaking is expected to start at water depths of ~16 m for the Wadden Coast for a 7 m storm with a return period of ~6 years. (based on Schiermonnikoog-Noord data). Wave conditions are milder along the Holland Coast, and wave breaking is expected to become important at ~12 m water depth for a 5 m wave with a return period of ~1.5 years (based on Meetpost Noordwijk data).

In literature we found expressions to analytically compute wave-driven cross-shore and alongshore currents. We have also derived a new expression to compute the alongshore current based on the wave breaking dissipation. Although not directly tested against data, it has the advantage of a smooth cross-shore shape of the alongshore direction and it is independent of a choice for the onset of (irregular) wave breaking.

From initial calculations, it is concluded that the alongshore current in the deep shoreface (~10-20 m water depth) is of the order of ~0.1 m/s for high waves. This is small compared to the tidal current but could contribute to the net sand transport as the alongshore is a steady current. The near-bed offshore undertow is typically between 0-0.1 m/s, and not so much dependent of wave breaking. It is mainly the compensation for onshore-directed Stokes drift.

The following questions remain:

- Whether or not a depth-averaged wave-driven cross-shore current can be generated offshore from a tidal inlet.
- To what extent suspended sand is advected by the Eulerian or Generalized Lagrangian Mean velocity.
- How well the analytical expressions for the cross- and alongshore current match with lab and field data.

Based on the current system understanding it is recommended to compute the wave-driven currents in the offline sand transport calculation (with input from FM model simulations without waves) in the following way:

- Use of  $U_{GLM}$  velocities to compute the current-related suspended load with zero compensating mass flux in the case of open coast ( $U_{GLM} = U_s$ ). When the waves approach the coast under an angle this also contributes to an alongshore drift velocity with no alongshore compensating return flow ( $V_{GLM} = U_s$ ).

The expressions for the alongshore currents need to be tested first, before they can be applied.

The onshore-directed Longuet-Higgins streaming was already part of the Van Rijn bedload computation and is therefore not scope of this study.

## B Offshore wave statistics

Roscoe (2009) analysed wave data from 1979 to 2002/2008, and derived spectral mean wave heights ( $H_{m0} \approx H_s$ , with  $H_s$  the significant wave height) and the spectral mean periods  $T_{m01}$  for different return periods (Table B.1, Figure B.1, Figure B.2). The largest wave heights occurred during the following storm events

- 31 October – 1 November 2016 (northwesterly, “Allerheiligenvloed”),
- 18 January 2007 (southwesterly),
- 25 January 1990 (northwesterly?).

Table B.1 shows that the wave heights and wave periods are smaller at MPN (Noordwijk) and SWB (Schouwenbank) than at SON (Schiermonnikoog Noord), especially for the longer return periods of 10 and 100 years.

Table B.1 Spectral mean wave heights and mean wave periods for stations Schiermonnikoog-Noord (SON), Meetpost Noordwijk (MPN) and Schouwenbank (SWB) for different return periods. Data extracted manually from Roscoe (2009). (later we need figure showing locations)

Station	1 year		10 years		100 years	
	$H_{m0}$ (m)	$T_{m01}$ (s)	$H_{m0}$ (m)	$T_{m01}$ (s)	$H_{m0}$ (m)	$T_{m01}$ (s)
SON	5.5	10.5	7.4	12.6	8.6	14.1
MPN	4.8	9.2	5.8	10.6	6.6	11.4
SWB	4.5	8.3	5.3	9.0	5.8	9.4

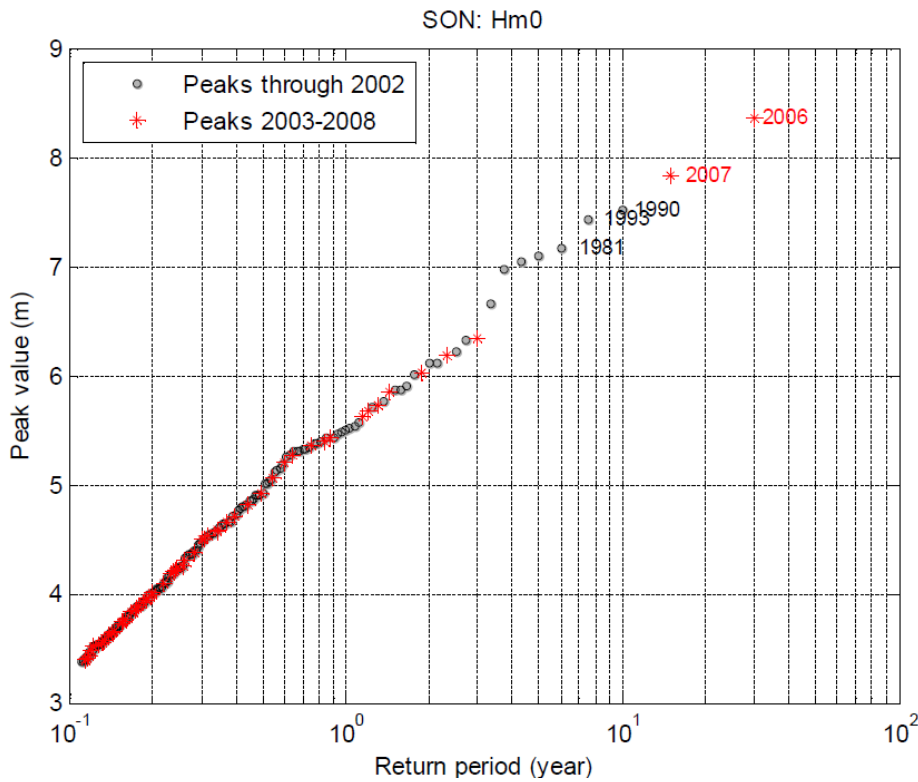


Figure B.1 Measured significant wave heights at Schiermonnikoog-Noord (SON). Figure taken from Roscoe (2009).

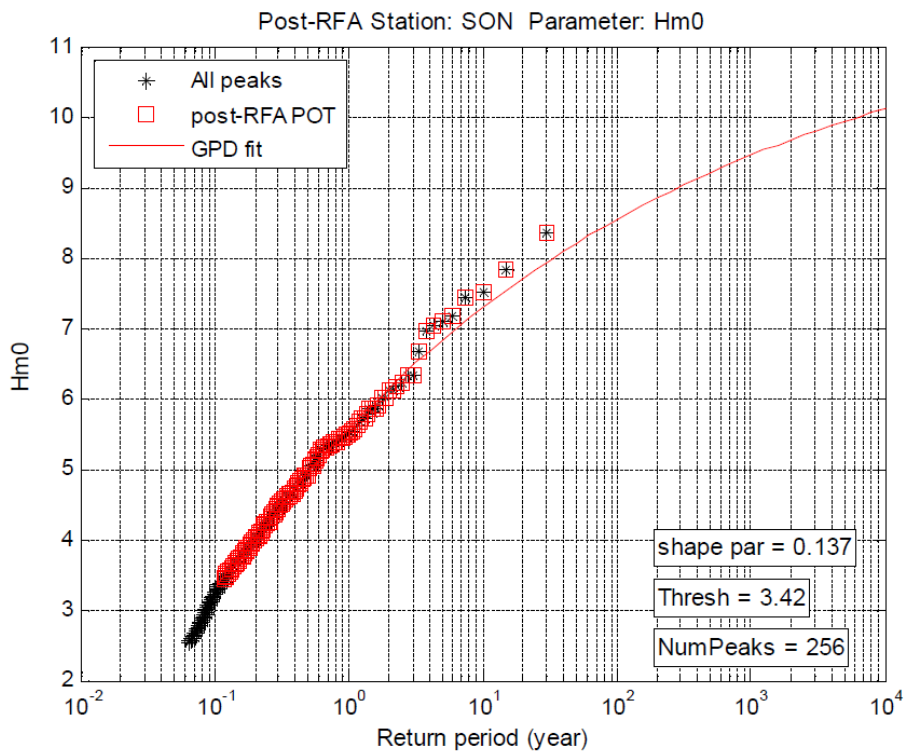


Figure B.2 Measured and fitted significant wave heights at Schiermonnikoog-Noord (SON). Figure taken from Roscoe (2009).

## C Annual mean residual flow velocities

To illustrate the variation of these flows along the Dutch coast, here we present the mean annual velocity vectors near the bed, near the surface and depth-averaged as computed with the 3D DCSM-FM model. We use the year 2016 as an example and subdivide the Dutch coast in 5 sections, e.g. southern coast, central Holland coast, northern Holland coast, northwestern coast along the Wadden islands and northeastern coast along the Wadden islands.

To illustrate the cross-shore variations, in addition to vector plots we present the computed annual mean residual flow velocities and directions at nine different JARKUS transects along the Dutch coast, i.e. at Ouddorp, Westkapelle, Scheveningen, IJmuiden, Callantsoog, Texel, Terschelling, Ameland and Schiermonnikoog.

Figure 7.1 shows the computed annual mean flow velocities for the year 2016 along the southern Dutch coast. The present coastal foundation is indicated with the solid green line and the NAP-15 m contour suggested by Vermaas et al. (2015) is indicated with the dashed green line. Selected JARKUS transects are shown also.

Figure 7.1 shows that residual flow velocities are generally small (few cm/s) along the coast between Westkapelle and Ouddorp and increase towards Hoek van Holland. There is a difference in magnitude and direction between the near-bed (blue arrows) and near-surface flows (red arrows) due to wind and due to density differences from the freshwater outflow of the Haringvliet (north of Ouddorp) and Rhine River (south of Hoek van Holland) into the saline North Sea. This causes the near-bed velocities to be more shoreward directed. The near-surface flows are clearly larger at Hoek van Holland because of the River Rhine outflow and flow contraction due to the presence of Maasvlakte II.

Figure 7.2 shows the residual flow magnitudes and directions in the Westkapelle transect and the same in the Ouddorp transect (see for transect locations). The presented statistics are based on annual means over years 2013-2017 and error bars indicate the standard deviation between the years. The lower panel shows the bed levels along this transect.

The depth-averaged annual mean residual flows in the Westkapelle transect amount to about 0.01-0.02 m/s. The depth-averaged residual flow direction is about  $100^\circ$  at 9 km offshore (15 m depth). It decreases to about  $-20^\circ$  at 14 km offshore (22 m depth) and increases again to  $80^\circ$  at 21 km offshore. The coast angle is about  $60^\circ$  measured from the horizontal axis. This means that near the coast the depth-averaged flow has a small offshore directed component at 9 km, an onshore directed component at 14 km and an offshore directed component at 22 km. The near-bed residual flows are smaller than the depth-averaged values and the flow angle is generally smaller than the coast angle, which means that also here the near-bed residual flow has a small onshore directed component.

The depth-averaged annual mean residual flow amounts to about 0.02 m/s and this value is more or less constant in the Ouddorp transect. The depth-averaged residual flow direction varies from about  $90^\circ$  at 7 km offshore (15 m depth) to about  $60^\circ$  at 25 km offshore (26 m depth), where angles are measured anticlockwise from the horizontal x-axis. This depth-averaged flow angle is larger than the coast angle (based on JARKUS or tide), which means that the depth-averaged residual flow has a small offshore directed component. The near-bed residual flows are slightly smaller in magnitude and the direction varies between  $-40^\circ$  and  $20^\circ$ . This is smaller than the coast angle, which means that the near-bed residual flow has a small onshore directed component.

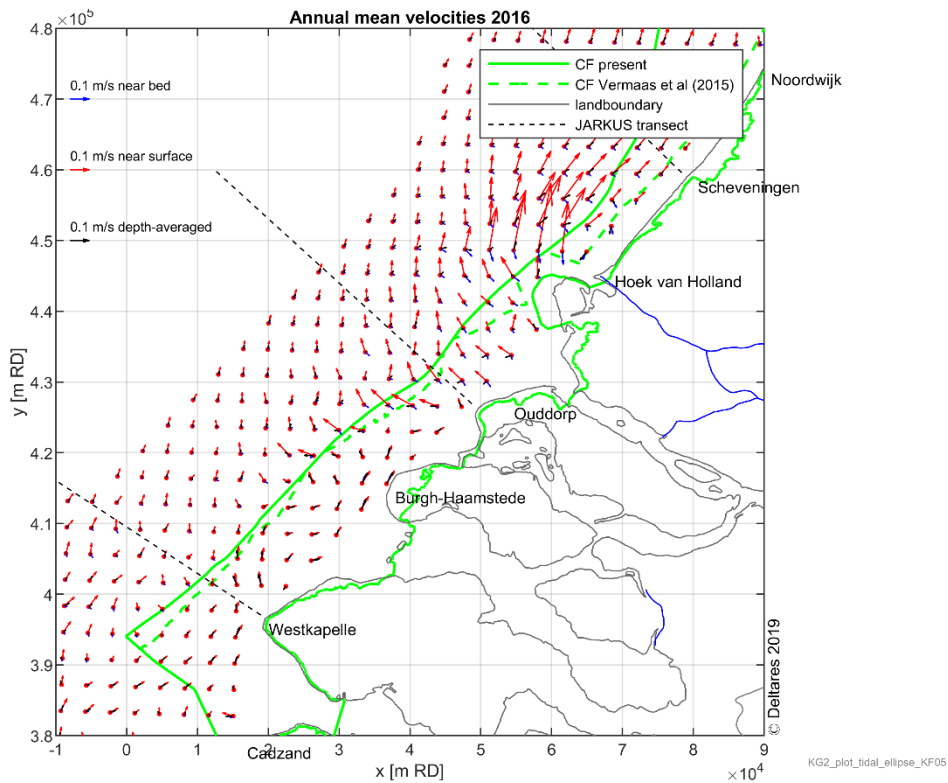


Figure 7.1 Annual mean velocities near bed (blue), near surface (red) and depth-averaged (black) computed with 3D DCSM-FM model for the year 2016, southwestern Dutch coast. The transects at Westkapelle and Ouddorp are indicated with the dashed black line.

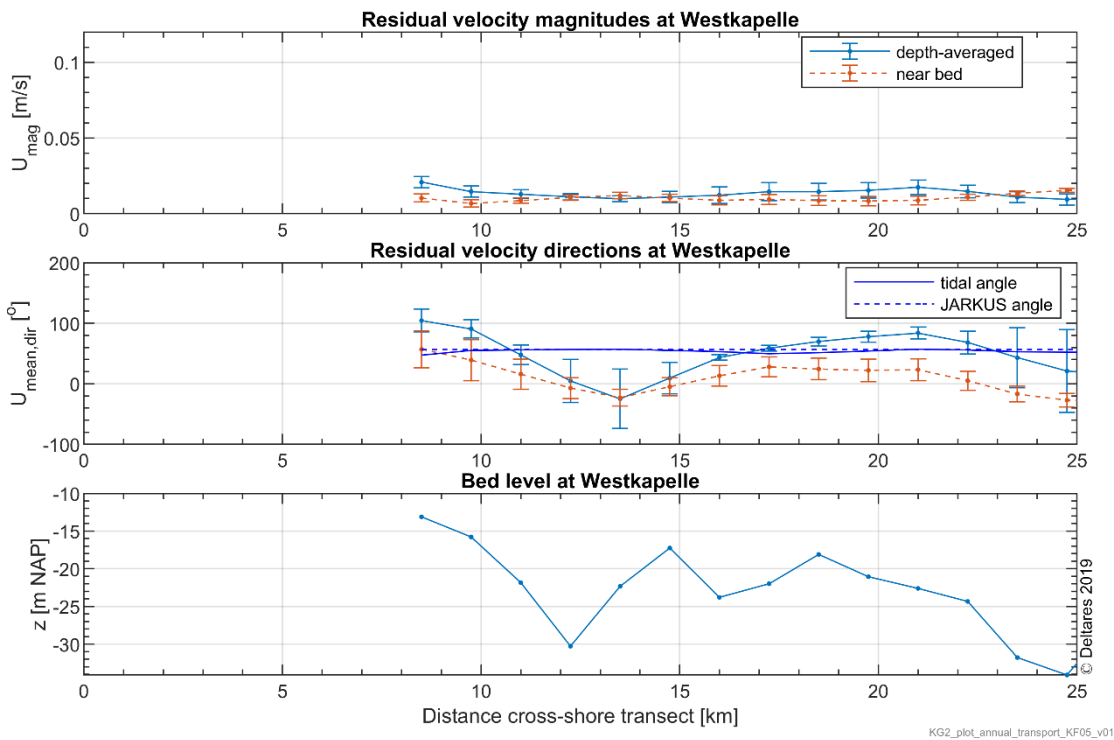


Figure 7.2 Annual mean residual velocities and directions computed with 3D DCSM-FM model along Westkapelle transect. Statistics are based on annual means over years 2013-2017 and error bars indicate the standard deviation between the years. The lower panel shows the bed levels along this transect.



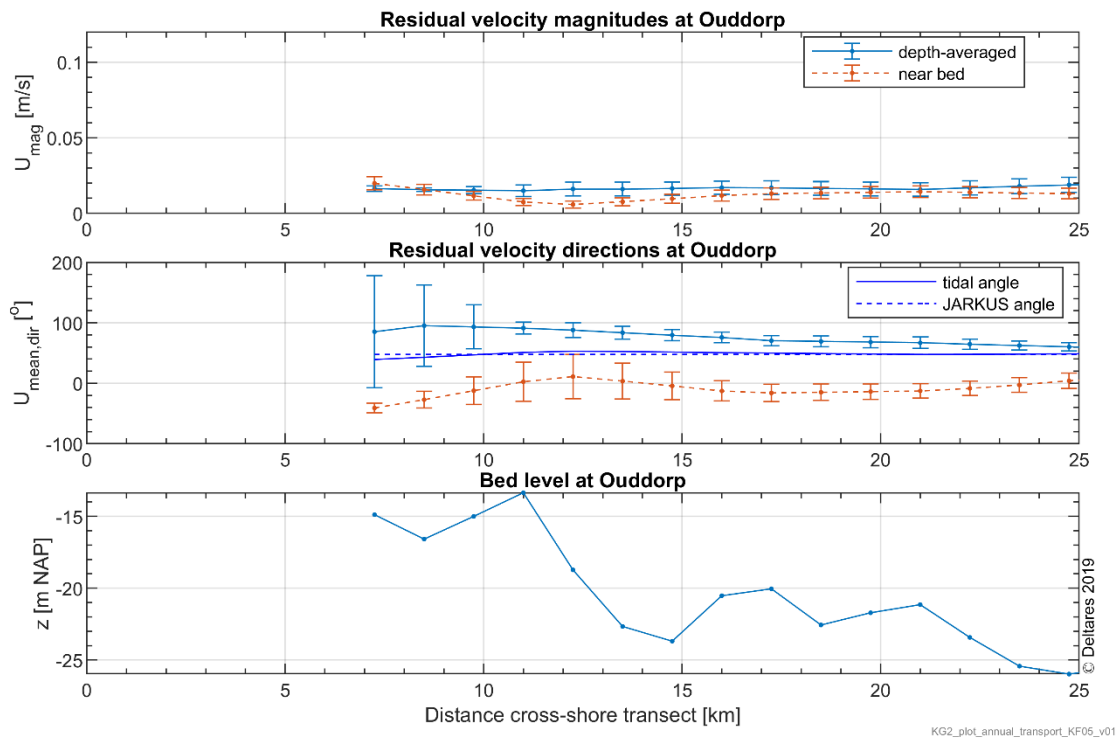


Figure 7.3 Annual mean residual velocities and directions computed with 3D DCSM-FM model along Ouddorp transect. Statistics are based on annual means over years 2013-2017 and error bars indicate the standard deviation between the years. The lower panel shows the bed levels along this transect.

Figure 7.4 shows the computed annual mean residual flow velocities along the central Holland coast. The residual flow velocities near the surface are largest near Hoek van Holland due to outflow of the river Rhine and decrease further north. Annual mean depth-averaged velocities are with a few cm/s generally relatively small. The direction is generally alongshore directed, except at Hoek van Holland where they tend to be onshore directed. Density effects can be seen here also with near-surface flow more alongshore directed and near-bed flows showing a tendency to be onshore directed.

Figure 7.5 shows the residual flow magnitudes and directions in the Scheveningen transect and Figure 7.6 the same in the IJmuiden transect. Annual mean depth-averaged flows vary between 0.01 and 0.03 m/s and generally follow the coast angle here. Near-bed residual flows are 0.01-0.02 m/s and directed at an angle of about  $-40^\circ$  measured from the horizontal x-axis. This is smaller than the coast angle of about  $45^\circ$ , which means that the near-bed flows have a clear onshore directed component in this transect.

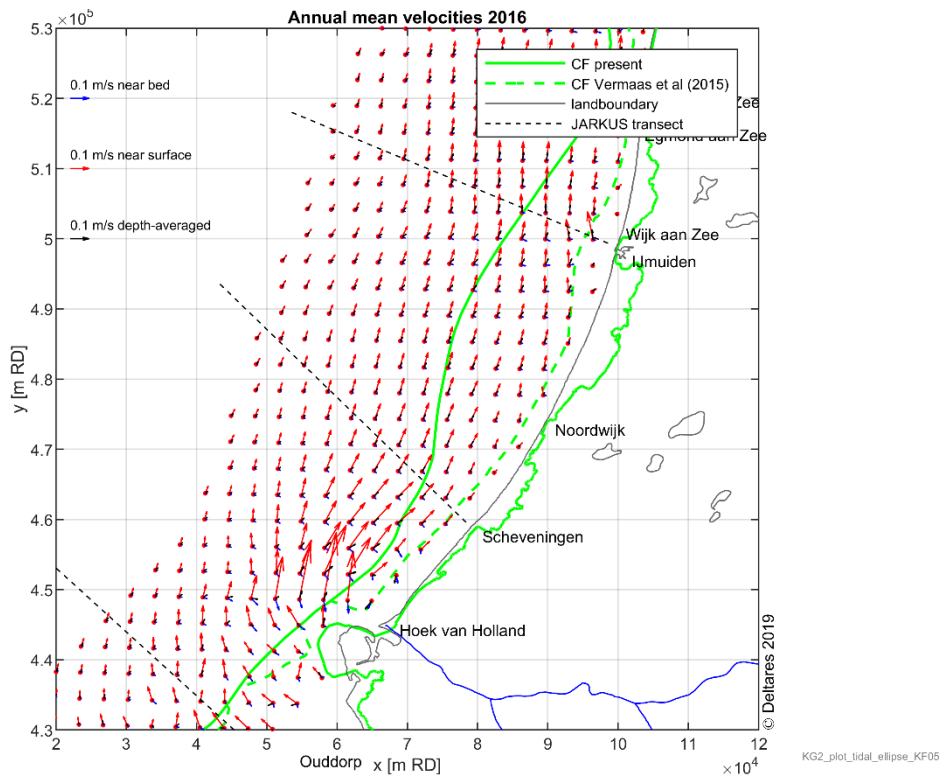


Figure 7.4 Annual mean velocities near bed (blue), near surface (red) and depth-averaged (black) computed with 3D DCSM-FM model for the year 2016, central Dutch coast.

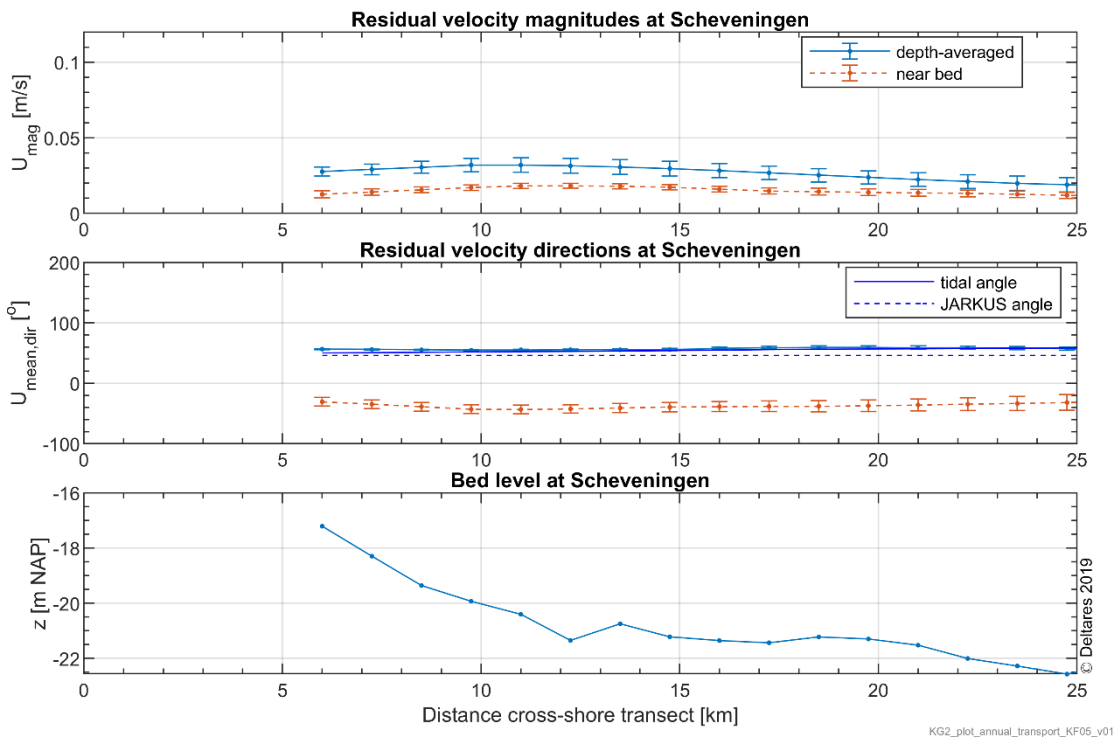


Figure 7.5 Annual mean residual velocities and directions computed with 3D DCSM-FM model along Scheveningen transect. Statistics are based on annual means over years 2013-2017 and error bars indicate the standard deviation between the years. The lower panel shows the bed levels along this transect.

The depth-averaged annual mean residual flows amount to 0.03-0.05 m/s in the IJmuiden transect and the near-bed values are 0.01-0.02 m/s transect (Figure 7.6). The depth-averaged residual annual mean residual flow angle varies between  $80^\circ$  at 4 km offshore and  $65^\circ$  at 25 km offshore. This is generally larger than the coast angle, which means that the depth-averaged residual flows have an offshore directed component. In contrast, the flow angle of the residual near bed flows is smaller than the coast angle, resulting in an onshore directed component in the entire IJmuiden transect.

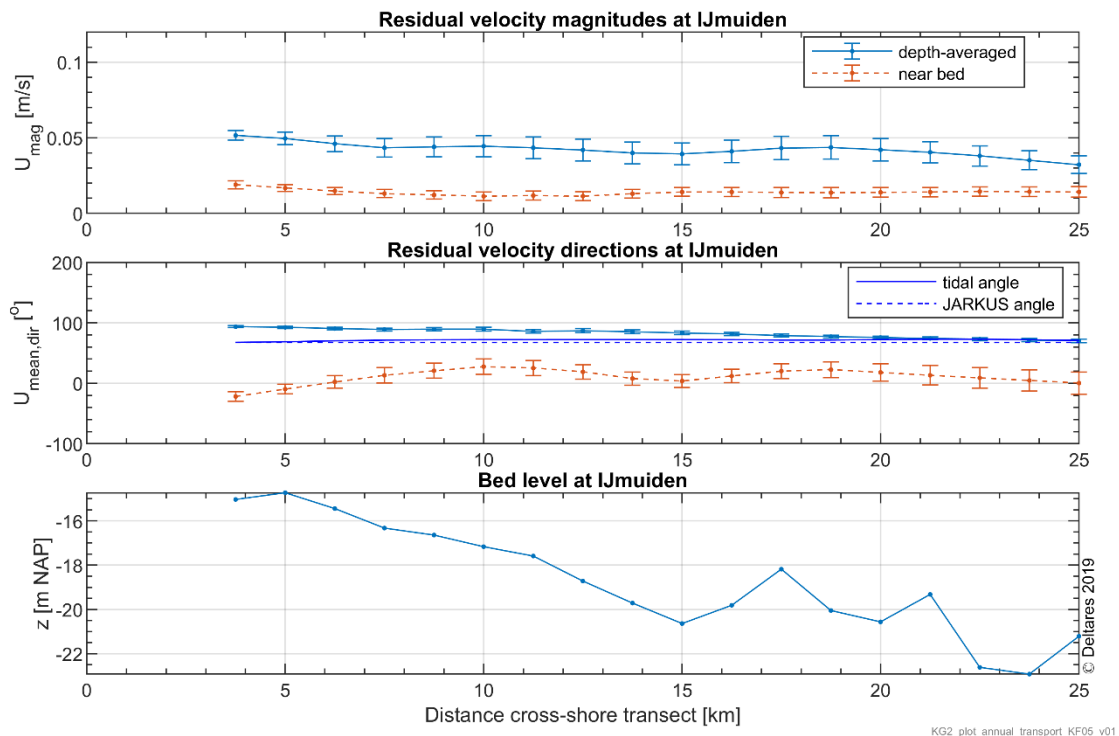


Figure 7.6 Annual mean residual velocities and directions computed with 3D DCSM-FM model along IJmuiden transect. Statistics are based on annual means over years 2013-2017 and error bars indicate the standard deviation between the years. The lower panel shows the bed levels along this transect.

Figure 7.7 shows that the annual mean residual flow velocities increase from IJmuiden to Callantssoog and Texel. The direction is generally alongshore directed except near Den Helder and Texel where velocities are affected by the Marsdiep tidal inlet and the ebb tidal delta here (see bathymetry in Figure 2.5).

Figure 7.8 shows the annual mean residual flows in the Callantssoog transect. Depth-averaged residual flows vary between 0.04 and 0.08 m/s. The coast angle is about  $80^\circ$  measured anticlockwise from the horizontal x-axis. The angle of the depth-averaged mean annual residual flow varies from  $100^\circ$  at 5 km offshore to  $70^\circ$  at 25 km offshore. This means that there is a small offshore directed component between 5 km and about 16 km offshore (25 m depth) and a small onshore directed component between 16 and 25 km offshore.

Near the bed the mean annual residual flow velocities are 0.02 to 0.03 m/s. The angle varies between  $100^\circ$  at 5 km and about  $10^\circ$  at 11 km. The first is larger than the coast angle and the second much smaller than the coast angle. This means that the near-bed annual mean residual flow has a small offshore directed component between 5 km and about 8 km (18 m depth) and an onshore directed component between 8 km and 25 km.

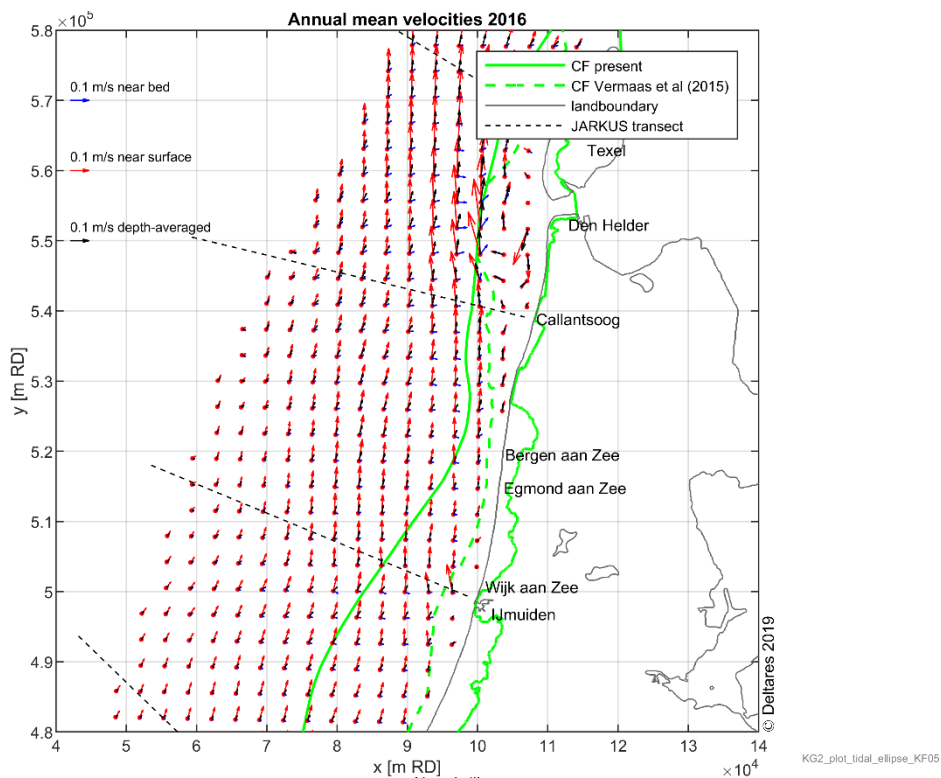


Figure 7.7 Annual mean velocities near bed (blue), near surface (red) and depth-averaged (black) computed with 3D DCSM-FM model for the year 2016, northern Dutch coast.

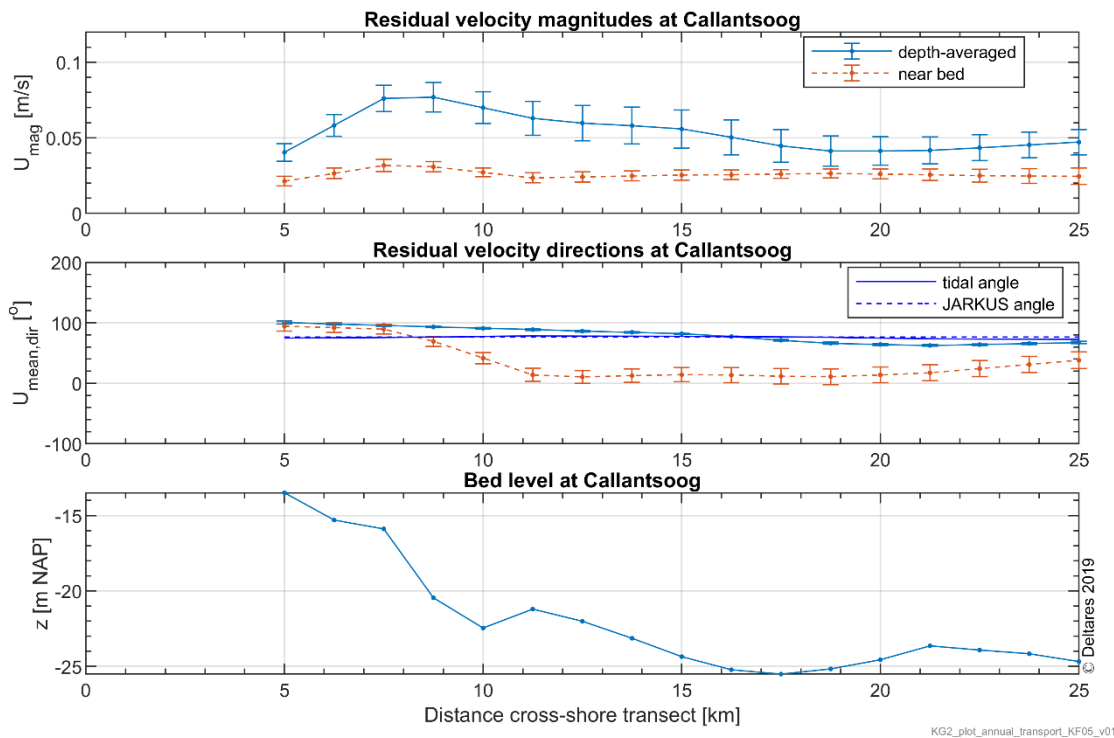


Figure 7.8 Annual mean residual velocities and directions computed with 3D DCSM-FM model along Callantssoog transect. Statistics are based on annual means over years 2013-2017 and error bars indicate the standard deviation between the years. The lower panel shows the bed levels along this transect.

The annual mean residual flow decreases in magnitude from Texel to Terschelling (Figure 7.9). The difference between the near surface flows and near-bed flows is clearly larger at Texel than at Terschelling. The vector plots also show effects of the tidal inlets.

Figure 7.10 shows the residual flows in the Texel transect and Figure 7.11 that in the Terschelling transect. The depth-averaged mean annual residual flow magnitude in the Texel transect increases from about 0.04 m/s at 5 km offshore to 0.08 m/s at 12 km offshore. It decreases again to 0.05 m/s at 25 km offshore. The coast angle is about 60° in this transect. The depth-averaged mean annual residual flow angle varies between 60° at 5 km to 80° at 25 km. This means that the flow is alongshore directed at 5 km (flow angle same as coast angle) and has a small offshore directed component at 25 km (flow angle larger than coast angle).

The near-bed annual residual flow magnitude varies between 0.02 and 0.03 m/s. The angle is 20° at 5 km (16 m depth), 60° at 9 km (21 m depth), about 15° at 17 km (26 m depth) and about 40° at 25 km (30 m depth). This means that the near-bed residual flow generally has an onshore directed component that is largest at 5 km and 17 km and is smallest at 9 km (21 m depth).

In the Terschelling transect, the depth-averaged mean annual residual flow magnitude varies between 0.03 and 0.04 m/s. The coast angle is about 20° here. The angle of the depth-averaged mean annual residual flow increases from 20° at 5 km offshore to about 40° at 20 km offshore, which means that the it has an increasing offshore directed component moving further from the coast.

The near-bed mean annual residual flow magnitude is about 0.02 m/s with angle 0° at 5 km, 16° at 15 km and -18° at 25 km. This means that the near-bed flow has an onshore directed component that is largest at 5 km (17 m depth) and 25 km (27 m depth) and smallest at 15 km (21 m depth)

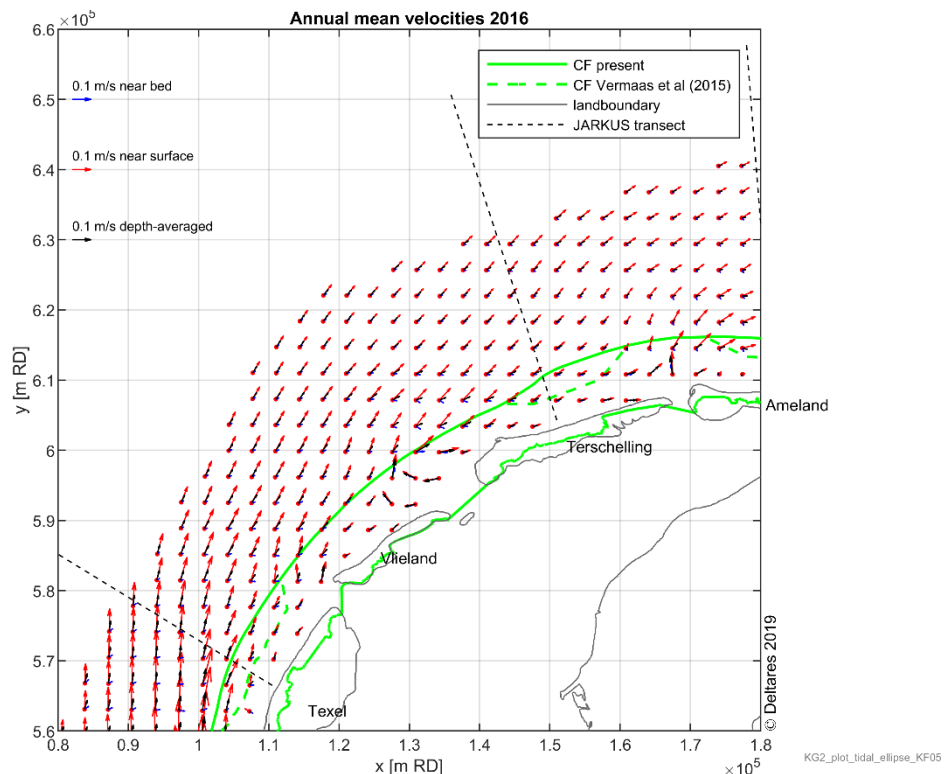


Figure 7.9 Annual mean velocities near bed (blue), near surface (red) and depth-averaged (black) computed with 3D DCSM-FM model for the year 2016, northern Wadden coast.

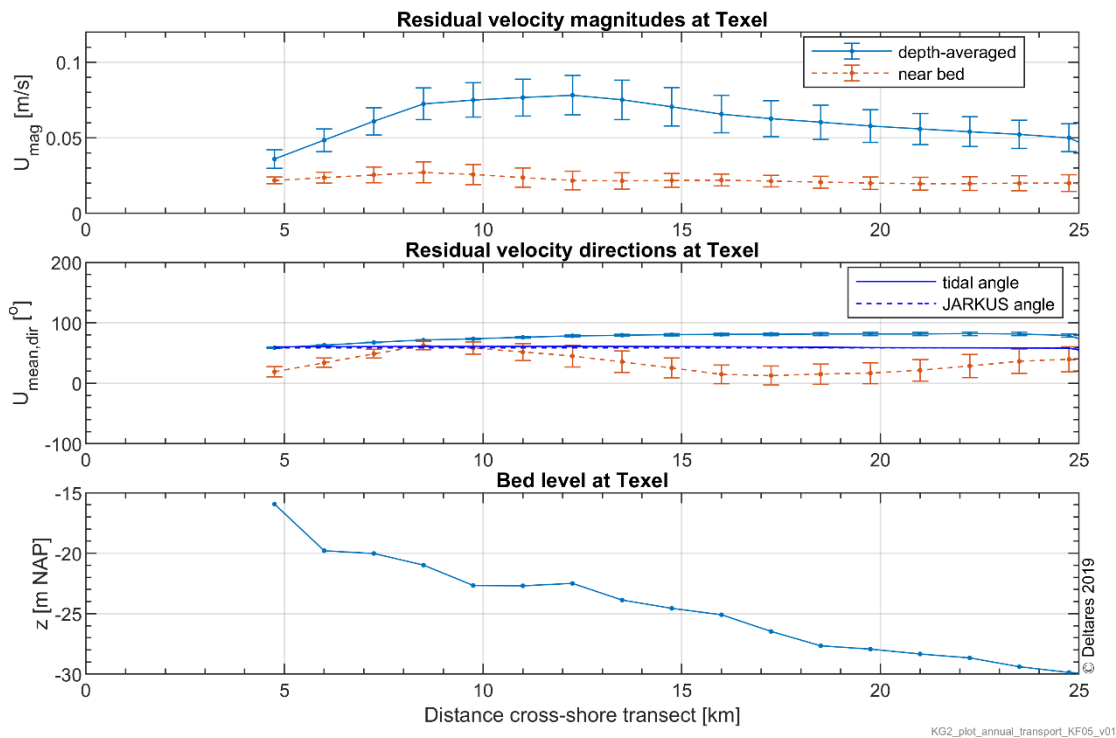


Figure 7.10 Annual mean residual velocities and directions computed with 3D DCSM-FM model along Texel transect. Statistics are based on annual means over years 2013-2017 and error bars indicate the standard deviation between the years. The lower panel shows the bed levels along this transect.

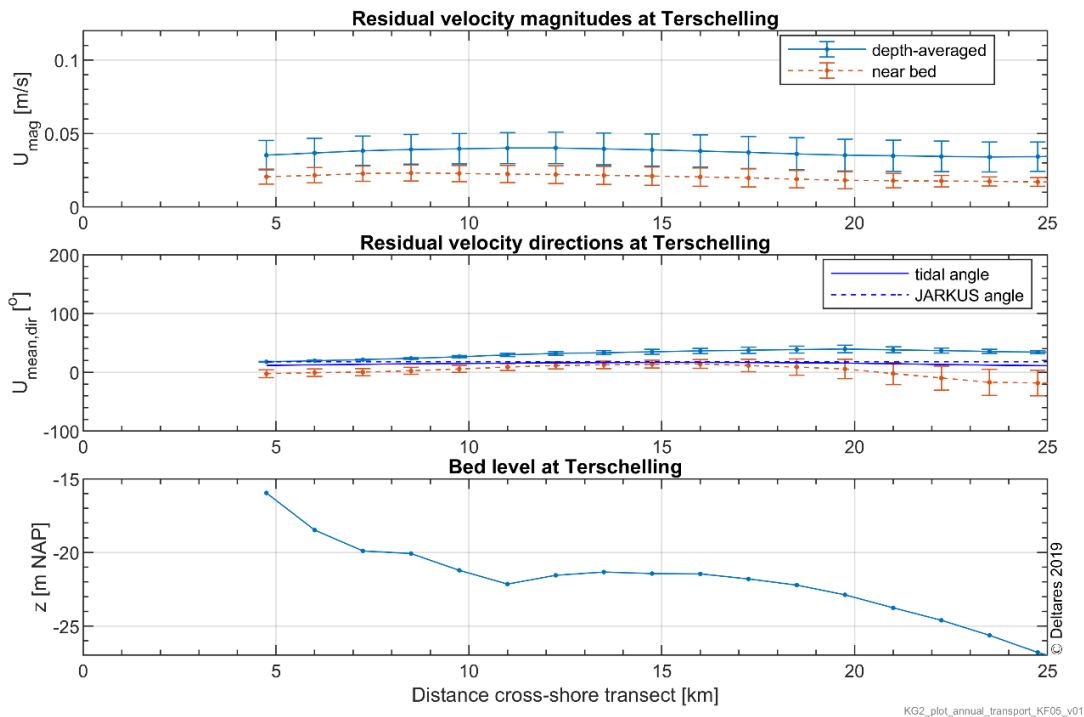


Figure 7.11 Annual mean residual velocities and directions computed with 3D DCSM-FM model along Terschelling transect. Statistics are based on annual means over years 2013-2017 and error bars indicate the standard deviation between the years. The lower panel shows the bed levels along this transect.

The mean annual residual flows above Ameland and Schiermonnikoog show a similar behaviour (Figure 7.12). The depth-averaged flow are generally more or less alongshore directed and the near-surface flows are more NE directed due to the predominant SW wind directions. Effects of the tidal inlets can also be observed here.

Figure 7.13 shows the residual flows in the Ameland transect and Figure 7.14 that in the Schiermonnikoog transect. The depth-averaged mean annual residual flow magnitude in the Ameland transect is 0.02-0.03 m/s with angle varying between  $-20^\circ$  at 5 km offshore and  $5^\circ$  at 25 km offshore. The coast angle is  $5^\circ$  at this transect. This means that the coast angle is larger than the flow angle and that the depth-averaged mean annual residual flow generally has an onshore directed component in the Ameland transect.

The near-bed mean annual residual flow is about 0.02 m/s and the angle varies between about  $-60^\circ$  at 5 km offshore (15 m depth) and  $-50^\circ$  at 15 km offshore (24 m depth). These angles are much smaller than the coast angle due to which the near-bed residual flow has an onshore directed component in the Ameland transect.

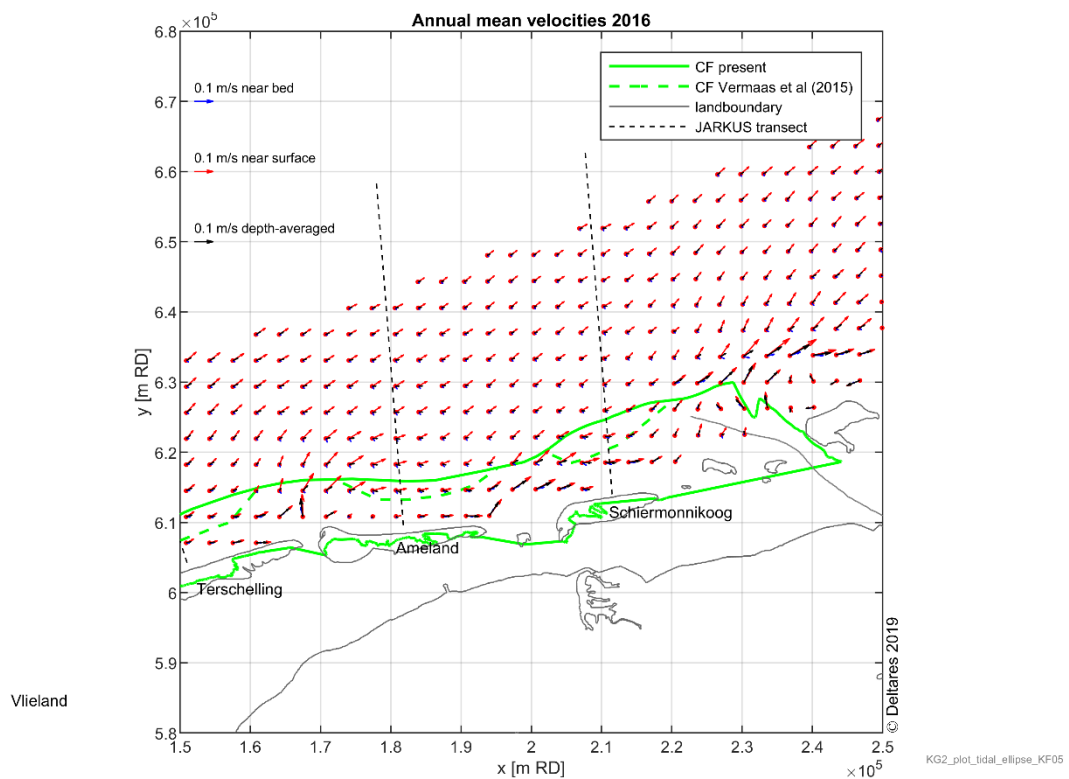


Figure 7.12 Annual mean velocities near bed (blue), near surface (red) and depth-averaged (black) computed with 3D DCSM-FM model for the year 2016, northeastern Wadden coast.

The depth-averaged mean annual residual flow magnitude decreases from about 0.05 m/s at 7 km offshore to about 0.02 m/s at 25 km offshore in the Schiermonnikoog transect. The angle is about  $5^\circ$ , which is about the same as the coast angle.

The near-bed mean annual flows decrease from 0.03 m/s at 5 km to 0.02 m at 25 km offshore. The angle varies from about  $-20^\circ$  at 7 km to about  $-55^\circ$  at 25 km. This means that the near-bed flows have an onshore directed component in the entire transect.

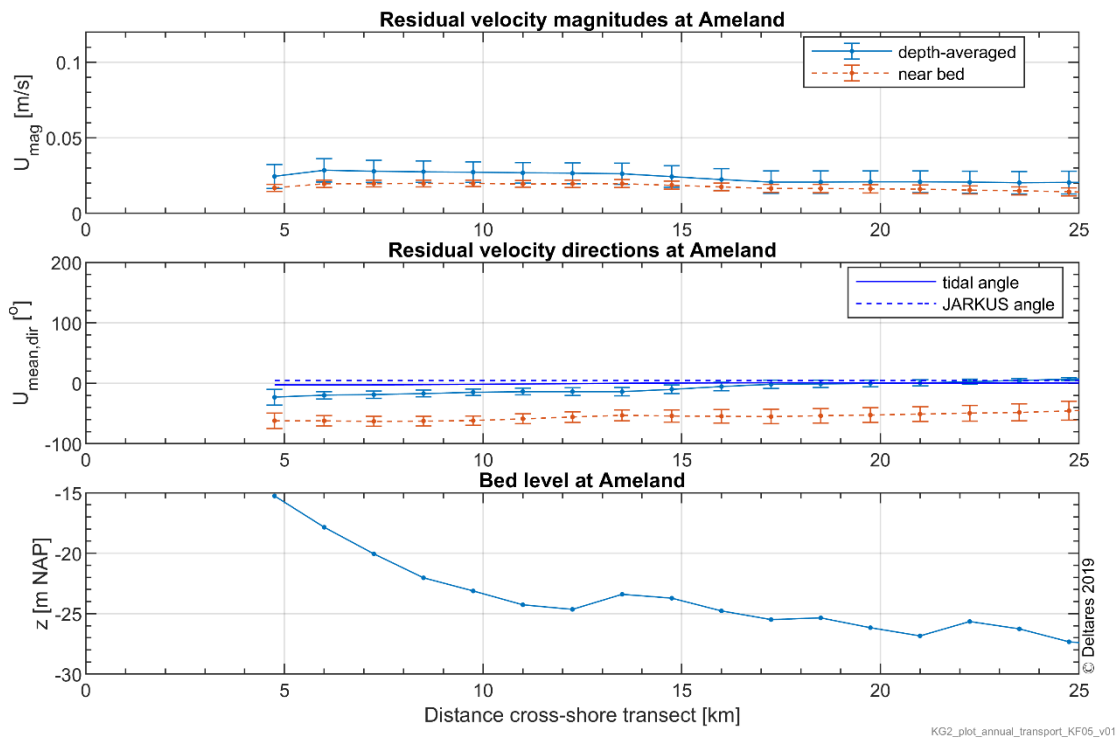


Figure 7.13 Annual mean residual velocities and directions computed with 3D DCSM-FM model along Ameland transect. Statistics are based on annual means over years 2013-2017 and error bars indicate the standard deviation between the years. The lower panel shows the bed levels along this transect.

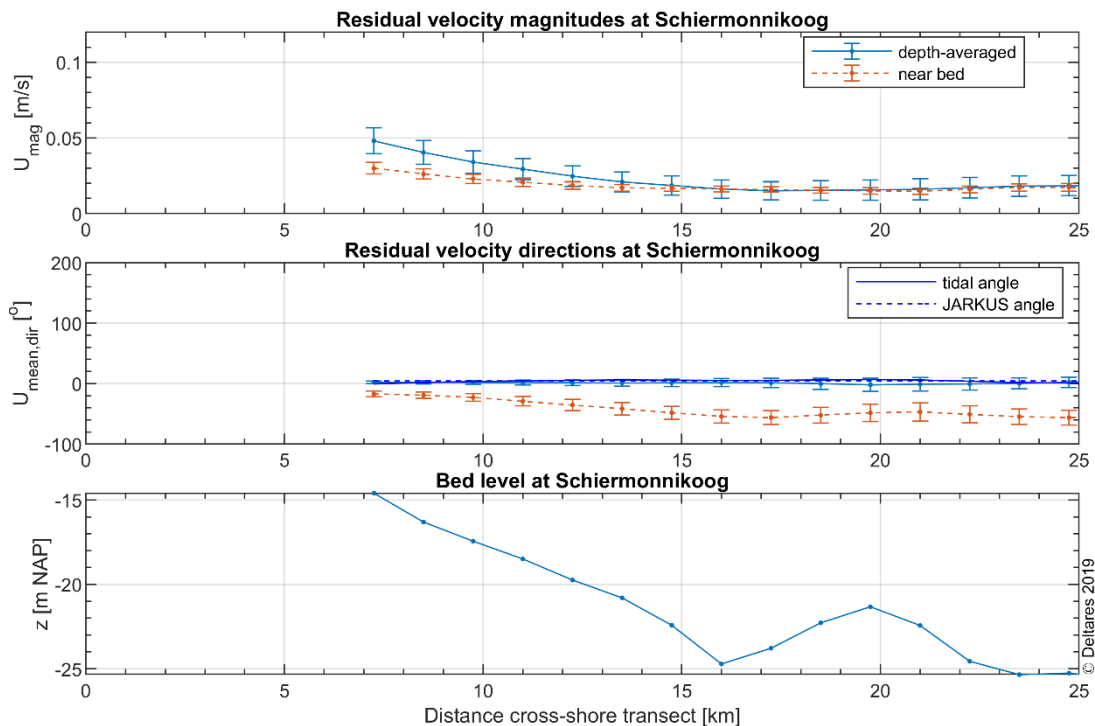


Figure 7.14 Annual mean residual velocities and directions computed with 3D DCSM-FM model along Schiermonnikoog transect. Statistics are based on annual means over years 2013-2017 and error bars indicate the standard deviation between the years. The lower panel shows the bed levels along this transect



## D Annual mean peak tidal velocities

Here we plot the annual mean peak flood and ebb velocities as vector plots for five different stretches along the Dutch coast. The peak flood values have been determined as the mean of all peak flood and ebb velocities in a year. As a year has 365 days, there are 24 hours per days and a tidal period is about 12.5 hours, this is the mean of about  $365 \cdot 24 / 12.5 \approx 700$  peak tidal velocities per year.

Figure 7.15 shows the computed annual mean peak tidal depth-averaged velocities along the southwestern Dutch coast near Westkapelle and Ouddorp. Tidal velocities are generally alongshore directed in deeper waters and can be observed to be affected by the tidal inlet closer to the shore shows a clear effect of the Westerschelde south of Westkapelle and the Oosterschelde north of Westkapelle.

Figure 7.16 shows the annual mean peak tidal flood and ebb velocities and directions computed with 3D DCSM-FM model along Westkapelle transect. Statistics are based on annual means over years 2013-2017 and error bars indicate the standard deviation between the years. The lower panel shows the bed levels along this transect.

The mean annual peak flood velocities increase from about 0.66 m/s at 8 km offshore (13 m depth) to 0.82 m/s at 16 km offshore (24 m depth). Annual mean peak ebb velocities are 0.57 m/s at 8 km offshore and 0.82 m/s at 16 km offshore. The asymmetry of the peak tidal velocities varies from 0.54 at 8 km (larger flood than ebb currents) to 0.50 at 16 km (no asymmetry).

Peak tidal velocities are of similar magnitude in the Ouddorp transect with peak flood velocities of 0.79 m/s at 8 km (15 m depth) and 0.84 m/s at 12 km (19 m depth) as shown in Figure 7.17. The asymmetry of the peak tidal velocities is 0.53 at 8 km and 0.52 at 12 km.

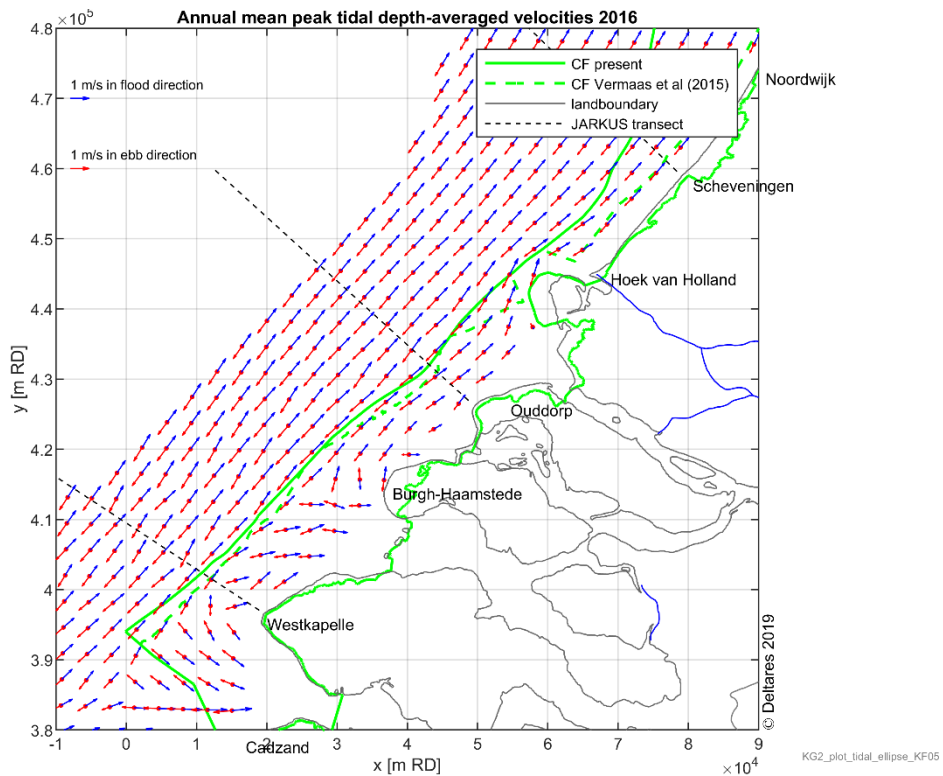


Figure 7.15 Annual mean peak flood (blue) and ebb (red) depth-averaged velocities computed with 3D DCSM-FM model for the year 2016, southwestern Dutch coast.

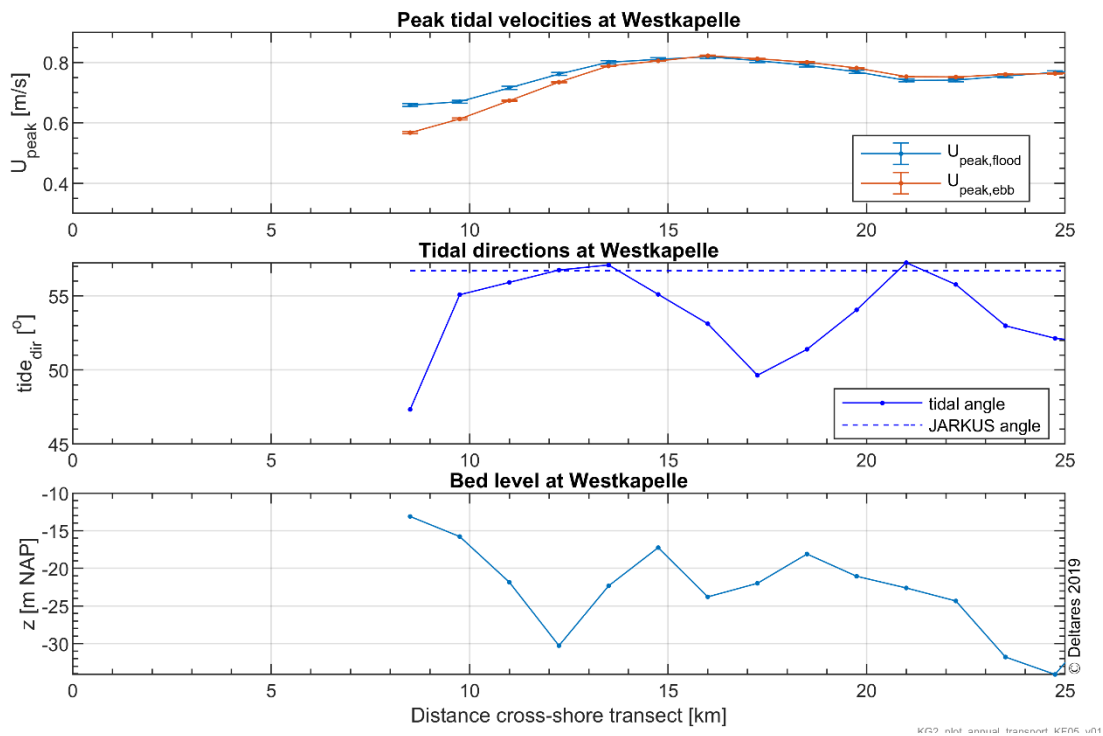


Figure 7.16 Annual mean peak tidal flood and ebb velocities and directions computed with 3D DCSM-FM model along Westkapelle transect. Statistics are based on annual means over years 2013-2017 and error bars indicate the standard deviation between the years. The lower panel shows the bed levels along this transect

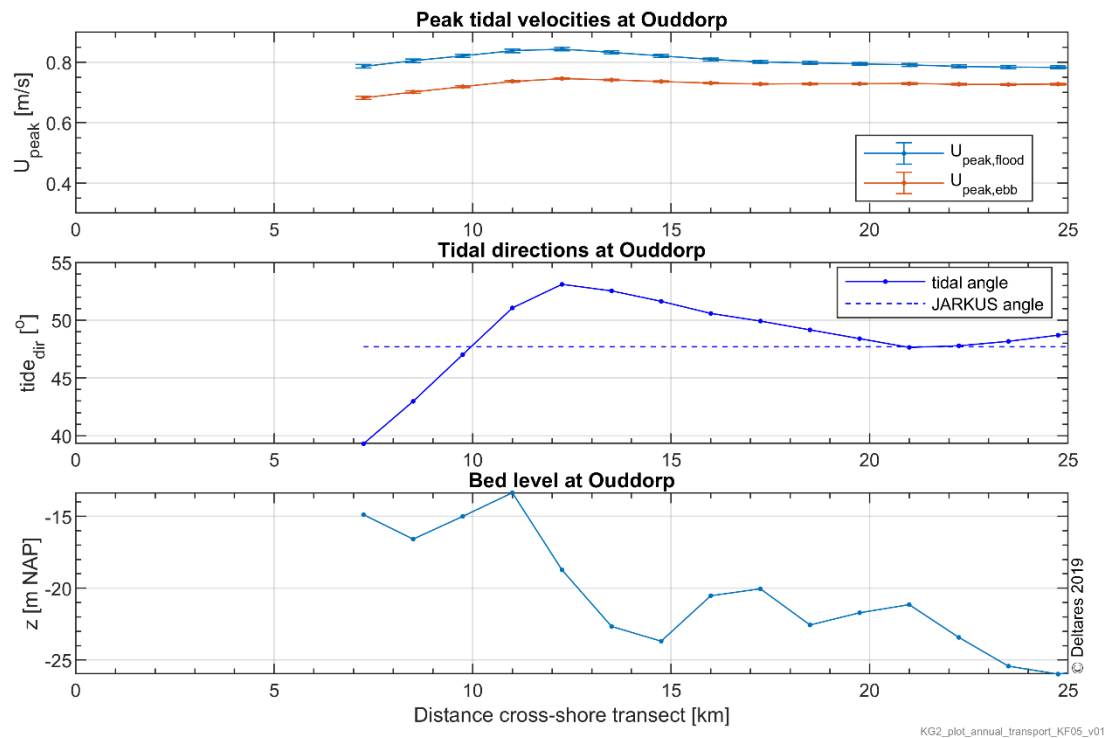


Figure 7.17 Annual mean peak tidal flood and ebb velocities and directions computed with 3D DCSM-FM model along Ouddorp transect. Statistics are based on annual means over years 2013-2017 and error bars indicate the standard deviation between the years. The lower panel shows the bed levels along this transect

Figure 7.18 shows the annual mean peak tidal velocities along the coast between Hoek van Holland and IJmuiden. Peak tidal velocities are generally alongshore directed except near Hoek van Holland. Peak flood velocities are generally larger than the peak ebb velocities.

Figure 7.19 shows the annual mean peak tidal flood and ebb velocities along Scheveningen transect. The peak flood velocities are about 0.72 m/s along the entire transect from 6 km to 25 km offshore. The peak ebb velocities increase from 0.54 m/s at 6 km (17 m depth) to 0.60 m/s at 25 km (23 m depth). The asymmetry of the peak tidal velocities is 0.57 at 6 km and 0.54 at 25 km. This is larger than in the Ouddorp transect further south.

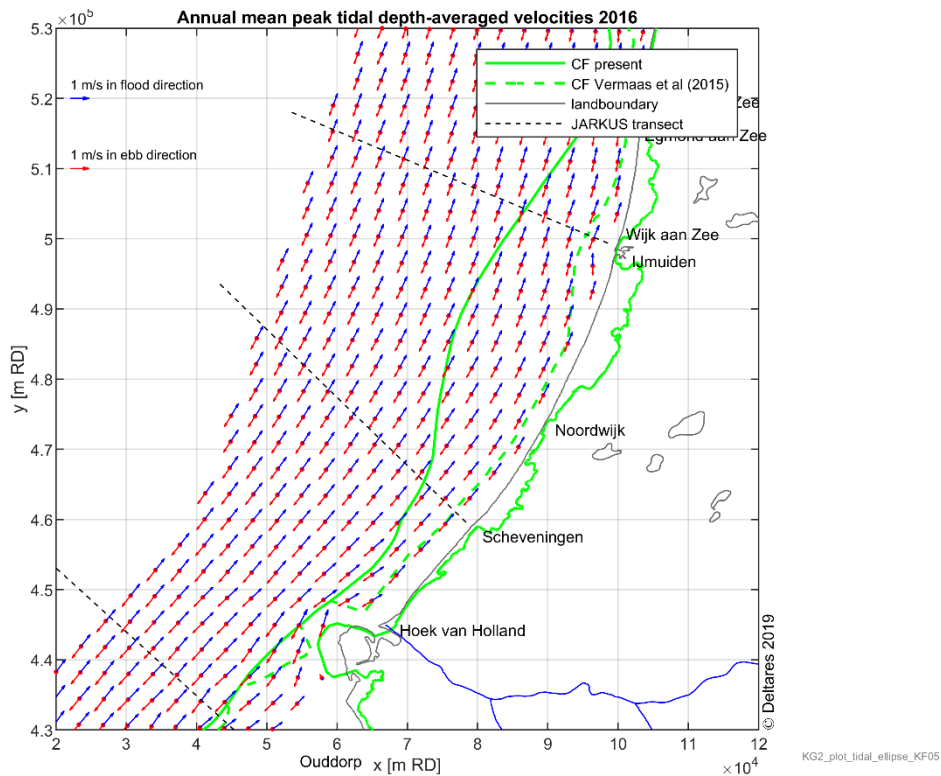


Figure 7.18 Annual mean peak flood (blue) and ebb (red) depth-averaged velocities computed with 3D DCSM-FM model for the year 2016, central Dutch coast.

The annual mean peak flood velocities are 0.76 m/s at 6 km (15 m depth) and 0.71 m/s at 25 km (21 m depth) in the IJmuiden transect (Figure 7.20). The peak ebb velocities are 0.52 m/s at 6 km and 0.54 m/s at 25 km. The asymmetry of the peak tidal velocities range between 0.59 at 6 km to 0.57 at 25 km. This is larger than in the Scheveningen transect.

The peak tidal velocities along the coast of IJmuiden, Callantssoog and Den Helder show a further increase of the flood velocities northward and a clear effect of the tidal inlet between Den Helder and Texel (Marsdiep) with flood velocities directed towards the inlet (Figure 7.21).

Annual mean peak flood velocities vary between 0.81 m/s at 6 km (15 m depth) and 0.74 m/s at 25 km (25 m depth) in the Callantssoog transect (Figure 7.22). The peak ebb velocities are 0.55 m/s at 6 km and 0.51 m/s at 25 km. The asymmetry is about 0.60. This is larger than the asymmetry in the IJmuiden transect further south.

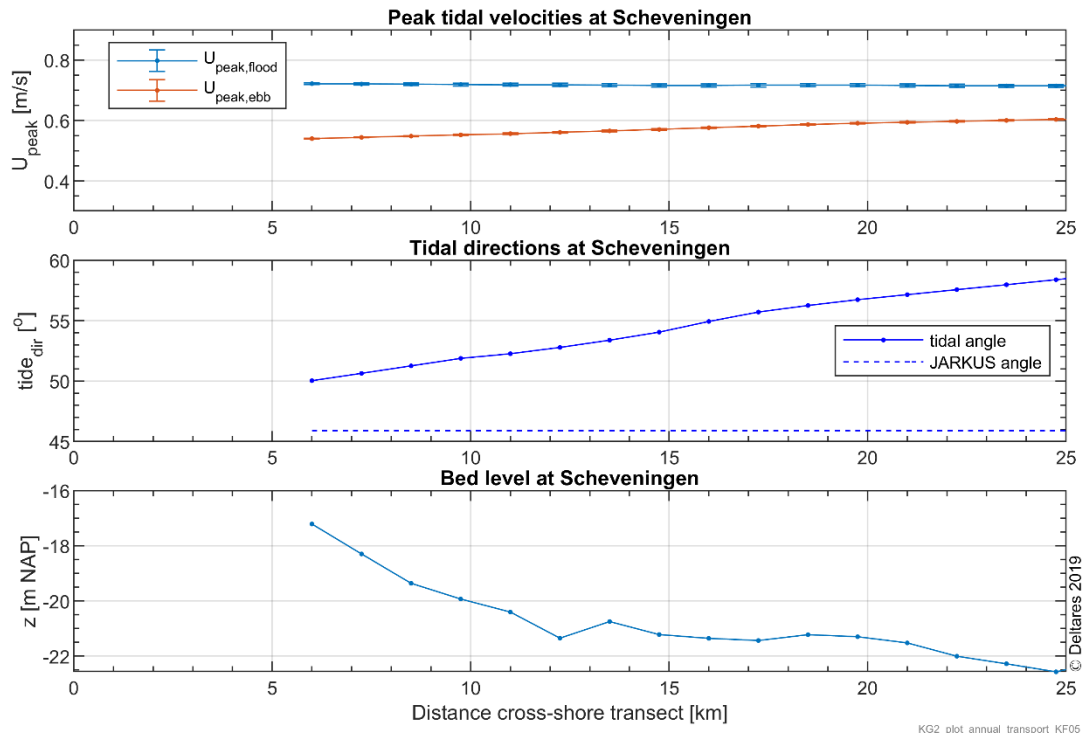


Figure 7.19 Annual mean peak tidal flood and ebb velocities and directions computed with 3D DCSM-FM model along Scheveningen transect. Statistics are based on annual means over years 2013-2017 and error bars indicate the standard deviation between the years. The lower panel shows the bed levels along this transect

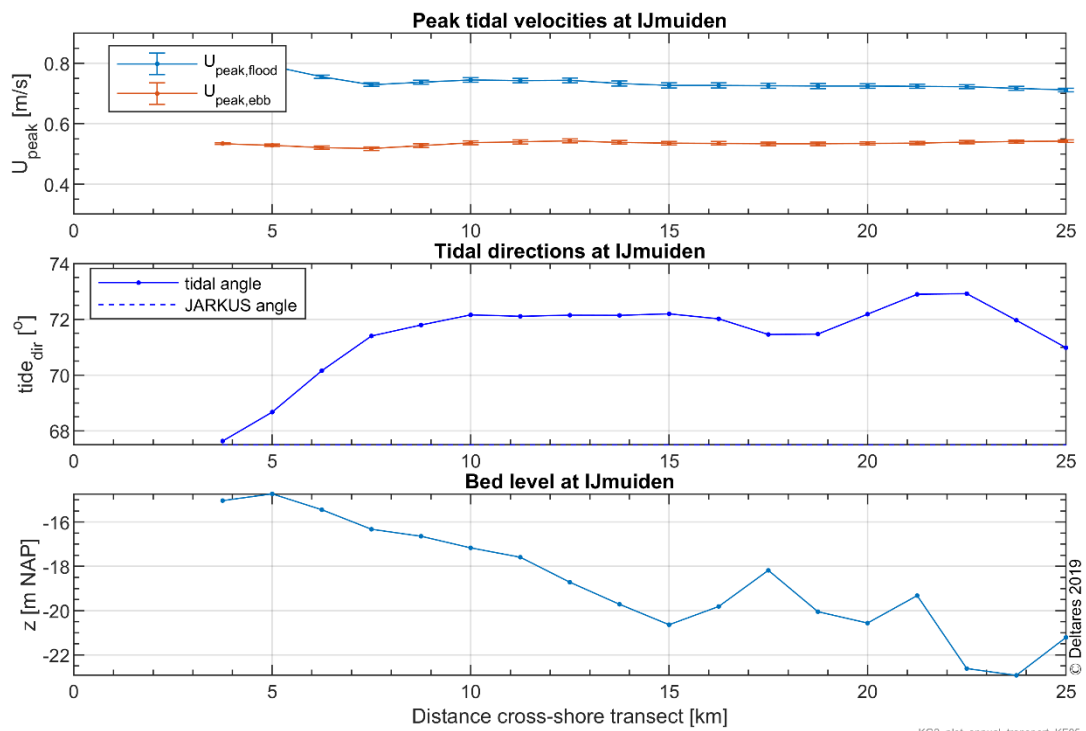


Figure 7.20 Annual mean peak tidal flood and ebb velocities and directions computed with 3D DCSM-FM model along IJmuiden transect. Statistics are based on annual means over years 2013-2017 and error bars indicate the standard deviation between the years. The lower panel shows the bed levels along this transect

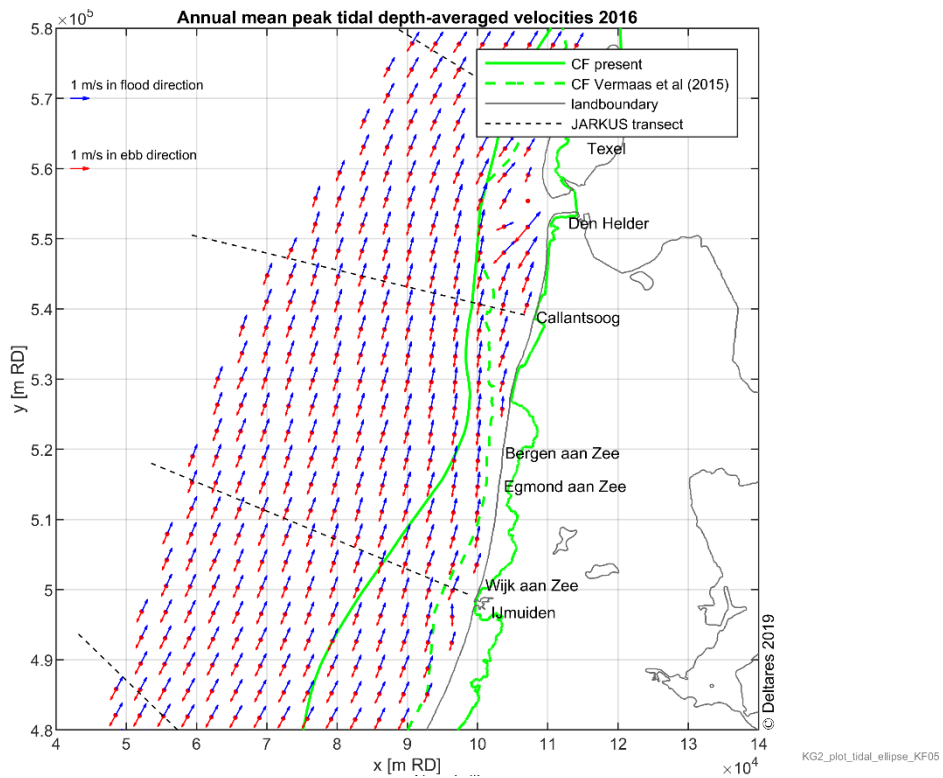


Figure 7.21 Annual mean peak flood (blue) and ebb (red) depth-averaged velocities computed with 3D DCSM-FM model for the year 2016, northern Dutch coast.

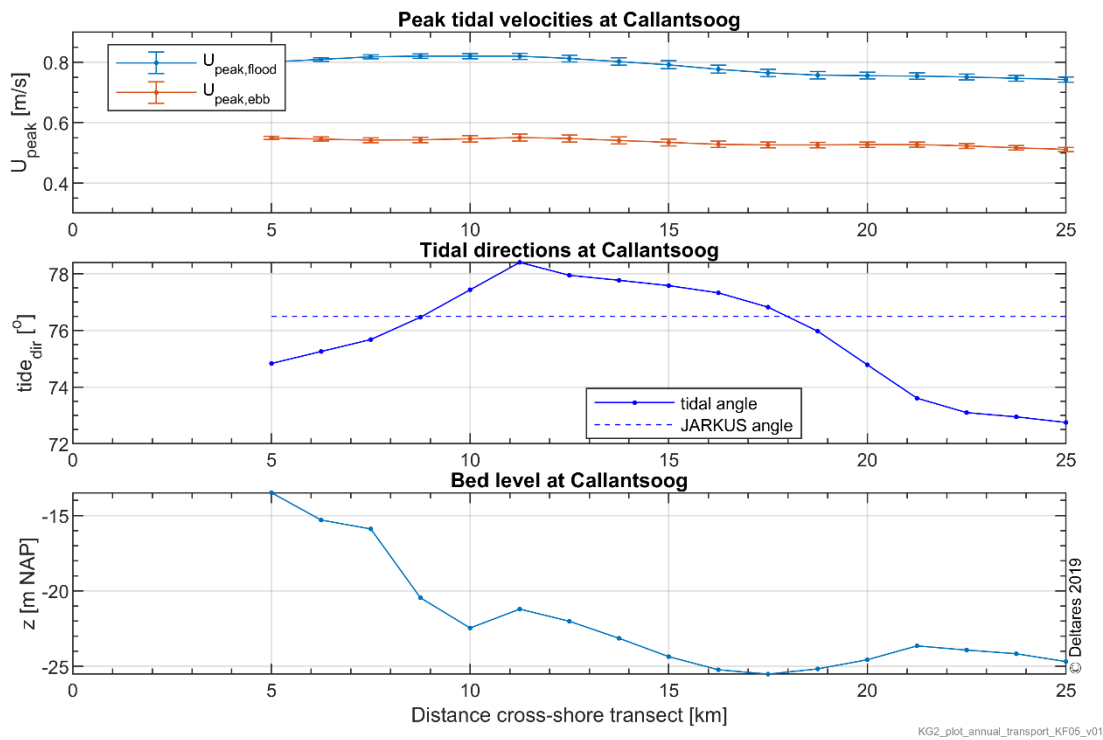


Figure 7.22 Annual mean peak tidal flood and ebb velocities and directions computed with 3D DCSM-FM model along Callantsoog transect. Statistics are based on annual means over years 2013-2017 and error bars indicate the standard deviation between the years. The lower panel shows the bed levels along this transect

Figure 7.23 shows the peak tidal velocities along the coasts of Texel, Vlieland and Terschelling. The peak tidal velocities follow the coastline more or less. Peak flood velocities decrease from Texel to Terschelling. The tidal velocities show a clear effect of the tidal inlet between Vlieland and Terschelling (Vliestroom) with flood velocities directed towards the inlet.

The annual mean peak flood velocities are 0.81 m/s at 6 km (20 m depth), 0.84 m/s at 9 km (21 m depth) and 0.68 m/s at 25 km (30 m depth) in the Texel transect (Figure 7.24). The peak ebb velocities are 0.53 m/s at 6 km, 0.56 m/s at 9 km and 0.47 m/s at 25 km. The asymmetry is 0.60. This is the same as in the Callantssoog transect.

In the Terschelling transect (Figure 7.25), the annual mean peak flood velocities are 0.66 m/s at 6 km (18 m depth), 0.68 m/s at 9 km (20 m depth) and 0.56 m/s at 25 km (27 m depth). The peak ebb velocities are 0.56 m/s at 6 km, 0.61 m/s at 9 km and 0.52 m/s at 25 km. The asymmetry decreases slightly from 0.54 to 0.52 when moving offshore. The asymmetry of the peak tidal velocities in this Terschelling transect is smaller than in the Texel transect.

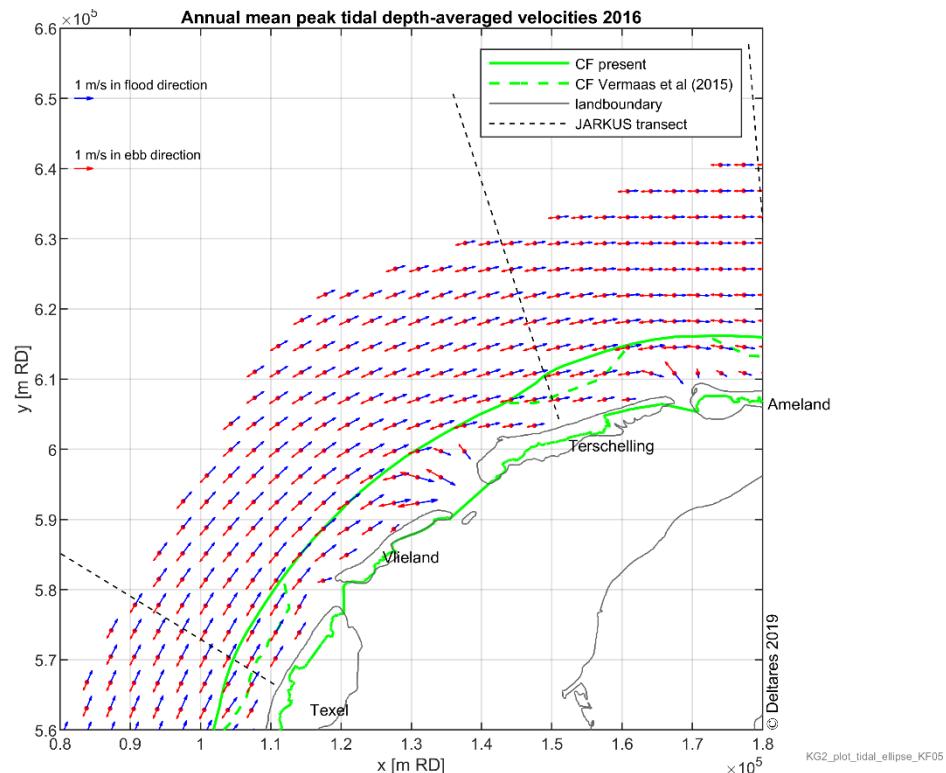


Figure 7.23 Annual mean peak flood (blue) and ebb (red) depth-averaged velocities computed with 3D DCSSM-FM model for the year 2016, northwestern Wadden coast.

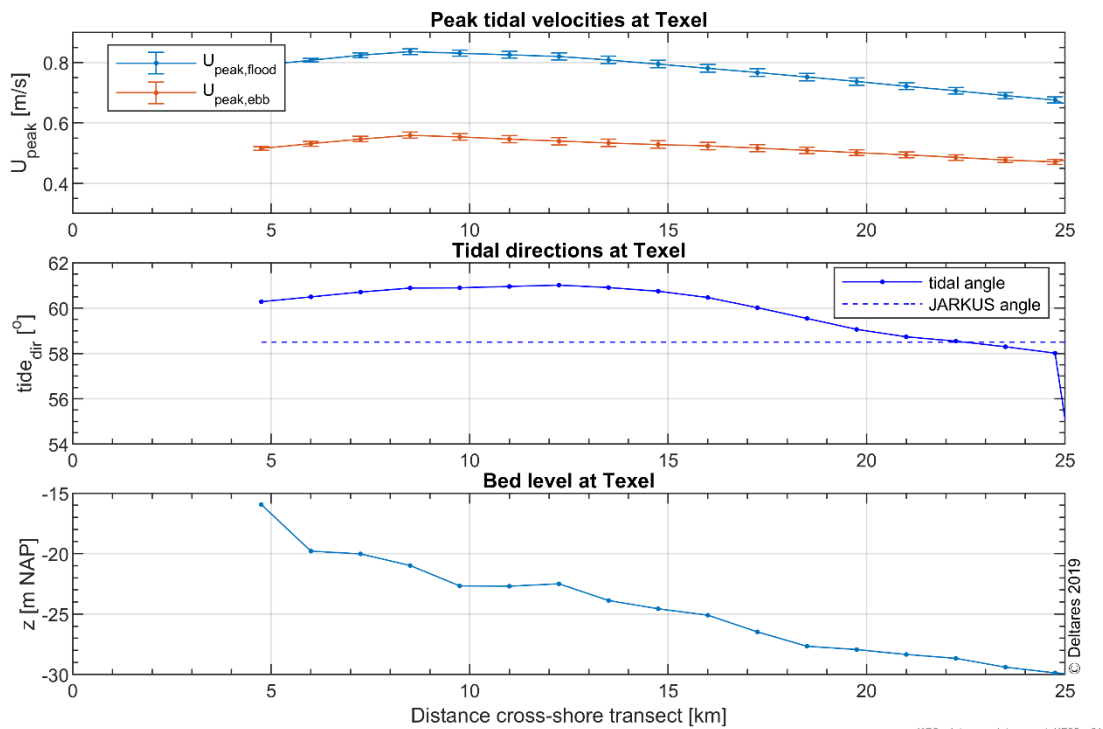


Figure 7.24 Annual mean peak tidal flood and ebb velocities and directions computed with 3D DCSM-FM model along Texel transect. Statistics are based on annual means over years 2013-2017 and error bars indicate the standard deviation between the years. The lower panel shows the bed levels along this transect

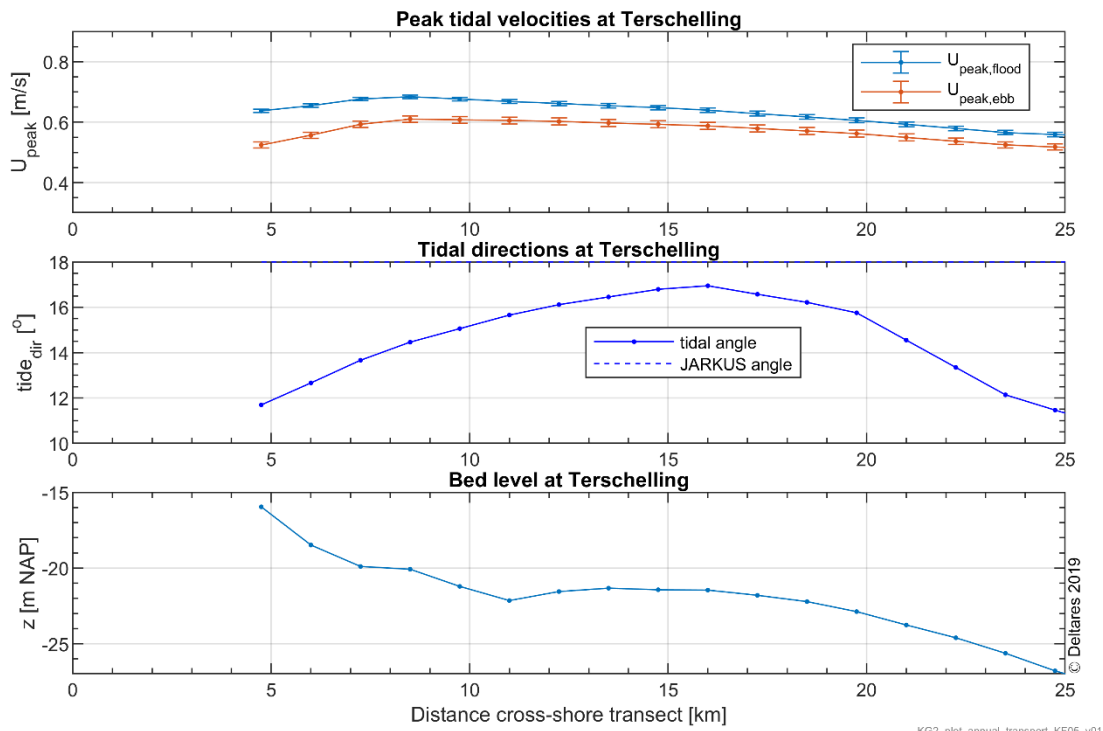


Figure 7.25 Annual mean peak tidal flood and ebb velocities and directions computed with 3D DCSM-FM model along Terschelling transect. Statistics are based on annual means over years 2013-2017 and error bars indicate the standard deviation between the years. The lower panel shows the bed levels along this transect



Peak tidal velocities decrease further along the coast from Terschelling to Ameland and Schiermonnikoog (Figure 7.26). Annual mean peak flood velocities are 0.50 m/s at 6 km (18 m depth) and 0.54 m/s at 25 km (27 m depth) at Ameland (Figure 7.27). Peak ebb velocities are 0.43 m/s at 6 km and 0.49 at 25 km. The tidal velocity asymmetry is 0.54 at 6 km and 0.52 at 25 km. This is similar to the asymmetry in the Terschelling transect.

The annual mean peak flood velocities are 0.56 m/s at 7 km (15 m depth) and 0.55 m/s at 25 km (25 m depth) in the Schiermonnikoog transect (Figure 7.28). The peak ebb velocities are 0.43 m/s at 7 km and 0.49 m/s at 25 km. The peak tidal velocity asymmetry is 0.57 at 7 km and 0.53 at 25 km. Although slightly larger, this is similar to the Ameland transect.

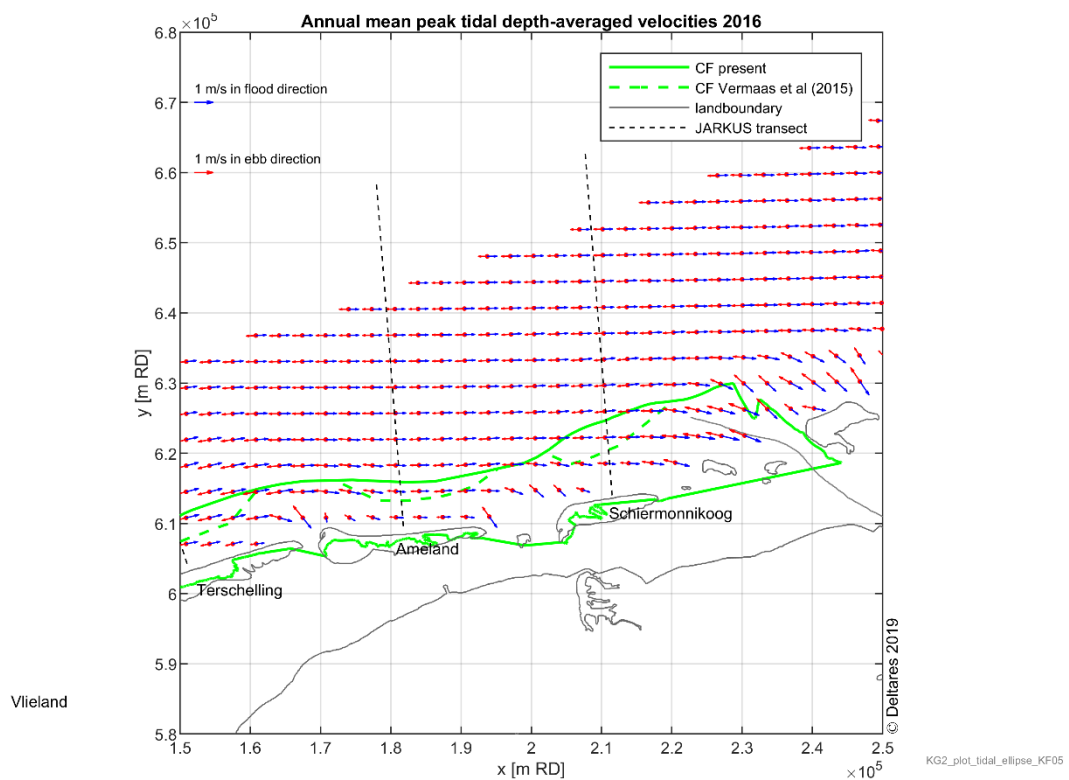


Figure 7.26 Annual mean peak flood (blue) and ebb (red) depth-averaged velocities computed with 3D DCSM-FM model for the year 2016, northeastern Wadden coast.

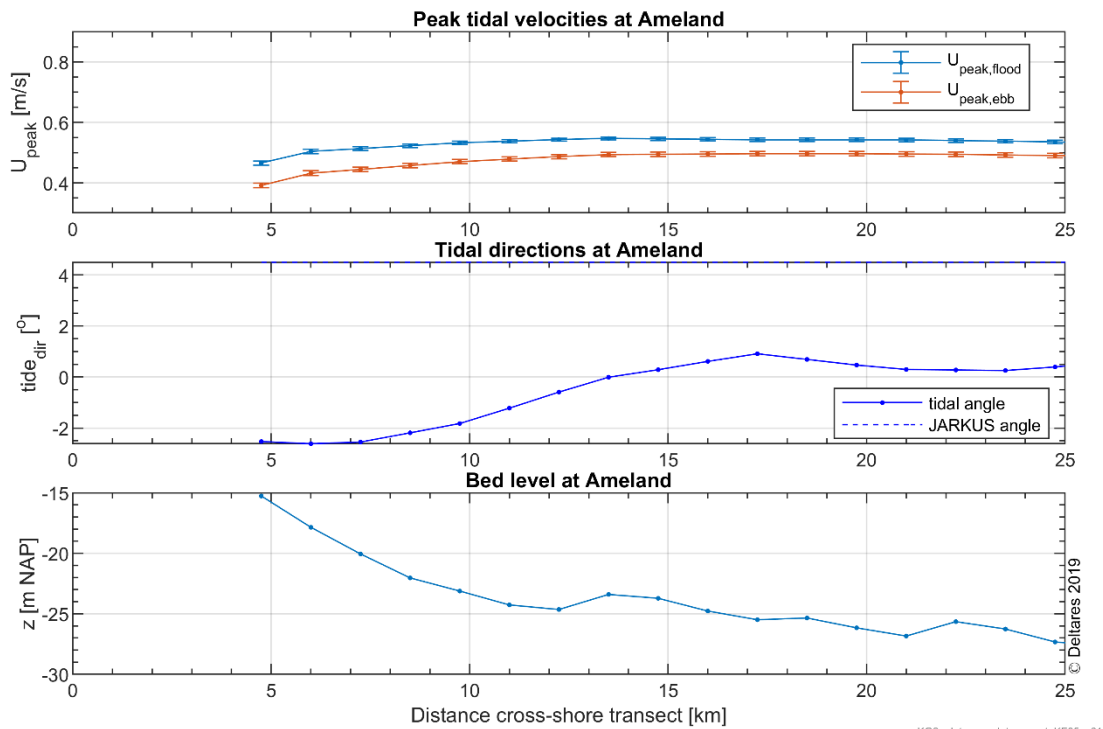


Figure 7.27 Annual mean peak tidal flood and ebb velocities and directions computed with 3D DCSM-FM model along Ameland transect. Statistics are based on annual means over years 2013-2017 and error bars indicate the standard deviation between the years. The lower panel shows the bed levels along this transect

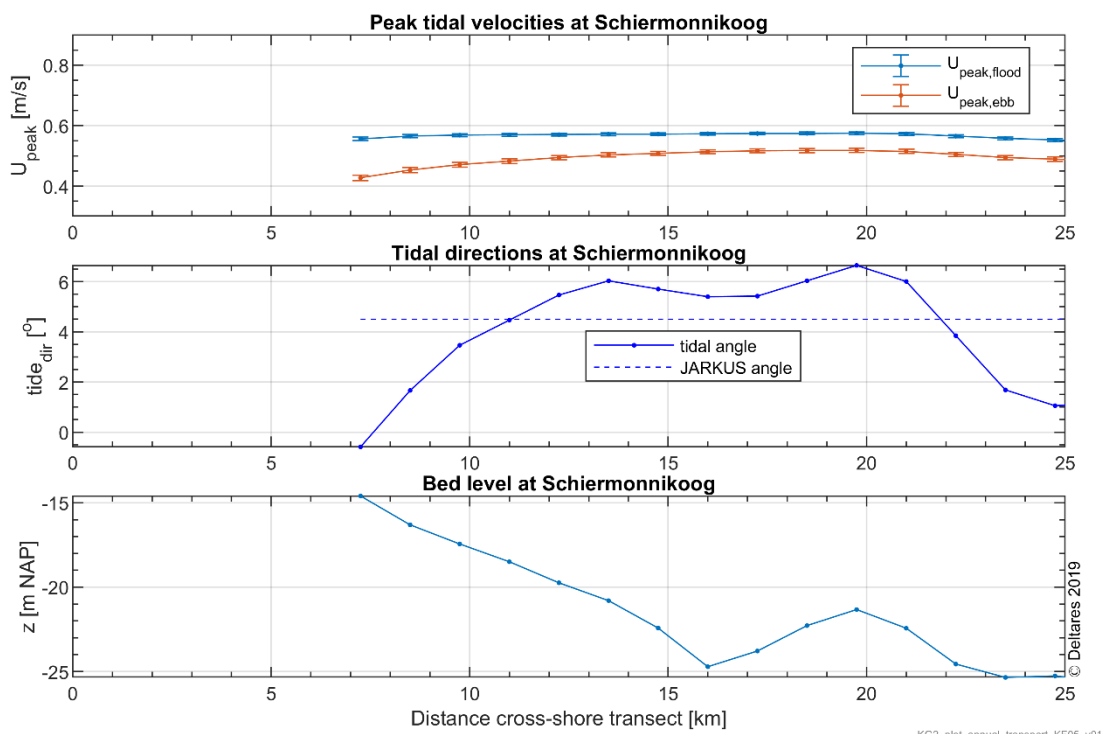


Figure 7.28 Annual mean peak tidal flood and ebb velocities and directions computed with 3D DCSM-FM model along Schiermonnikoog transect. Statistics are based on annual means over years 2013-2017 and error bars indicate the standard deviation between the years. The lower panel shows the bed levels along this transect